Modeling past, present and future climate induced vegetation changes in East Africa

Dissertation von

Istem Fer

Kumulative Dissertation
zur Erlangung des akademischen Grades
"Doctor Rerum Naturalium"
(Dr. rer. nat.)
in der Wissenschaftsdisziplin
"Vegetationsökologie und Naturschutz"

Eingereicht an der Biochemie und Biologie Fakultät
der Universität Potsdam

Potsdam, Januar 2018

Published online at the
Institutional Repository of the University of Potsdam:
https://doi.org/10.25932/publishup-42777
https://nbn-resolving.org/urn:nbn:de:kobv:517-opus4-427777

This work has not been submitted to any other institution of higher education, and that it was prepared independently and exclusively with the specified funds, the graduate school GRK1364 "Shaping Earth's Surface in a Variable Environment: Interactions between tectonics, climate and biosphere in the African-Asian monsoonal region" of the German Science Foundation (DFG, Deutsche Forschungsgemeinschaft; Project GRK 1364/2) and by German Academic Exchange Service (DAAD, Deutscher Akademischer Austauschdienst, 12/2011).

Abstract

East Africa is a natural laboratory, both to test the fundamentals of ecological theory, and to study many of the contemporary ecosystem research questions. First of all, it has a unique geological and biological evolutionary history. Studying its past can help us better inform our theories and models, and as a result, make more accurate predictions into the future. Secondly, East Africa is also sensitive to the current climate variability and global climate change due to its present biogeographical setting. Finally, East Africa hosts major hotspots of global biodiversity, and supports some of the fastest growing populations in the developing world. East African vegetation plays a central role in all these aspects, and this dissertation aims to quantify its transient dynamics through simulations using a process-based vegetation model.

Dynamic vegetation models (DVMs) can capture the biotic and abiotic interactions within terrestrial ecosystems in a spatially explicit way, which makes them suitable tools to study the questions asked in this dissertation. However, these models may need to be calibrated and validated for the particular study system if they were originally developed for another system. Therefore, I first simulated the present-day and mid-Holocene vegetation of East Africa with a DVM, namely LPJ-GUESS, and conducted an exhaustive area-wise comparison of model outputs with maps of potential modern vegetation distribution, and point-wise comparison with local pollen records (both modern and fossil). This was an effort to evaluate the model performance in East Africa, as well as to evaluate the applicability of point-wise model-data comparison approach with pollen data. Because when we study the past, we do not have vegetation maps that are based upon observations. We only have proxy data, such as pollen, which require extra modelling efforts to extract information about past vegetation, and which often provides highly localized signals as opposed to the spatial scales investigated with DVMs. Given that the topographical and climatic conditions change within very short distances in East Africa, I hypothesized that running the model at higher spatial resolutions would contribute to resolve the vegetation distribution better and have a better comparison scale with vegetation maps and pollen data. I used statistical downscaling methods to obtain finer resolution of model drivers and simulated the vegetation at these finer spatial scales. This study

showed that, overall, the model was able to reproduce the observed spatial patterns of East African vegetation. Both the area- and point-wise comparison showed that a higher spatial resolution does indeed allow a better comparison between predicted vegetation and data in East Africa.

Once the model was tested and validated for the region, it became possible to probe one of the long standing questions regarding East African vegetation: How did East Africa lose its tropical forests? The present-day vegetation in the tropics is mainly characterized by forests worldwide except in tropical East Africa, where forests only occur as patches at the coast and the highlands. Previous studies indicate that these patches are most likely the remnants of a once continuous and intact forest belt along the tropical East Africa that fragmented in time due to increasing aridity in the region over the late Cenozoic. In a series of simulation experiments where I systematically altered the environmental conditions, I investigated under which conditions these forest patches could have been connected, and a preceding continuous forest belt could have extended and fragmented. Results indicate that it is likely that the region indeed hosted conditions supporting forest biomes and a continuous forest belt during the late Cenozoic. This study once again established the sensitivity of East African vegetation to climate change and variability while providing an interpretation of the environmental changes that could have accompanied the hominin evolution that took place during this period.

The sensitivity of East African vegetation to climate change and climate variability continues to play a critical role for ecosystem services and biodiversity conservation in this region. In particular, the El Niño Southern Oscillation (ENSO) influence and its potential future impacts on East African vegetation need to be well understood in order to predict the vegetation responses and inform management decisions. With this goal in mind, I removed the ENSO signal from the climate data using Empirical Orthogonal Teleconnections (EOT) analysis and simulated the vegetation under the historical climate without components related to ENSO teleconnections, in order to differentiate the vegetation variability due to ENSO. This analysis revealed three important findings: 1) EOT analysis can successfully produce coupled tropical Pacific Sea Surface temperature-East African rainfall teleconnection from observational climate datasets, 2) there are

ENSO driven patterns in East African vegetation response, 3) the ENSO signal extracted from the climate model outputs, applying the same analysis, showed a weak correlation with the recorded one, meaning the climate models are still not good at predicting ENSO teleconnections. These findings led to the next step of the study: If there is a known relationship between East African rainfall and ENSO events, and climate models are not good at capturing this rainfall variability due to ENSO, then what is the extent of this discrepancy in our future projections? Using the same approach, I extracted the future ENSO signal from climate model projections, manipulated this signal to be as strong as it should be according to present-day observations, merged it back with the future climate data, and simulated the future vegetation under this manipulated climate dataset. I also simulated the vegetation under the climate model outputs as they are and compared the predictions. Indeed, future simulations showed considerable differences in East African vegetation under these two future climate drivers. This implies that the future vegetation would be different from what is simulated under these climate model outputs that lack accurate ENSO contribution, and this is a further uncertainty in our future global carbon budget calculations.

Overall, each component of this dissertation helped to fill both knowledge and methodology gaps in understanding East African vegetation dynamics, as well as to provide ancillary data for related studies such as palaeohydrology and palaeontology. I conclude with highlighting the importance of quantifying terrestrial ecosystem responses to changing climatic conditions to test and synthesize our understanding of how these natural systems work. Finally, I point out to future directions and research needs in modeling vegetation of East Africa in particular, and dryland ecosystems in general.

Kurzfassung

Ostafrika ist ein natürliches Labor zur Überprüfung der Grundlagen ökologischer Theorien und zum Studium vieler gegenwärtiger Forschungsfragen auf dem Gebiet der Ökosysteme. Insbesondere hat Ostafrika eine einzigartige geologische und biologische Evolutionsgeschichte. Daher lassen sich durch ein Studium dieser Vergangenheit aktuelle Theorien und Modelle überprüfen und verbessern, was zu genaueren Vorhersagen über die Zukunft führen kann. Desweiteren unterliegt Ostafrika aufgrund seiner biogeographischen Rahmenbedingungen den gegenwärtigen Klimaschwankungen und dem globalen Klimawandel. Darüber hinaus beherbergt Ostafrika bedeutende Hotspots globaler Artenvielfalt und einige der am schnellsten wachsenden Bevölkerungsgruppen in Entwicklungsländern. Bei all diesen Punkten spielt die ostafrikanische Vegetation eine zentrale Rolle, und Ziel dieser Dissertation ist es, durch Simulationen mit einem prozessbasierten Vegetationsmodell die transienten Dynamiken dieser Vegetation zu quantifizieren.

Dynamische Vegetationsmodelle (DVM) können sowohl biotische als auch abiotische Interaktionen innerhalb eines terrestrischen Ökosystems räumlich explizit erfassen. Damit sind sie geeignete Instrumente zum Studium der in dieser Dissertation behandelten Fragen. Es kann jedoch sein, dass diese Modelle für das Studiensystem neu kalibriert und validiert werden müssen, falls sie ursprünglich für ein anderes System entwickelt wurden. Daher wurden zunächst die aktuelle und die im Mittelholozän vorherrschende Vegetation Ostafrikas mit einem DVM simuliert, und zwar mit LPJ-GUESS. Mithilfe von Karten potentieller heutiger Vegetationsverteilung wurde ein gründlicher großräumiger Vergleich von Modell-Outputs durchgeführt. Mit lokalen Pollen-Daten (sowohl aktuellen als auch fossilen) erfolgte ein punktueller Vergleich. Dadurch sollte die Leistungsfähigkeit des Modells in Ostafrika abgeschätzt werden, sowie die Anwendbarkeit des Ansatzes mit einem punktuellen Modell-Daten-Vergleich mit Pollen-Daten. Beim Studium der Vergangenheit verfügt man nämlich über keine auf Beobachtungen beruhenden Vegetationskarten, sondern nur über Proxy-Daten, wie etwa Pollen, die einen zusätzlichen Modellaufwand zur Beschaffung von Informationen über frühere Vegetation nötig machen und im Gegensatz zu den über DVMs

untersuchten räumlichen Skalen oft sehr lokalisierte Signale liefern. Aufgrund der Tatsache, dass in Ostafrika die topographischen und klimatischen Umstände oft auf kleinem Raum rasch wechseln, ging ich davon aus, dass eine Anwendung des Modells mit höheren räumlichen Auflösungen dazu beitragen kann, die Vegetationsverteilung besser zu klären und zu einer besseren Vergleichsskala mit Vegetationskarten und Pollen-Daten zu gelangen. Um eine genauere Auflösung der Modelltreiber zu erhalten, wurden statistische Downscaling-Methoden verwendet, und die Vegetation wurde auf diesen genaueren Skalen simuliert. Es zeigte sich, dass das Modell insgesamt in der Lage war, die beobachteten räumlichen Muster der ostafrikanischen Vegetation zu reproduzieren. Sowohl aus dem großräumigen als auch aus dem punktuellen Vergleich ergab sich, dass eine höhere räumliche Auflösung tatsächlich einen besseren Vergleich zwischen vorhergesagter Vegetation und Daten in Ostafrika ermöglicht.

Nachdem das Modell getestet und für die Region validiert war, konnte eine der seit langem offenen Fragen über die ostafrikanische Vegetation angegangen werden, nämlich wie Ostafrika seines Tropenwaldes verlustig gehen konnte. In den Tropen wird die heutige Vegetation weltweit hauptsächlich von Wäldern dominiert, mit Ausnahme der Tropengebiete Ostafrikas, wo Wälder nur noch stellenweise an der Küste und im Hochland vorkommen. Aus früheren Studien hatte sich ergeben, dass diese Waldreviere höchstwahrscheinlich die Reste eines durchgehenden, intakten Waldgürtels sind, der sich durch das ganze tropische Ostafrika zog und aufgrund der zunehmenden Trockenheit im späten Känozoikum fragmentiert wurde. In dieser Studie wurden in einer Reihe von Simulationsexperimenten die Umweltbedingungen systematisch verändert, sodass untersucht werden konnte, unter welchen Bedingungen die Waldgebiete miteinander verbunden gewesen sein konnten, und wo sich ein früherer durchgehender Waldgürtel vermutlich erstreckte und schließlich fragmentiert wurde. Es ergab sich, dass in der Region in der Tat mit hoher Wahrscheinlichkeit Bedingungen herrschten, die auf Waldbiome und einen durchgehenden Waldgürtel im späten Känozoikum schließen lassen. Meine Studie hat somit erwiesen, wie empfindlich die ostafrikanische Vegetation für Klimawandel und Klimaschwankungen ist. Sie lässt eine Interpretation der Umweltbedingungen zu, unter denen die damalige Evolution der Hominiden stattgefunden haben könnte.

Die Empfindlichkeit der ostafrikanischen Vegetation für Klimawandel und Klimaschwankungen spielt weiterhin eine kritische Rolle für die ökosystemaren Dienstleistungen und die Bewahrung der Artenvielfalt in der Region. Insbesondere muss gut erforscht werden, wie sich das El Niño/Southern Oscillation--Phänomen (ENSO) in Zukunft auf die ostafrikanische Vegetation auswirken könnte, damit sich die Vegetationsreaktionen vorhersagen lassen und geeignete Maßnahmen getroffen werden können. Im Hinblick darauf wurde in dieser Studie unter Benutzung der Empirical Orthogonal Teleconnections (EOT)-Analyse das ENSO-Signal aus den Klimadaten entfernt, und die Vegetation unter dem historischen Klima wurde ohne Komponenten simuliert, die in Bezug zu ENSO-Telekonnektionen stehen. Damit sollten die auf das ENSO-Phänomen zurückgehenden Vegetationsschwankungen herausgearbeitet werden. Aus dieser Analyse haben sich drei wichtige Faktoren ergeben: 1) Die EOT-Analyse kann aus empirischen Klima-Datasätzen eine Telekonnektion zwischen der Meerestemperatur im tropischen Pazifik und den Niederschlägen in Ostafrika nachweisen 2) In der ostafrikanischen Vegetationsreaktion gibt es ENSO-bedingte Muster, 3) Das aus den Klimamodell-Outputs extrahierte ENSO-Signal wies bei der Anwendung der gleichen Analyse nur eine schwache Korrelation zum aufgenommenen Signal auf, was bedeutet, dass Klimamodelle immer noch nicht gut genug sind, um ENSO-Telekonnektionen vorherzusagen. Aus diesen Erkenntnissen leitete sich der nächste Schritt der Studie ab: Wenn es bekanntermaßen einen Zusammenhang zwischen den Niederschlägen in Ostafrika und dem ENSO-Phänomen gibt, und wenn Klimamodelle diese auf ENSO zurückgehenden Niederschlagsschwankungen nicht gut genug erfassen können, wie hoch ist dann das Ausmaß dieser Diskrepanz in unseren zukünftigen Projektionen? Unter Anwendung desselben Ansatzes wurde das künftige ENSO-Signal aus den Klimamodellprojektionen herausgenommen und so manipuliert, dass es so stark war, wie es laut den heutigen Beobachtungen sein müsste. Daraufhin wurde es in die künftigen Klimadaten zurückgerechnet, und die künftige Vegetation wurde mit diesem manipulierten Klima-Datensatz simuliert. Die Vegetation wurde auch mit den tatsächlichen Klimamodell-Outputs simuliert, und die jeweiligen Vorhersagen wurden verglichen. Zukunftssimulationen ergaben, dass zwischen diesen beiden künftigen Klimatreibern in der ostafrikanischen Vegetation erhebliche Unterschiede bestehen. Daraus leitet sich ein Unterschied zwischen der künftigen Vegetation und den Simulationen ab, die

mit Klimamodell-Outputs erfolgen, bei denen der genaue ENSO-Beitrag nicht berücksichtigt werden kann. Bei der Berechnung der künftigen weltweiten CO_2-Bilanz stellt dies daher einen zusätzlichen Unsicherheitsfaktor dar.

Insgesamt hat jeder Teilaspekt dieser Dissertation dazu beigetragen, beim Verständnis der ostafrikanischen Vegetationsdynamik Wissens- und Methodenlücken zu füllen und zusätzliche Daten für verwandte Studien wie etwa in Paläohydrologie und Paläontologie zu erheben. Abschließend wird hervorgehoben, wie wichtig es ist, terrestrische Ökosystemreaktionen auf wechselnde klimatische Bedingungen zu quantifizieren, um unser Verständnis davon, wie diese natürlichen Systeme wirken, zu testen und zusammenzufassen. Es werden auch Hinweise darauf gegeben, in welcher Richtung bei der Modellierung der ostafrikanischen Vegetation im besonderen und Trockenland-Ökosystemen im allgemeinen weitergeforscht werden sollte.

Publications and author contributions

This thesis is comprised of three independent studies published in high impact peer review journals. Chapters 2 through 4 correspond to the individual studies.

Chapter 2

High-resolution modelling closes the gap between data and model simulations for Mid-Holocene and present-day biomes of East Africa

Istem Fer, Britta Tietjen, Florian Jeltsch

All authors contributed to the design of the study. Istem Fer conducted the study and the analyses. Istem Fer wrote the manuscript with contribution from all co-authors.

Chapter 3

Modelling vegetation change during Late Cenozoic uplift of the East African plateaus

Istem Fer, Britta Tietjen, Florian Jeltsch, Martin H. Trauth

All authors contributed to the design of the study. Istem Fer conducted the study and the analyses. Istem Fer wrote the manuscript with contribution from all co-authors.

Chapter 4

Influence of El Niño-Southern Oscillation regimes on East African vegetation and its future implications under RCP 8.5 warming scenario

Istem Fer, Britta Tietjen, Florian Jeltsch, Christian Wolff

Christian Wolff proposed the study theme. All authors contributed to the design of the study. Istem Fer conducted the study and the analyses. Istem Fer wrote the manuscript with contribution from all co-authors.

Table of Contents

List of abbreviations

ITCZ: Intertropical Convergence Zone

CAB: Congo Air Boundary

MER: Main Ethiopian Rift

EARS: East African Rift System

ENSO: El Niño Southern Oscillation

SST: Sea Surface Temperatures

DVM: Dynamic Vegetation Model

PFT: Plant Functional Type

LPJ-GUESS: Lund-Potsdam-Jena General Ecosystem Simulator

AHP: African Humid Period

NEE: Net Ecosystem Exchanges

NPP: Net Primary Productivity

List of Figures

List of Tables

Acknowledgements

Above all, I would like to express my deepest gratitude to my guiding and inspiring advisors Prof. Dr. Florian Jeltsch and Prof. Dr. Britta Tietjen. Without their insightfulness and stimulation this work would not have been achievable. Thank you for supporting me and allowing me to develop my own research.

I cannot thank my family enough: first and foremost to my father, Metin Fer, for all his selfless hard work and generosity; to my mother, Şenay Fer for always encouraging me; to my dear sister Evrim Fer and brother Yetkin Fer; Kadir Polat, Imran Polat and Ozge Polat for always being there for me, and last but not least, to my precious partner, Uygar Polat, for helping me find all the important things in life, and for his limitless support and warmth. I feel so lucky and strong with these wonderful people by my side.

I am grateful to everyone who made the whole experience of Graduate School GRK 1364, "Shaping Earth's Surface in a Variable Environment: Interactions between tectonics, climate and biosphere in the African-Asian monsoonal region" possible. To Dr. Henry Wichura for all his organizational efforts, especially for the unforgettable field schools in East Africa and the Himalayas, to Prof. Manfred Strecker for encouraging me into this wonderful program, to Prof. Martin Trauth and Dr. Christian Wolff for all their valuable teaching and collaboration, and to all DFG school participants who were good peers and friends. I would like to thank Prof. Annett Junginger in particular for sharing her enthusiasm and research with me. I also would like to appreciate the PENCies whose constructive comments and discussions always helped me improve my scientific work.

Thank you my dear friends Michael Hayn, Anne-Karoline Distel, and Yildiz Goney for all the good memories we created together. You are partly to blame why I loved Germany this much. I owe a special thanks to Gerhard Meier for the German translation of my abstracts, you are the best.

Finally, I would like to thank Prof. A. M. Celâl Şengör, for truly infecting me with his love and appetite for science. I hope this thesis was my first step to a scientific journey of a thousand miles like his.

Chapter 1: Introduction

1.1 Motivation

Almost everything about East Africa is scientifically intriguing: the formation of the Great Rift Valley, dynamics of its lakes and plateaus, its fluctuating climate, diversity of its biomes, its evolutionary past and uncertain future. And what makes it even more fascinating is the interconnectedness of them all. It is almost never enough to study one without the other and each is a piece of a bigger puzzle. Therefore, this dissertation does not only takes an ecological approach but a whole earth system perspective.

First, and foremost, the main motivation of this study was to learn more about the past vegetation of East Africa. Vegetation sets the scene for other earth system processes to take place: from affecting denudation rates (Torres Acosta et al., 2015) to changing migratory routes (Cowlings et al., 2008) in East Africa. However, reconstructing palaeovegetation is a challenge in general, and in East Africa in particular. Because continuous records of palaeoecological change are rare from terrestrial sequences in East Africa as active faulting, erosion, and non-deposition often punctuate the geologic record, and they often provide localized signals (Potts, 1998; Kingston, 2007). Tools such as dynamic vegetation models (DVMs) can help us incorporate information from other paleo-proxies and allow us to reconstruct the regional palaeovegetation in a spatially explicit way (Cowlings et al., 2008).

While studying palaeoecology has its own value; the tools, the data and the knowledge emerged from these studies can also be used for predicting future changes. DVMs are central instruments for projecting future as well. However, there are substantial disagreements in their future predictions (Friedlingstein et al., 2014). Therefore, testing their performance in reproducing the past environmental changes has become a common benchmarking effort to distinguish the reasons behind these disagreements and understand their sensitivities to different drivers (Monserud et al., 1993; Shellito & Sloan, 2006; Henrot et al., 2017). In line with

these efforts, while this dissertation investigates past vegetation dynamics in the region, it also provides a basis for more robust future projections for East Africa.

We need robust projections for East Africa as it is sensitive to climate change and climate variability while hosting major hotspots of global biodiversity, and some of the fastest growing human populations in the developing world. Furthermore, dryland ecosystems such as East African savannas also play an important role in global carbon budget (Poulter et al., 2014; Ahlström et al., 2015). Both the geographical distribution and ecosystem services of drylands will be affected by climate change with unclear consequences on global carbon budget and sustainable livelihood (Tietjen et al., 2017). Moreover, the El Niño Southern Oscillation (ENSO) influence brings further uncertainties into the future predictions of terrestrial ecosystem responses in this region. Again, DVMs can help us quantify these uncertainties and inform our management strategies of these natural system as demonstrated in this dissertation.

1.2 East Africa

1.2.1 Geology

Geology has a lot to do with vegetation when it comes to East Africa. A brief summary of geological history of East Africa during the Cenozoic (period between 66-0 million years ago, Ma hereinafter) is as follows: During Early Paleogene (66-50 Ma) African Continent was positioned south of its current location and the Tethys Sea in its north was still open. Together with the currents over Atlantic Ocean in the west and Indian Ocean in the east, northern part of the continent was moist and covered with forests from coast to coast (Lovett and Wasser, 1993). As the continent moved northwards from early to middle Miocene (around 20 Ma), the Tethys Sea closed when Africa collided with Eurasia. This ended the flow of oceanic currents around northern Africa, limiting moisture transport to the Sahara and the Arabian Peninsula (Lovett and Wasser, 1993). However, lower topographical setting was still allowing zonal circulations to bring precipitation to East Africa that could support forest biomes in the region (Sepulchre et al., 2006). Around this time, development of Ethiopian dome also

started (20±2 Ma), followed by volcanism in northern Kenya (15±2 Ma), southward propagation of the rifting (8±2 Ma), advanced development of the East African Rift System (3±1 Ma), leading to today's high topography of the region (MacGregor, 2015). Especially the uplift during the last 10 million years is associated with the aridification of East Africa, accompanying other environmental factors such as atmospheric CO_2 decrease (8 to 6 Ma), Indian Ocean sea surface temperature cooling and the onset of glacial-interglacial cycles (5 to 3 Ma) that further influenced the East African vegetation (Sepulchre et al., 2006). The change of East Africa from a relatively flat, homogeneous landscape covered with mixed tropical forests, to a heterogeneous one with high mountains and diverse vegetation might have facilitated the traits that enabled human ancestors to adjust to environmental change (Trauth et al., 2010; Maslin et al., 2014). These topographical features continue to affect the climate of East Africa today.

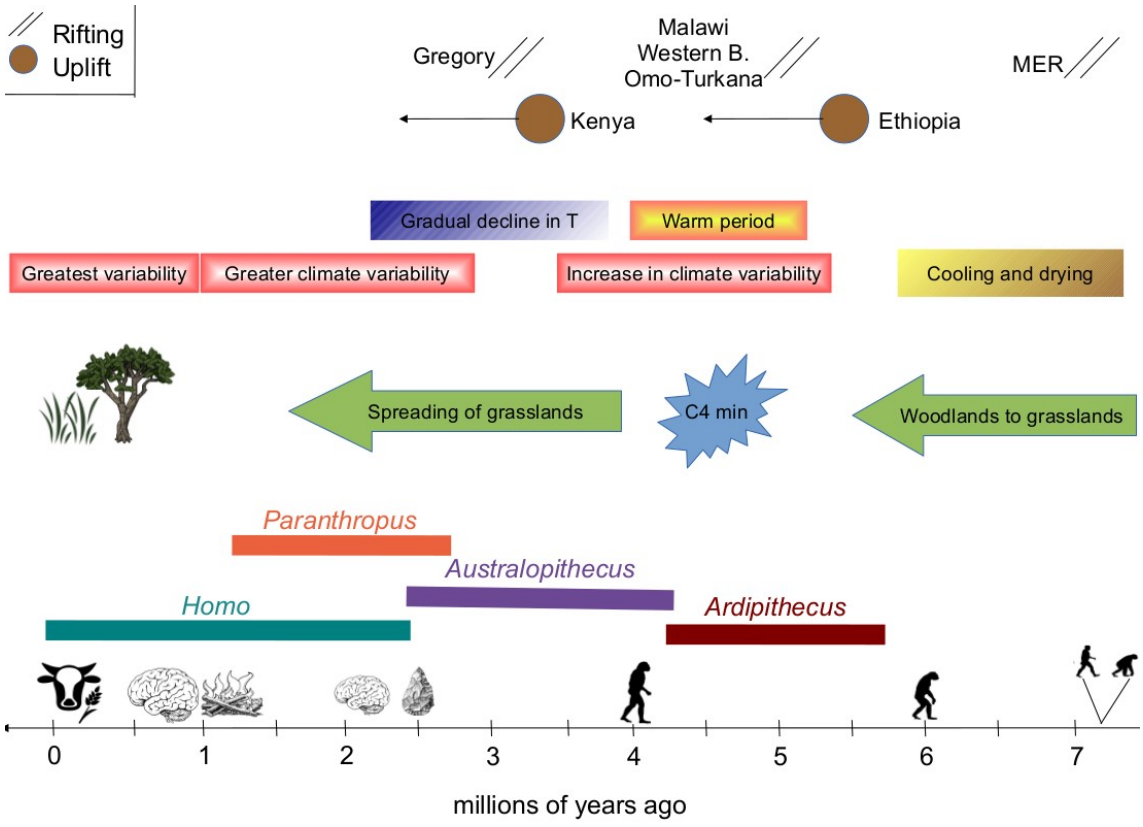

Figure 1.1 A brief summary and compilation of environmental changes accompanying human evolution in East Africa. From top to bottom, the panels show geological, climatological, ecological, and evolutionary changes. Multiple, intertwined factors are influential on human evolution. (MER: Main Ethiopian Rift, C4 min: C4 grass minimum in abundance)

1.2.2 Climate

East African climate is mainly under the influence of seasonal movement of the east-west oriented Intertropical Convergence Zone (ITCZ) and the northeast-southwest oriented Congo Air Boundary (CAB) (Figure 2). CAB is basically the area where Indian and West African Monsoonal air movements interact. In addition to major regional climatic factors, the topography also impacts local climate conditions in eastern Africa, causing a more complex and different climatic behaviour than in the rest of the Africa (Junginger et al., 2014). For instance, CAB's location is determined partly by Ethiopian and Kenyan Domes. While Ethiopia, the western branch of EARS and most of western Tanzania receives seasonal rainfalls, the Horn of Africa and coastal East Africa are isolated orographically from convergence along CAB and consequently these regions are more arid. As a result, western Ethiopia and north of Lake Victoria have the highest rainfall amount (2000 mm/yr) whereas Afar, Somali and the Awash valley receives the lowest (150 mm/yr) (Nicholson, 2000).

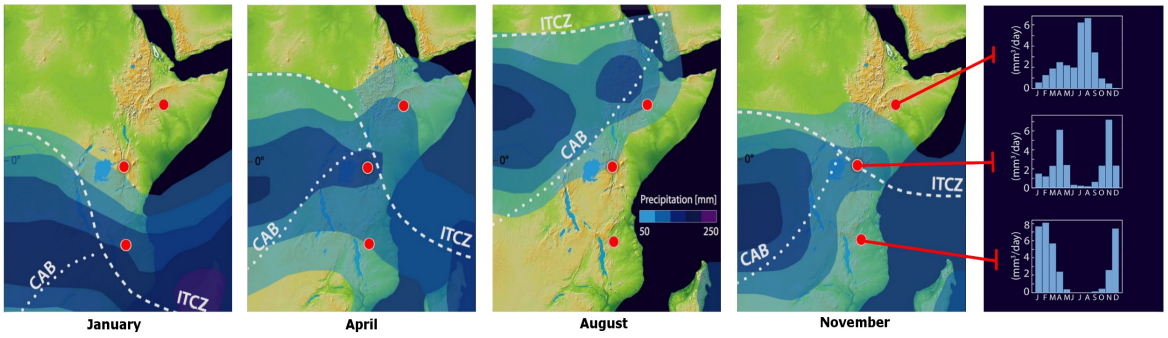

Figure 1.2 Distribution and amount of precipitation in East Africa (after Junginger et al., 2014). Rainfall closely follows the movement of Intertropical Convergence Zone (ITCZ) and the Congo Air Boundary (CAB) in the region. The modality of the rainfall for three locations (red dots) on a north-south gradient can be seen in the last column.

This topography – precipitation interplay had an interesting impact in East Africa during the African Humid Period (AHP, 15-5 ka BP). During that time, changes in solar radiation increased the pressure gradient over the northern hemisphere resulting in northeastward shifts in ITCZ and CAB positions (Junginger et al., 2014). With this pressure gradient, CAB was able overcome the orographic barrier, bringing precipitation to the drier parts of East Africa, filling out the rift lakes (Junginger et al., 2014). Increase in boreal summer season insolation also

enhanced evaporation and precipitation together with more inland movement of the West African Monsoon due to land-sea pressure gradients. The structural changes East African terrestrial ecosystems went through during this time are detectable in the proxy data (Peyron et al., 2000; Garcin et al., 2006).

Being in the tropics and adjacent to the Indian Ocean, East Africa is also susceptible to inter-annual climate variability due to fluctuations in atmospheric and oceanic currents (Nicholson, 2000). Two main atmospheric circulations affecting the region is the Hadley Circulation that moves the air along latitudes (north-south) and the Walker Circulation that moves the air along the tropical longitudes (east-west). The strength of Hadley and Walker cells is affected by land-atmosphere-ocean temperature and pressure gradients.

The branches of Walker circulations involve uplifts of air masses over Africa, Indonesia and South America, and subsidence in-between these areas (Figure 1.3, top panel). The cell over the Indian Ocean consists of uplift over Indonesia (rising air, wetter conditions) and subsidence occurring over the coast of East Africa (sinking air, drier conditions). The stronger this circulation becomes, the drier East Africa gets. On the contrary, when this cell weakens or shifted, more moisture from Indian Ocean can reach East Africa and wetter conditions occur (Lau and Yang, 2002).

The interplay between Hadley and Walker circulations is also responsible for the teleconnection between Pacific Ocean Sea Surface Temperatures (SSTs) and East African rainfall (Schreck and Semazzi, 2004). When the trade winds (the part of Hadley cell where air masses move back towards the equator) weaken, the warm water in the western Pacific oscillates backwards to the eastern Pacific and this slows or stops the upwelling of cooler water along the coast (warm event, El Niño phase of the El Niño Southern Oscillation -ENSO-). As a result, the Walker circulation shifts with rising air over Pacific Ocean and East Africa, bringing more rainfall to the region (Figure 1.3, middle panel). When the opposite occurs and the trade winds strengthen, it causes even more upwelling of the cooler water in eastern Pacific, followed by a stronger Walker Circulation and less rainfall in East Africa (cold event, La Niña phase of ENSO, Figure 1.3, bottom panel). The inter-annual variability of precipitation is also influential on the East African

vegetation.

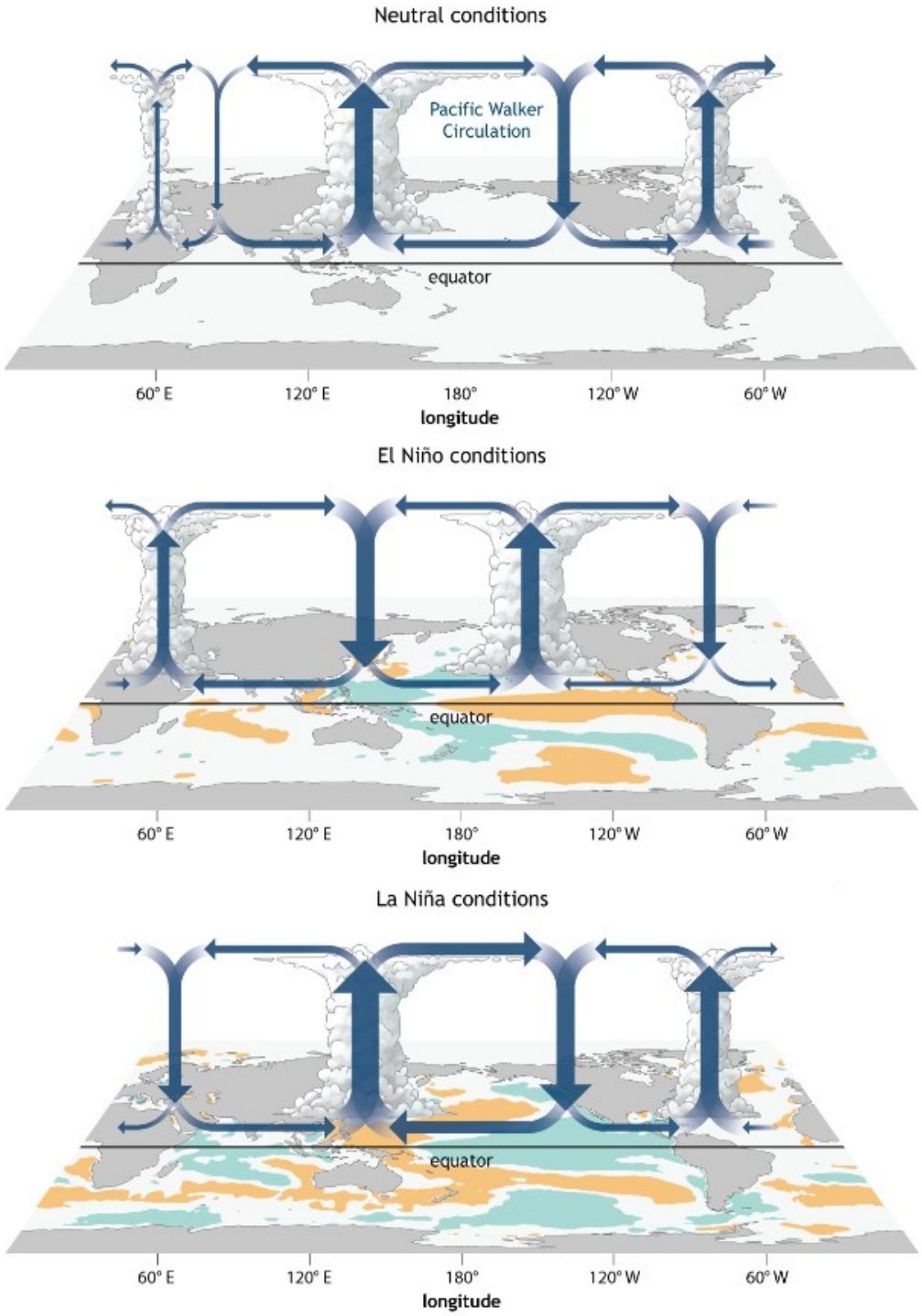

Figure 1.3 Walker circulation moves the air masses across the tropics. (Source NOAA Climate.gov, drawing by Fiona Martin)

1.2.3 Vegetation

The East African vegetation distribution and composition follows the precipitation patterns closely, whereas temperature is also effective on the rift mountains (Figure 1.4). As a result, within a relatively small region, East Africa hosts biomes ranging from deserts to afro-alpine grasslands, and from tropical rainforests to afromontane forests (White, 1983). However, arid and semi-arid environments still dominate the region with a proportion of 83.2% (excluding agriculture) which is even greater relative to their proportion in the whole Africa 70.1% (Bobe, 2006).

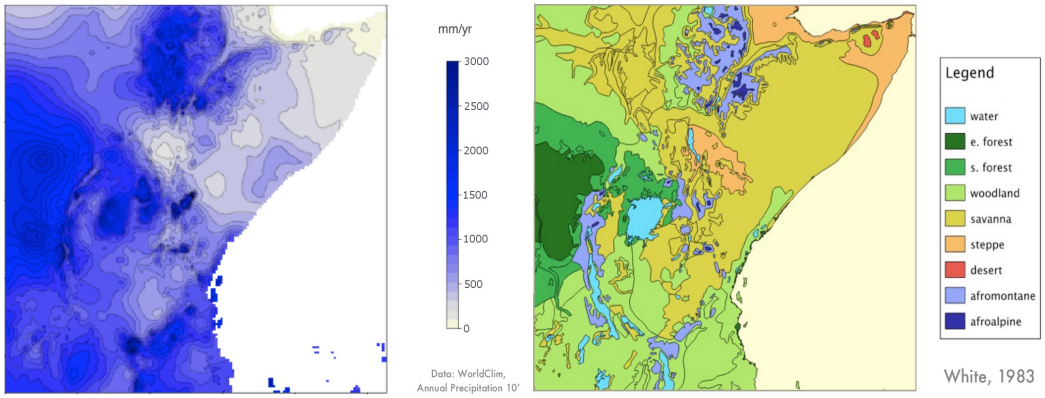

Figure 1.4 Precipitation (left; WordClim) and vegetation (right; White, 1983) patterns in East Africa. Biomes are distributed in accordance with the annual mean precipitation.

The complexity of East African topography and climate dynamics requires a comprehensive study of its vegetation which sustains a great biodiversity and human population. However, the East African vegetation is relatively under-studied due to the remoteness and the socio-economic history of the region. In the recent years, especially with the development of remote sensing technologies, this knowledge gap closes. However, long term monitoring and observation systems are still lacking for the region whereas such systems are vital for ground validation of the remote sensing data and forecasting the future responses of the terrestrial ecosystems. Although they cannot substitute for the observations and they themselves are data hungry, Dynamic Vegetation Models (DVMs) can help us bring pieces of information together and provide a more comprehensive picture of East African vegetation dynamics. For example, a model that can successfully reproduce the vegetation composition and distribution which is comparable to

satellite-based vegetation maps that we have for East Africa, may also be trusted for reproducing the fluxes correctly which we do not have from East Africa.

Studying the palaeovegetation dynamics can partly be a remedy for the lack of long-term observations from East Africa. Thanks to its variable climatological history, East African vegetation has already experienced considerable changes in the past (for an example, see African Humid Period in the previous section), which can help us understand the conditions that they have adopted or sensitive to through time. Once more, DVMs can act as a scaffold: biome composition extracted from fossil pollen data can be compared to plant functional type composition predictions from a DVM, while surface runoff values calculated from palaeo-lake level reconstructions can be compared to its runoff predictions, and from that we can make interpretations about total biomass of that particular ecosystem through the DVM. In addition to connecting one pattern to the other through underlying mechanistic processes, DVMs could also connect them through space.

1.3 Dynamic vegetation models

Dynamic Vegetation Models (DVMs) are computer models that simulate the vegetation dynamics according to the underlying equations of ecosystem processes coded in their framework. They can be very simple with a few processes and a few hundred lines of code (Simplified Photosynthesis and Evapotranspiration -SIPNET- model; Braswell et al., 2005) or very complex (Community Land Model -CLM-; Oleson et al., 2010). DVMs were developed to simulate terrestrial ecosystem responses under rapid environmental changes and predict global vegetation patterns (Prentice et al., 1992). They are now also widely used to recreate past settings (Allen et al., 2010), forecast into the future (Hickler et al., 2012) or conduct simulation experiments that we cannot easily perform in the field (Higgins and Scheiter, 2012).

DVMs generally combine biogeochemistry, ecophysiology, demography and disturbance submodels. Disturbance is often limited to wildfires, but implementations for land-use changes, pests and hurricanes also exist. DVMs usually “spin up” their simulations from bare ground to “equilibrium” vegetation

to establish realistic initial values for their various "pools". Alternatively, they can also be started from prescribed initial conditions. The model used in this dissertation, Lund-Potsdam-Jena General Ecosystem Simulator (LPJ-GUESS: Smith et al., 2001; Sitch et al., 2003; Gerten et al., 2004), uses spin-up approach in its simulations and simulates the potential natural vegetation (i.e. does not include anthropogenic land-use changes). More details regarding this model are given in the following chapters.

In DVMs, the simulated units are usually Plant Functional Types (PFTs). The PFT concept is used to reduce the complexity in ecosystem modelling and is built on the similarities that plants show in their resource use and response to environmental changes. PFT parameters are distinguished according to the morphology, physiology and life history traits of plants, and are determined by field/laboratory measurements when possible. Then, the dynamics of a particular set of PFTs would be simulated according to these parameters, under a given input dataset including climatic variables (temperature, precipitation, insolation), soil type and atmospheric CO_2 concentration.

There are several important issues that needs to be considered while working with DVMs. First, these models are usually developed and tested for a particular system (e.g. temperate forests) or for reproducing global vegetation patterns. As a result, their PFTs and parameters, and even processes, could be tuned for increasing their predictive performance for such settings. Therefore, they need to be validated for the study system (in this case tropical systems) if it is different from the original development and validation system. Second, as these models are mainly developed for reproducing regional or global patterns, they accept gridded input datasets and they produce gridded outputs on the same spatial resolution as their inputs are. In other words, the model spatial resolution is contingent upon the spatial resolution of its inputs. However, spatial resolutions of gridded input datasets are often on the order of 100 km (as in one side of a square grid) if not coarser. Whereas, simulating East African vegetation (and other systems with similar topographical and climatological complexity) would require finer resolutions than that, as the topographical and climatological features change within distances as short as 10-20 km. Besides, if the model outputs are

considered to be compared to point-scale data such as pollen, finer simulation resolutions are expected to provide a better comparison scale with such data. Finally, both the model parameters and drivers include uncertainties. Therefore, the model predictions should be interpreted accordingly, and these uncertainties should be investigated and reported along with the model predictions.

1.4 Objectives

This dissertation aims to understand the transient East African vegetation dynamics through mechanistic process-based model simulations while filling the methodological gaps. The main objectives of this project are:

1. Validating a widely-used dynamic vegetation model in East Africa and testing its performance against observations at different spatial resolutions.
2. Understanding the responses of East African vegetation during the African Humid Period and its interaction with climate and hydrology.
3. Comparison of drivers in the past and present, and understanding their relative importance at different periods.
4. Investigating the influence of topographical changes on region's climatic and ecological fluctuations.
5. Understanding the sensitivity of East African vegetation to climate variability and quantifying uncertainties related to future interannual climate change and variability.

Chapters 2 through 4 address these objectives as independent studies published in peer-reviewed journals. Chapter 2, „High-resolution modelling closes the gap between data and model simulations for Mid-Holocene and present-day biomes of East Africa“, by Istem Fer, Britta Tietjen and Florian Jeltsch, addresses research objectives 1 to 3 and has been published in Palaeogeography, Palaeoclimatology, Palaeoecology (doi: 10.1016/j.palaeo.2015.12.001). Research objective 3 is addressed in Chapter 3, „Modelling vegetation change during Late Cenozoic

uplift of the East African plateaus“, by Istem Fer Britta Tietjen, Florian Jeltsch and Martin H. Trauth and has also been published in Palaeogeography, Palaeoclimatology, Palaeoecology (doi: 10.1016/j.palaeo.2016.04.007). Chapter 4 addresses research objective 5 and is titled „Influence of El Niño-Southern Oscillation regimes on East African vegetation and its future implications under RCP 8.5 warming scenario“ which is published in the journal EGU Biogeosciences (doi: 10.5194/bg-14-4355-2017).

1.5 References

Ahlström, A., Raupach, M. R., Schurgers, G., Smith, B., Arneth, A., Jung, M.,Reichstein, M., Canadell, J. G., Friedlingstein, P., Jain, A. K., Kato, E., Poulter, P., Sitch, S., Stocker, B. D., Viovy, N., Wang, Y. P., Wiltshire, A., Zaehle, S., Zeng, N., 2015, The dominant role of semi-arid ecosystems in the trend and variability of the land CO_2 sink, Science, 348(6237), 895-899. dx.doi.org/10.1126/science.aaa1668

Allen, J. R. M., Hickler, T., Singarayer, J. S., Sykes, M. T., Valdes, P. J., Huntley, B., 2010. Last glacial vegetation of northern Eurasia. Quaternary Science Reviews. 29, 2604-2618. http://dx.doi.org/10.1016/j.quascirev.2010.05.031

Bobe, R. (2006): The evolution of arid ecosystems in eastern Africa, Journal of Arid Environments, 66, 564-584.

Cowlings, S. A., Cox, P. M., Jones, C. D., Maslin, M. A., Peros, M. and Spall, S. A., 2008, Simulated glacial and interglacial vegetation across Africa: implications for species phylogenies and trans-African migration of plants and animals. Global Change Biology, 14: 827–840.

http://dx.doi.org/10.1111/j.1365-2486.2007.01524.x

Friedlingstein, P., M. Meinshausen, V.K. Arora, C.D. Jones, A. Anav, S.K. Liddicoat, and R. Knutti, 2014, Uncertainties in CMIP5 Climate Projections due to Carbon Cycle Feedbacks. J. Climate, **27**, 511–526,

https://doi.org/10.1175/JCLI-D-12-00579.1

Garcin, Y., Vincens, A., Williamson, D., Guiot, J., Buchet, G., 2006, Wet phases in tropical southern Africa during the last glacial period, Geophysical Research Letters, 33(7), dx.doi.org/10.1029/2005GL025531

Gerten, D., Schaphoff, S., Haberlandt, U., Lucht, W., Sitch, S., 2004. Terrestrial vegetation and water balance – hydrological evaluation of a dynamic global vegetation model. Journal of Hydrology, 286, 249–270. http://dx.doi.org/10.1016/j.jhydrol.2003.09.029

Henrot, A. -J., Utescher, T., Erdei, B., Dury, M., Hamon, N., Ramstein, G., Krapp, M., Herold, N., Goldner, A., Favre, E., Munhoven, G., François, L., 2017, Middle Miocene climate and vegetation models and their validation with proxy data, Palaeogeography, Palaeoclimatology, Palaeoecology, 467, 95-119.

https://doi.org/10.1016/j.palaeo.2016.05.026

Hickler, T., Vohland, K., Freehan, J., Miller, P. A., Smith, B., Costa, L., Giesecke, T., Fronzek, S., Carter, T. R., Cramer W., Kühn, I., Sykes, M. T., 2012. Projecting the future distribution of European potential natural vegetation zones with a generalized, tree species-based dynamic vegetation model. Global Ecology and Biogeography. 21, 50-63.

http://dx.doi.org/10.1111/j.1466-8238.2010.00613.x

Higgins, S.I., Scheiter, S., 2012, Atmospheric CO2 forces abrupt vegetation shifts locally, but not globally, Nature, 488, 209-212, http://dx.doi.org/10.1038/nature11238

Junginger, A., Roller, S., Olaka, L.A., Trauth, M.H., 2014, The effects of solar irradiation changes on the migration of the Congo Air Boundary and water levels of paleo-Lake Suguta, Northern Kenya Rift, during the African Humid Period (15–5ka BP), Palaeogeography, Palaeoclimatology, Palaeoecology, 396, 1-16, https://doi.org/10.1016/j.palaeo.2013.12.007

Kingston, J.D., 2007, Shifting adaptive landscapes: progress and challenges in reconstructing early Hominid environments, Yearbook of Physical Anthropology, 50:20-58. dx.doi.org/10.1002/ajpa.20733

Lau, K.M., Yang, S. (2002): Walker Circulation in: Encyclopedia of Atmospheric Sciences, edited by: Holton, J., Pyle, J. P., and Curry, J., 2505–2509, Academic, San Diego, Calif.

Lovett J.C., Wasser S.K., 1993. Biogeography and Ecology of the Rainforests

of Eastern Africa. Cambridge: Cambridge University Press.

Macgregor, D., 2015. History of the development of the East African Rift System: A series of interpreted maps through time. Journal of African Earth Sciences 101, 232-252. http://dx.doi.org/10.1016/j.jafrearsci.2014.09.016

Maslin, M.A., Brierley, C.M., Milner, A.M., Shultz, S., Trauth, M.H., Wilson, K.E., 2014. East African climate pulses and early human evolution, commissioned review paper. Quaternary Science Reviews, 101, 1-17. http://dx.doi.org/10.1016/j.quascirev.2014.06.012

Monserud, R. A., Denissenko, O. V., Tchebakova, N. M., 1993, Comparison of Siberian paleovegetation to current and future vegetation under climate change, Climate Research, 3-3, 143-159

http://www.jstor.org/stable/24863391

Nicholson, S.E., 2000, The nature of rainfall variability over Africa on time scales of decades to millennia, Global Planet Change, 26, 137–158. https://doi.org/10.1016/S0921-8181(00)00040-0

Oleson, K.W., D.M. Lawrence, G.B. Bonan, M.G. Flanner, E. Kluzek, P.J. Lawrence, S. Levis, S.C. Swenson, P.E. Thornton, A. Dai, M. Decker, R. Dickinson, J. Feddema, C.L. Heald, F. Hoffman, J.-F. Lamarque, N. Mahowald, G.-Y. Niu, T. Qian, J. Randerson, S. Running, K. Sakaguchi, A. Slater, R. Stockli, A. Wang, Z.-L. Yang, Xi. Zeng, and Xu. Zeng, 2010: Technical Description of version 4.0 of the Community Land Model (CLM). NCAR Technical Note NCAR/TN-478+STR, National Center for Atmospheric Research, Boulder, CO, 257 pp.

Peyron, O., Jolly, D., Bonnefille, R., Vincens, A., Guiot, J., 2000, Climate of East Africa 6000 ^{14}C yr B.P., as inferred from pollen data, *Quaternary Research*, 54, 90– 101.

https://doi.org/10.1006/qres.2000.2136

Potts, R., 1998, Environmental hypotheses of Hominin evolution, Yearbook of Physical Anthropology, 41:93-136.

Poulter, B., Frank, D., Ciais, P., Myneni, R. B., Andela, N., Bi, J., Broquet, G., Canadell, J. G., Chevallier, F., Liu, Y. Y., Running, S. W., Sitch, S., van der Werf, G., 2014, Contribution of semi-arid ecosystems to interannual variability of global carbon cycle, Nature, 509, 600-603, dx.doi.org/10.1038/nature13376

Schreck, C. J. and Semazzi, F. H. M., 2004, Variability of the re- cent climate of East Africa, Int. J. Climatol., 24, 681–701,

https://doi.org/10.1002/joc.1019

Sepulchre, P., Ramstein, G., Fluteau, F., Schuster, M., Tiercelin, J.-J., Brunet, M., 2006. Tectonic uplift and eastern Africa aridification. Science 313, 1419–1423.

http://dx.doi.org/10.1126/science.1129158.

Shellito, C. J. and Sloan, L. C., 2006, Reconstructing a lost Eocene Paradise, Part II: On the utility of dynamic global vegetation models in pre-Quaternary climate studies, Global and Planetary Change, 50-1, p. 18-32 https://doi.org/10.1016/j.gloplacha.2005.08.002

Sitch, S., Smith, B., Prentice, I.C., Arneth, A., Bondeau, A., Cramer, W., Kaplan, J.O., Levis, S., Lucht, W., Sykes, M.T., Thonicke, K., Venevsky, S., 2003. Evaluation of ecosystem dynamics, plant geography and terrestrial carbon cycling in the LPJ dynamic global vegetation model. Global Change Biology. 9, 161–185.

Smith, B., Prentice, I.C., Sykes, M.T., 2001. Representation of vegetation dynamics in the modelling of terrestrial ecosystems: comparing two contrasting approaches within European climate space. Global Ecology and Biogeography. 10, 621–637.

http://dx.doi.org/10.1046/j.1466-822X.2001.t01-1-00256.x

Tietjen, B., Schlaepfer, D. R., Bradford, J. B., Lauenroth, W. K., Hall, S. A., Duniway, M. C., Hochstrasser, T., Jia, G., Munson, S. M., Pyke, D. A. and Wilson, S. D., 2017, Climate change-induced vegetation shifts lead to more ecological droughts despite projected rainfall increases in many global temperate drylands. Glob Change Biol, 23: 2743–2754. doi:10.1111/gcb.13598

Torres Acosta, V., Schildgen, T. F., Clarke, B. A., Scherler, D., Bookhagen, B.,

Wittmann, H., von Blanckenburg, F., Strecker, M. R., 2015, Effect of vegetation cover on millennial-scale landscape denudation rates in East Africa, Lithosphere, 7-4, p. 408-420. https://doi.org/10.1130/L402.1

Trauth, M.H., Maslin, M.A., Deino, A., Junginger, A., Lesoloyia, M., Odada, E.O., Olago, D.O., Olaka, L., Strecker, M.R., Tiedemann, R. 2010, Human evolution in a variable environment: the amplifier lakes of East Africa, Quaternary Science Reviews.

White, F., 1983, The vegetation of Africa, a descriptive memoir to accompany the UNESCO/AETFAT/UNSO vegetation map of Africa. UNESCO, *Natural Resour. Res*. 20: 1-356.

Chapter 2:

High-resolution modelling closes the gap between data and model simulations for Mid-Holocene and present-day biomes of East Africa

Abstract

East Africa hosts a striking diversity of terrestrial ecosystems, which vary both in space and time due to complex regional topography and a dynamic climate. The structure and functioning of these ecosystems under this environmental setting can be studied with dynamic vegetation models (DVMs) in a spatially explicit way. Yet, regional applications of DVMs to East Africa are rare and a comprehensive validation of such applications is missing. Here, we simulated the present-day and mid-Holocene vegetation of East Africa with the DVM, LPJ-GUESS and we conducted an exhaustive comparison of model outputs with maps of potential modern vegetation distribution, and with pollen records of local change through time. Overall, the model was able to reproduce the observed spatial patterns of East African vegetation. To see whether running the model at higher spatial resolutions (10'x10') contribute to resolve the vegetation distribution better and have a better comparison scale with the observational data (i.e. pollen data), we run the model with coarser spatial resolution (0.5ºx0.5º) for the present-day as well. Both the area- and point-wise comparison showed that a higher spatial resolution allows to better describe spatial vegetation changes induced by the complex topography of East Africa. Our analysis of the difference between modelled mid-Holocene and modern-day vegetation showed that whether a biome shifts to another is best explained by both the amount of change in precipitation it experiences and the amount of precipitation it received originally. We also confirmed that tropical forest biomes were more sensitive to a decrease in precipitation compared to woodland and savanna biomes and that Holocene vegetation changes in East Africa were driven not only by changes in annual precipitation but also by changes in its seasonality.

2.1 Introduction

East Africa hosts a striking diversity of terrestrial ecosystems, ranging from deserts to rainforests and mountainous forests (White, 1983) as a function of its geography and highly variable topography which consists of central and coastal lowlands, elevated plateaus and adjacent rift basins (Pik, 2011). Superimposed on this complex topography, a dynamic system of Atlantic- and Indian Ocean-related air movements (monsoon systems) determine the amount of precipitation and its timing in the region (Tierney et al., 2011). The varied and heterogeneous ecosystems of East Africa are sensitive to the temporal and spatial changes in this environmental setting in terms of structure and functioning, all of which can be studied by predictive tools such as dynamic vegetation models (DVMs) (Cramer et al., 2001). Yet, regional applications of DVMs to East Africa are rare and a comprehensive validation of such applications is missing.

The present-day vegetation of East Africa has been simulated by DVMs as a part of global (Hickler et al., 2006) and continental studies (Jolly et al., 1998a; Scheiter and Higgins, 2009), and even in regional studies (as control runs in Sepulchre et al., 2006; Doherty et al., 2010; Prömmel et al., 2013). However neither of these studies validated their findings specifically and extensively for East Africa, and it is therefore not clear, if they can adequately represent the abrupt changes in biomes induced by the complex topography of the area. In this study, we apply a process-based DVM, LPJ-GUESS (Lund-Potsdam-Jena General Ecosystem Simulator) for East Africa at two different spatial resolutions and compare the resulting biome distributions with vegetation maps as well as with pollen data. LPJ-GUESS is suitable for regional scale studies with its detailed representation of vegetation dynamics (Smith et al., 2001) and has been applied and validated for West Africa before (Hely et al., 2006). However unlike East Africa, West Africa does not have a highly variable topography. Here, we aim to assess if East African biome distribution can be adequately described by low resolution models at it has been done until now, or if a higher resolution significantly improves the representation of vegetation patterns due to the requirement of a spatially detailed approach under the complex climatic and topographic conditions.

In addition, we apply LPJ-GUESS to simulate the mid-Holocene biomes of East Africa. During the early- to mid-Holocene, the higher summer insolation over the Northern Hemisphere due to changes in Earth's orbital parameters caused more heating of the continents and altered the land-sea pressure gradients (Bosmans et al., 2012). This resulted in both intensification and displacement of moisture related air circulations over East Africa, bringing more precipitation to the north-eastern parts of the region (Junginger and Trauth, 2013). Meanwhile the Southern Hemisphere was partly in antiphase, experiencing less insolation and weaker monsoons which decreased the rainfall in south-eastern parts of the region (Castañeda et al., 2007). Our motivations in simulating mid-Holocene biomes are twofold: First, it provides a realistic scenario to test the regional application of LPJ-GUESS under different climatic conditions and understand the vegetation distribution, composition and its response to changing climate in East Africa. Second, for this period, high resolution climate outputs of global climate models (GCMs) to drive DVMs have recently been available. Here, we use the outputs of such an atmosphere-ocean coupled climate model, EC-Earth, which has one of the most sophisticated model parameterizations and highest resolution amongst the GCMs that simulated mid-Holocene so far (Bosmans et al., 2012).

Our approach follows these steps: (i) simulating the potential modern East African vegetation with regional application of LPJ-GUESS, and area- and point-wise validation of the model outputs, (ii) assessing the level of agreement for model-data comparison with different spatial resolutions (iii) reconstructing the mid-Holocene biomes with more detailed representation of the mid-Holocene climate (iv) analysis of the vegetation changes between the two periods and the drivers these changes.

2.2 Methods

Dynamic Vegetation Models (DVMs) are widely accepted model platforms that simulate vegetation response to changing climatic variables and atmospheric CO_2 concentrations for both future (Koca et al., 2006; Doherty et al., 2010; Hickler et al., 2012) and past studies (Jolly et al., 1998a; Hely et al., 2009; Allen et al., 2010, François et al., 2011). In this study we analyze modern and palaeo-vegetation dynamics of East Africa simulated by the DVM, Lund-Potsdam-Jena General

Ecosystem Simulator (LPJ-GUESS). In order to assess the performance of the model in simulating the complex East African vegetation distribution, we first evaluated modern vegetation under modern climate data and compared the outputs with observational data (i.e. vegetation maps, modern pollen data). Afterwards, we simulated the mid-Holocene biomes and compared the outputs with fossil pollen data. Finally, by comparing the vegetation composition and distribution of both periods, we assessed the drivers behind the simulated differences and sensitivity of biomes to changes in precipitation regimes.

2.2.1 LPJ-GUESS Model

LPJ-GUESS is a mechanistic dynamic vegetation model in which ecosystem processes are simulated via explicit equations (Smith et al., 2001; Sitch et al., 2003; Gerten et al., 2004). It has been successfully applied worldwide both regionally and locally (e.g. Koca et al., 2006; Tang and Beckage, 2010; Hickler et al., 2012) and recently to tropical regions (Hely et al., 2006, 2009; Doherty et al., 2010).

LPJ-GUESS consists of communicating submodules, each corresponding to different subsets of ecosystem processes, in order to provide a realistic representation of how the physiological and biophysical components and functions are linked in nature. In the model, the status of the processes is updated in either daily or annual time step. The physiological processes such as photosynthesis and plant respiration are simulated on a daily time step whereas establishment, growth, reproduction, mortality and disturbance are updated annually. Vegetation is represented as a mixture of plant functional types (PFTs), which are characterized by their life-form, phenology, physiology and other biological requirements and limits. Based on descriptions of these ecosystem processes and PFTs, LPJ-GUESS then provides gridded values of outputs of different PFTs (e.g. biomass, leaf area index (LAI) etc.), which can be used to assess the vegetation composition of an ecosystem. The spatial resolution of the outputs depends on the resolution of the inputs. In this study we simulated the vegetation at two different spatial resolutions: 10'x10' (higher) and 0.5ºx0.5º (coarser). Model parameters are provided in the Supplementary Material, Appendix I (for more detailed descriptions of the model structure, its

(biogeochemical) computational background and hydrological updates, see also Smith et al. (2001), Sitch et al. (2003) and Gerten et al. (2004), respectively).

2.2.2 PFT parameterizations and classification rules

LPJ-GUESS requires a list of PFT parameters to simulate the vegetation dynamics. A set of PFTs representing the vegetation of Africa has been parameterized and used in previous studies (Hely et al., 2006; Doherty et al., 2010). Following the previous PFT sets and parameterizations (Hely et al., 2006; Doherty et al., 2010; Allen et al., 2010), with a number of changes, we used twelve PFTs in this study. In order to better represent tropical African biomes, we not only used tropical broadleaved evergreen/raingreen types, but we also split them into shade-tolerant and shade-intolerant types. Together with shade tolerance-intolerance distinction, we assumed shade intolerant trees to be more fire and drought resistant too, in order to distinguish them as savanna-type trees from forest-type trees. (Further details of PFT parameterizations can be seen in the Supplementary Material, Appendix I, Table A1.2 to A1.5)

Classification of the outputs in terms of biomes is necessary in order to be able to compare the simulated vegetation with observational data. Amongst the outputs of the model, LAI provides an important representation of canopy structure and vegetation composition (ranging from 0 in bare soil to 7 in dense evergreen forests). Therefore, the resulting composition of annual LAI (averaged over the entire 111 years of simulation) was used to classify the corresponding biome of each grid cell according to a set of assignment rules (Table 1.1). As starting point for these rules we used comparable studies for West Africa (Hely et al., 2006, 2009) and East Africa (Doherty et al., 2010). Then, we determined the final set of assignment rules by calibrating them to five East African study sites, for which biome classification according to modern pollen data (see section 2.3) and White's vegetation map (see section 2.4) were in agreement.

Table 2.1. Biome classification rules. Rules are based on total leaf area index (LAI) and proportions of LAIs of different plant functional types (PFT) and **are applied in the given order** to classify biomes.

Rules	**Biome**
(1): If (MNE LAI >0.01 or MBS LAI > 0.01) and C3CG LAI > 2.0	XERO
(2): If TeNE LAI > 0.01 or TeBE LAI > 0.1 TeBS LAI > 0.1	AFRO
(3): If Tot. LAI >= 6.0 and woody LAI >=5.0 and TrBE is the dominant PFT	TEFO
(5): If Tot. LAI > 5.0 and woody LAI> =4.0	TSFO
(5): If Tot. LAI > 2.5 and woody LAI> =1.5	WOOD
(6): If Tot. LAI > 0.5 and woody LAI > 0	SAVA
(7): If Tot. LAI >= 0.1	STEP
(8): If Tot. LAI < 0.1	Bare Soil

XERO=Afroalpine, AFRO=Afromontane, TEFO=Tropical Evergreen Forest, TSFO=Tropical Seasonal Forest, WOOD=Woodland, SAVA=Savanna, STEP=Steppe, MNE=Mountainous Needle-leaved Evergreen, MBS=Mountainous Broad-leaved Summergreen, C3CG=Cold C3 Grass, TeNE=Temperate Needle-leaved Evergreen, TeBE=Temperate Broad-leaved Evergreen, TrBE=Tropical (Shade-tolerant) Broad-leaved Evergreen.

2.2.2 Climate data and Downscaling

LPJ-GUESS requires climate data (gridded monthly values of temperature (°C), precipitation (mm) and cloud cover (%), atmospheric CO_2 concentration and soil type data as an input. For modern climate, we used the Climate Research Unit (CRU) time series dataset CRU TS3.20 at 0.5° spatial resolution, spanning 1901-2011 (Harris et al., 2014). For mid-Holocene climate, we used data from atmosphere-ocean coupled climate model, EC-Earth at 1.125° spatial resolution (Bosmans et al., 2012, for monthly temperature and precipitation anomaly maps see supplementary Figure A3. 1 and A3.2 respectively). For present-day run we used the atmospheric CO_2 concentration data compiled by NASA (GISS Website, last accessed November 2015) from 1901 (296 ppm) to 2011 (390 ppm), and for the mid-Holocene run, we fixed the value to 280 ppm.

As the topography of the region can change in very short distances, we downscaled the climate data in order to resolve the vegetation distribution better and have a better comparison scale with the observational data (i.e. pollen data). To do this, we followed the method given in Tang and Beckage (2010). For the

modern climate data, we first calculated the lapse rate of each grid cell by fitting a regression model to the 0.5° CRU TS3.20 climate dataset that treats the climatic value at each grid cell as a function of its latitude, longitude and elevation. Then we targeted a finer 10'x10' resolution elevation dataset and interpolated the coarser resolution climate values using the lapse rates.

For the mid-Holocene climate data, in order to eliminate model biases, we first calculated the anomalies between pre-industrial and mid-Holocene climate data that were simulated by EC-Earth model (for temperature the differences, and for precipitation and cloud cover the percentages of changes are calculated). Then, these anomalies were downscaled on the same finer 10'x10' resolution as explained above and added to the monthly time series of modern climate data in order to obtain the interannual variability.

2.2.3 Pollen data and biomization

In this study pollen data was used for calibration of the classification rules, and for comparison of modern simulations and paleo-simulations at point scale. Both modern and fossil pollen data were obtained from the African Pollen Database (APD, last accessed February 2015). Pollen data, consist of pollen counts of identified taxa and each needs to be assigned to a biome so that the pollen record can be comparable with the simulated biomes. The pollen data and taxa from East Africa have been biomized extensively by previous studies (Jolly et al., 1998b; Peyron et al., 2000; Elenga et al., 2000; Mumbi et al., 2008; Lebamba et al., 2009, Vincens et al., 2006, 2010). As biomization of the pollen data was not the main focus of this study, we followed these earlier studies and constructed a 'taxon x biome' matrix, by assigning each taxon to the biomes (see Supplementary Material, Appendix II), based on their known biology, ecology and physiology. Finally, we assigned the pollen samples to a biome by calculating the affinity scores as described in Prentice et al. (1996). For the 'taxon x biome' matrix used in calculating the affinity scores and the assigned biomes to pollen sites, see Supplementary Material, Appendix II. In total, we used modern-day pollen spectra from 135 samples from East Africa. Thereof, five used for calibration of the classification rules, and 130 were used for comparison with the simulated modern biomes. In addition, fifteen of these 130 samples also provide fossil

pollen-derived records of vegetation change between the mid-Holocene (6000 yr BP) and today.

2.2.4 Map Comparison: Vegetation Maps and Kappa Statistics

For the validation of the model at regional scale we used White's Vegetation map (White, 1983; Figure 1a) as it is considered to be the closest vegetation map to the potential natural vegetation (PNV) of Africa and has been widely used for validation of vegetation model outputs for Africa (Hely et al., 2006, 2009; Scheiter and Higgins, 2009). To be able to compare the map with our model outputs, different biome classifications of White's vegetation map were aggregated into new classes (see Supplementary Material, Appendix III, Table A3.1). These new classes were comparable with the reconstructed biomes from pollen data and eight types of simulated biomes by LPJ-GUESS, namely, desert (or bare soil), steppe, savanna, woodland, seasonal forest, evergreen forest, afromontane and afroalpine. Additionally, we also compared our present-day simulation results with a satellite derived Global Land Cover 2000 Map (GLC2000, Mayaux et al., 2004), although GLC2000 was also classifying anthropogenically altered areas such as urban areas and croplands. As LPJ-GUESS simulates the PNV only, these areas were masked out for both maps in the comparison step and the remaining classes were aggregated into new classes (see Supplementary Material, Appendix III, Table A3.2). Also, in GLC2000, it was not possible to make a distinction between afromontane and afroalpine biomes. Therefore, while comparing LPJ-GUESS and GLC2000 we combined afroalpine biomes simulated by LPJ-GUESS together with the afromontane biomes, resulting in seven biome types for comparison.

To compare the simulated and observational maps in pairs, we used Kappa statistics as described by Prentice et al. (1992), and Monserud and Leemans (1992) to compute the level of agreement. With kappa statistics it is possible to compare two maps grid by grid with ruling out the agreement due to chance. When the value is close to zero, the agreement is no better than expected by chance. When it approaches to one, it suggests an excellent agreement. The comparisons between model outputs and vegetation maps were conducted at the resolution of LPJ-GUESS' outputs (10' x 10'), therefore vegetation maps with

higher resolution were first clipped to a subset of East Africa (25° E to 50° E, 12° N to 12° S) and then re-sampled at their nearest neighbour grid points to match the ones of LPJ-GUESS.

2.3 Results and Discussion

2.3.1 Present-day simulations

The simulated potential natural vegetation (PNV) distribution by LPJ-GUESS under present-day climatic conditions mainly shows dry steppe biome types in the northeastern parts, evergreen and seasonal forest biome types in the central tropical Africa region, mountainous biome types along the elevated areas of the rift system and savanna-woodland biomes in the remaining areas (Figure 2.1b).

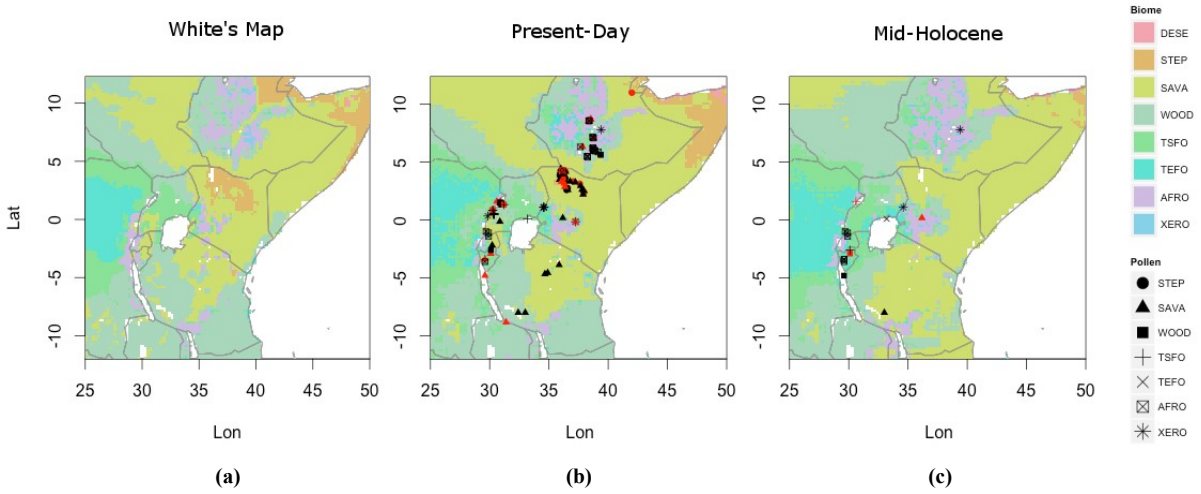

Figure 2.1. Biome distributions of East Africa. a) White's vegetation map, b) Present-day, and c) Mid-Holocene biomes simulated by LPJ-GUESS. Each color represents a different biome whereas white areas represents the masked-out water bodies. Smaller icons show the locations of pollen sites and the reconstructed biome from the pollen data. Where the icon is black, the biome derived from the pollen data agrees with the simulated biome; the icon is red where it does not.

XERO=Afroalpine, AFRO=Afromontane, TEFO=Tropical Evergreen Forest, TSFO=Tropical Seasonal Forest, WOOD=Woodland, SAVA=Savanna, STEP=Steppe, DESE=Desert

In order to asses the model performance for East Africa, we compared the simulated modern biomes grid by grid with two different observational vegetation maps (White's vegetation map and GLC2000). However, as they use different approaches and classification criteria, these vegetation maps differ in the biomes they represent and their distribution, and it was not always possible to match the corresponding biomes in each map. Thus, even the direct comparison between these two observational vegetation maps does not yield a one-to-one correspondence for East Africa, and in fact, their agreement was the lowest amongst others (fair: $0.4 < \kappa < 0.55$, Table 2.2). The accuracy assessment between GLC2000 and LPJ-GUESS also presented a fair agreement, while the agreement between White's vegetation map and LPJ-GUESS was higher on the level of agreement (good: $0.55 < \kappa < 0.7$, Table 2.2). The level of agreement with White's vegetation map of Africa (White, 1983) was also higher than it was in the continental study of Scheiter and Higgins (2009). A reason for this can be the higher spatial resolution and the better resolved vegetation patterns produced in this study. Another reason might be that as this is a regional study, our biome classification rules are more suitable for representing East African biomes. A third reason might simply be the different performance of the two dynamic vegetation models (DVMs) that were applied in the studies. Furthermore, the level of agreement with White's vegetation map in our study was only slightly lower than it was in the regional West African study of Hely et al. (2006), although their study region was especially selected for its relatively low variability in elevation which increases the predictive performance of the DVM.

The existence of transitional zones (heterogeneous areas with a continuum of vegetation that are difficult to classify in discrete biome categories, e.g. forest-woodland and woodland-savanna transitions), as it is the case in East Africa, tend to reduce the agreement between vegetation maps and simulated biomes (Hickler et al., 2006). Therefore, running the model at higher spatial resolution is expected to lead to a higher number of potentially disagreeing grid cells in such zones, and a reduced level of agreement. We run the model with coarser spatial resolution (0.5ºx0.5º grids) for the present-day in addition to our higher (10'x10' grids) resolution run and compared it with White's vegetation map. Contrary to expectations, we obtained no decrease in the level of agreement in such areas (Table 22.). Furthermore, our results show that, the high resolution simulation was

indeed able to resolve the evergreen forest and mountainous biomes of the region better, resulting in an even improved accuracy of simulated patterns of vegetation.

Table 2.2. Accuracy assessments between simulated map and vegetation maps. See the methods for the level of agreement classes.

	LPJ-GUESS vs. GLC2000		**LPJ-GUESS vs. White's map (10' x 10')**		**LPJ-GUESS vs. White's map (0.5º x 0.5º)**		**GLC2000 vs. White's map**	
Biomes	KIA		KIA		KIA		KIA	
Bare Soil	0.13		0.03		0		0.03	
Steppe	0.30		0.44		0.47		0.26	
Savanna	0.47		0.66		0.65		0.44	
Woodland	0.53		0.62		0.62		0.52	
Seasonal F.	0.36		0.50		0.49		0.34	
Evergreen F.	0.58		0.60		0.51		0.72	
Afromontane	0.31		0.62		0.53		0.36	
Afroalpine	-		0.49		0		-	
Overall	α	κ	α	κ	α	κ	α	κ
	0.56	0.44	0.71	0.60	0.70	0.59	0.57	0.43
#	12208		15864		1812		12147	

KIA = Kappa Index of agreement per biome; κ = Generalized Kappa value, α = the proportion of correctly classified cells; # = number of grid cells to compare (without the masked out cells). Levels of agreement: <0.4 poor, 0.4-0.55 fair, 0.55-0.7 good, 0.7-0.85 very good, >0.85 excellent (Monserud and Leemans,1992).

For present-day simulations, we additionally compared the model results (both higher -10'x10'- and lower -0.5ºx0.5º- resolutions) and White's vegetation map to modern pollen data (Table 2.3). This allowed us to (i) evaluate the comparability between biomized pollen data, the vegetation map and the simulated biomes, (ii) assess the level of agreement between the simulations and the pollen data at different spatial resolutions. Although the former exercise was not the main focus of this study, it was a necessary step before proceeding with the mid-Holocene simulations to show that biomes derived from pollen data can be used in model-data comparison independently for paleo-simulations where we only have fossil pollen data to compare our model outputs with. 97 out of 130 biomized pollen samples were in exact agreement with the simulated biomes (at 10'x10' resolution), while this number was 89 for the comparison with White's vegetation map (Table 2.3). The majority of the simulated biomes and White's classes were correctly assigned to the pollen derived biomes with the highest mismatch for savannas (Table 2.3). However, in this point-wise comparison there were not more

disagreements between model output and the pollen records than disagreements between the model output and the vegetation map, or between the vegetation map and the pollen data. These discrepancies in the comparison of the model outputs and vegetation map to the pollen records are expected because pollen data are point-wise and they can capture sub-scale spatial distribution of vegetation rather than the larger spatial scale of our grid cells. Ultimately, we found this point-wise comparison to be viable and used it for paleo-simulations as well. Moreover, the comparison of the modern pollen data with coarser (0.5ºx0.5º) simulations of the present-day biomes showed only 65 agreements out of 130 samples. The main importance of running the simulations at higher resolution manifested itself here. This finding clearly demonstrates that a higher the resolution leads to a better point-wise comparison, since model simulations can better capture site-specific characteristics.

Table 2.3. Numerical comparison between pollen derived and simulated biomes, and White's vegetation map classes. Each cell shows how well the pollen-derived (P) distribution of vegetation biomes (left column) correspond with the biomes inferred for those sites on White's vegetation map (W), and 10'x10' (high-resolution, H) or 0.5°x0.5° (low-resolution, L) present-day simulations with LPJ-GUESS. The bold numbers in the diagonal show the number of samples with exact agreement between P, and W, H and L for that particular biome.

W&H&L / P	XERO			AFRO			TEFO			TSFO			WOOD			SAVA			STEP			Exact agreement		
	W	H	L	W	H	L	W	H	L	W	H	L	W	H	L	W	H	L	W	H	L	W	H	L
XERO (7)	**7**	**7**	**-**	-	-	6				-	-	1												
AFRO (25)	1	1	-	**19**	**23**	**18**				-	-	2	1	-	4	-	1	1	4	-	-			
TEFO (0)																								
TSFO (14)				1	-	-	-	1	1	**13**	**13**	**1**	-	-	12									
WOOD (13)										3	3	-	**9**	**10**	**13**	1	-	-						
SAVA (42)				5	6	6	1	-	1	1	1	1	10	8	10	**14**	**24**	**21**	12	3	3			
STEP (29)																2	9	17	**27**	**20**	**12**			
Total (130)																						**89**	**97**	**65**

2.3.2 Mid-Holocene simulations

In our study we also simulated the mid-Holocene biomes of East Africa. The main differences between the simulated mid-Holocene (Figure 2.1c) and simulated modern vegetation of East Africa (Figure 2.1b) were as follows: (i) During the mid-Holocene, the afromontane biomes were extended in area with respect to their present-day distribution, (ii) the steppe biomes in the northeastern, savanna biomes in the northern part of East Africa were covering less area, (iii) in the southeastern-most part of our study region, savanna biomes were more extended during the mid-Holocene at the expense of woodland biomes. We have chosen 15 pollen sites such that they contain both mid-Holocene and modern pollen samples (Supplementary material, Appendix II). 12 out of 15 of these fossil pollen sites showed exact agreement with our mid-Holocene simulations. However, they do not fully capture the simulated differences in palaeo-vegetation with respect to present-day. Therefore we included comparison with available proxy records compiled by previous studies as well.

Extension of afromontane biomes

Two of the 15 sites that record both mid-Holocene and modern pollen samples (Rusaka and Kashiru) were biomized as afromontane biome for mid-Holocene while they no longer represent a mountainous biome today, which is in agreement with our simulations. As pollen samples are usually available from the elevated rift regions (where the lakes to preserve them are present), unsurprisingly most of them record afromontane biomes for both periods (Ahakagyezi, Rugezi, Mubwindi, Kuruyange, Koitoboss, Badda). Peyron et al. (2000) also reconstructed largely mountainous biomes around the rift vicinity.

Extension of biomes with more closed vegetation

We simulated extension of biomes with more closed vegetation during the mid-Holocene, mostly in the northern parts of the region. Samples from five of the pollen sites that record both mid-Holocene and modern pollen samples (Tanganyika, Pilkington, Ndrumu, Albert, Nyamuswaga) were assigned to biomes with more closed vegetation for mid-Holocene and biomes with more open vegetation for present-day conditions, supporting our simulations. Among these five sites, Tanganyika has a relatively southern location, and it extends from

latitude 3.20º S to 8.45 º S. While its northern end is well situated in the region where we simulated biome shifts towards more closed vegetation, its southern end is close to the transition zone between the northern and southern hemisphere patterns. Still, Tanganyika records (plant leaf waxes: Tierney e al., 2010) indicate humid conditions during the mid-Holocene.

Extension of biomes with more open vegetation

In our mid-Holocene simulation, an expansion of savanna biomes at the expense of woodlands was simulated. However, none of the pollen data used in our study records a more open vegetation in the mid-Holocene and a more closed vegetation in the present-day at the same site. This is because there is not much fossil pollen data from the southeastern-most parts of our study region that is simulated to have experienced drier conditions during the mid-Holocene. The only fossil pollen data situated near these parts was from Lake Rukwa (8º S, 33º E, 793 m a.s.l.) and this site has been biomized and simulated as savanna for both present-day and mid-Holocene in our study. A more detailed analysis of this fossil pollen data was given in Vincens et al. (2005) and it has been interpreted to record wetter conditions during the mid-Holocene as Tanganyika. However, a pollen data from Lake Masoko (which has a relatively more south-eastern location in our study area: 9.20º S, 33.45º E, 840 m a.s.l.) that was analyzed in detail by Garcin et al. (2006) records drier conditions during the mid-Holocene with respect to present-day, agreeing with our simulations. Another pollen record from Lake Malawi (south of 10º S), analyzed by deBusk (1998) suggests slightly drier conditions during mid-Holocene for Lake Malawi catchment. In addition to pollen, molecular isotopic records from Lake Malawi also indicate a drier early- to mid-Holocene and a wetter mid- to late-Holocene, although these records suggest an earlier mid-Holocene transition than 6000 ka (Castañeda et al., 2009). Moreover, carbon isotopic composition of fossil plant leaf waxes (Sinninghe-Damsté et al., 2011), and branched and isoprenoid tetraether index (Verschuren et al., 2009), from Lake Challa (3.19º S, 37.42º E, 880 m a.s.l.) indicate wetter conditions in the late Holocene than the mid-Holocene on average for the southeastern most parts of our study area.

2.3.3 Vegetation changes from mid-Holocene to present-day

After simulating both the present-day and mid-Holocene vegetation of East Africa, we conducted an analysis concentrating on the precipitation and temperature differences between these periods in order to understand which variables drove the biome shifts from mid-Holocene to the present-day. As expected, the main driver of the simulated shifts from mountainous biomes (afroalpine, afromontane) to non-mountainous biomes (steppe, savanna, woodland and forest biomes) was the increase in temperature from mid-Holocene to present-day. The monthly anomaly maps for temperature climatology (supplementary Figure A3. 1) indeed show higher present-day values in the vicinity of the elevated rift shoulders where the afromontane biomes occur (except for the JAS months). In this aspect, the simulated climate by Bosmans et al. (2012) agrees with the previous pollen-based reconstructions of cooler mid-Holocene temperatures in equatorial Africa (Bartlein et al, 2011).

For the shifts occurred within non-mountainous biomes, change in precipitation regime was the main driver. The monthly anomaly maps for precipitation climatology (supplementary Figure A3. 2) show that the spatial and temporal distribution of precipitation changes were not the same over the study region resulting in two types of shifts occurring from mid-Holocene to present-day, namely, (i) biomes shifting from more open (hence, lower LAI) to more closed (hence, higher LAI) vegetation: savanna to woodland, woodland to seasonal forest, seasonal to evergreen forest, and (ii) biomes shifting from more closed to more open vegetation: evergreen to seasonal forest, seasonal forest to woodland, woodland to savanna, savanna to steppe, steppe to desert (Figure 2.2). We applied a logistic regression analysis to assess which environmental variables help us explain these shifts occurring from mid-Holocene to present-day (detailed outputs of the regression analysis are given in Appendix 3, TableA3.3). When the biome was a savanna or woodland, the change in mean annual precipitation (MAP) is the main driver in whether the biome shifts to another or remains the same in a particular grid cell. When the biome was a seasonal or an evergreen forest, the MAP of the site during the mid-Holocene is more explanatory.

A same percentage of change in MAP may or may not cause a shift depending on the MAP amount of the site during the mid-Holocene in which the biome might generally be found. As tropical forest ecosystems of East Africa cover wider span in the MAP domain (~1500<MAP<3000 mm year^{-1}) compared to woodlands (~1000<MAP<1500 mm year^{-1}) and savannas (~250<MAP<1000 mm year^{-1}), the MAP of the site during the mid-Holocene becomes more relevant for explaining the shifts occurred from tropical forest biomes. Overall, the shifts were distinguished better under the combination of these two variables, and were plotted accordingly in this space as given in Figure 2.2. In the case of a biome shift towards more open vegetation (Figure 2.2b), based on the percentage of decrease in MAP necessary to shift from one biome to a drier one, forest biomes were more sensitive compared to woodland and savanna biomes, which is in agreement with the findings of Hely et al. (2006) for their study of West African biomes. It is interesting to note the shifts from seasonal to evergreen forest biomes (Figure 2.2a), although the MAP is decreasing from mid-Holocene to present-day. These sites were receiving enough precipitation to be an evergreen forest during the mid-Holocene, and even though their MAP decreased they are still receiving enough precipitation today. The reason behind the shifts from seasonal to evergreen forests is the higher atmospheric CO_2 concentrations today and resulting increase in woody vegetation due to enhanced photosynthesis and improved water use efficiency which in return increases productivity and vegetation growth (fertilization effect) in vegetation models (Hickler et al., 2008). When we look at the opposite shift (from evergreen to seasonal forest, Figure 2.2b), again we see that MAP is decreasing from mid-Holocene to present-day. Even though these sites also receive enough MAP to be an evergreen forest for both periods and the fertilization effect of increasing atmospheric CO_2 from mid-Holocene to present-day on woody vegetation still applies, the decrease in the length of wet season (< 8 months) prevents these sites to be an evergreen forest biome today. This finding demonstrate how the vegetation changes recorded during the Holocene in East Africa can be explained not only by changes in annual precipitation but also by changes in seasonality as suggested by previous sensitivity experiments (Hely et al.,2006; Gritti et al., 2010).

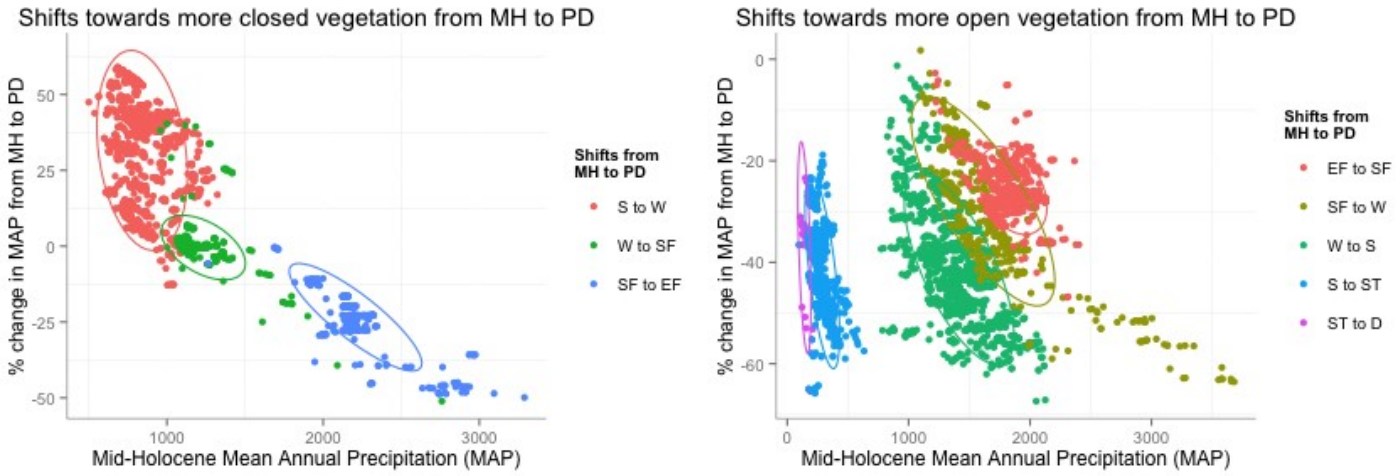

(a) **(b)**

Figure 2.2. Biome shifts from Mid-Holocene (MH) to Present-day (PD) in non-mountainous biomes: a) towards closed vegetation, b) towards open vegetation. Every data point represents a grid point site in our study area that was a different biome during the mid-Holocene and shifted to another today according to our simulations for these two periods. The ellipses indicate the concentration of 90% of sites for each group.

S to W = Savanna to Woodland, W to SF= Woodland to Seasonal Forest, SF to EF= Seasonal to Evergreen Forest, EF to SF= Evergreen to Seasonal Forest, SF to W=Seasonal Forest to Woodland, W to S= Woodland to Savanna, S to ST= Savanna to Steppe, ST to D= Steppe to Desert.

2.4 Conclusion

In our study, we have not only reproduced the past and present spatial patterns of the vegetation as suggested by the observational data, but also assessed the vegetation response and sensitivity to changing climate in East Africa in detail. Instead of focusing on specific locations, we included every grid point over the study region in our sensitivity analysis and confirmed the notion that Holocene vegetation changes in East Africa were driven not only by changes in annual precipitation but also by changes in its seasonality holds at regional scale. By driving a vegetation model with outputs of a high resolution climate model itself and running vegetation simulations at two different spatial resolutions, we clearly demonstrated that using a higher spatial resolution helps to close the gap between proxy data and model simulations, especially for topographically and climatologically complex regions like East Africa where environmental patterns can differ within very short distances. This is of particular concern to

palaeoecological studies where we need more applications of high resolution regional climate models for simulating past climates and for driving vegetation models with their outputs.

2.5 Acknowledgements

This project was funded by DAAD, grants to F. J. and German Research Foundation (DFG) Graduate School GRK1364 program (Shaping Earth's Surface in a Variable Environment – Interactions between tectonics, climate and biosphere in the African-Asian monsoonal region). FJ and BT acknowledge the support by the BMBF in the framework of the OPTIMASS project (01LL1302A and 01LL1302B). We would like to thank J. H. C. Bosmans for sharing the EC-EARTH climate data and Plant Ecology and Nature Conservation Group of Potsdam University for the fruitful discussions. We thank the two anonymous reviewers for their constructive comments.

2.6 References

Allen, J. R. M., Hickler, T., Singarayer, J. S., Sykes, M. T., Valdes, P. J., Huntley, B., 2010. Last glacial vegetation of northern Eurasia. Quaternary Science Reviews. 29, 2604-2618. http://dx.doi.org/10.1016/j.quascirev.2010.05.031

Bartlein, P. J., Harrison, S. P., Brewer, S., Connor, C., Davis, B. A. S., Gajewski, K., Guiot, J., Harrison-Prentice, T. I., Henderson, A., Peyron, O., Prentice, I. C., Scholze, M., Seppä, H., Shuman, B., Sugita, Thompson, R. S., Viau, A. E., Williams, J., Wu, H., 2011. Pollen-based continental climate reconstructions at 6 and 21 ka: a global synthesis. Climate Dynamics. 37(3), 775-802. http://dx.doi.org/10.1007/s00382-010-0904-1

Bosmans, J. H. C., Drijfhout, S. S., Tuenter, E., Lourens, L. J., Hilgen, F. J., Weber, S. L., 2012. Monsoonal response to mid-holocene orbital forcing in a high resolution GCM. Climate of the Past. 8, 723-740. http://dx.doi.org/10.5194/cp-8-723-2012

Castañeda, I. S., Werne, J. P., Johnson, T. C., 2007. Wet and arid phases in the southeast African tropics since the Last Glacial Maximum. Geology. 35(9), 823-826. http://dx.doi.org/10.1130/G23916A.1

Castañeda, I. S., Werne, J. P., Johnson, T. C.,, Filley, T. R., 2009. Late Quaternary vegetation history of southeast Africa: The molecular isotopic record from Lake Malawi. Palaeogeography, Palaeoclimatology, Palaeoecology. 275, 100-112. http://dx.doi.org/10.1016/j.palaeo.2009.02.008

Cramer, W., Bondeau, A., Woodward, F. I., Prentice, I. C., Betts, R. A., Brovkin, V., Cox, P. M., Fisher, V., Foley, J. A., Friend, A. D., Kucharik, C., Lomas, M. R., Ramankutty, N., Sitch, S., Smith, B., White, A., Young-Molling, C., 2001. Global Response of terrestrial ecosystem structure and function to CO_2 and climate change: results from six dynamic vegetation models. Global Change Biology. 7, 357-373. http://dx.doi.org/10.1046/j.1365-2486.2001.00383.x

DeBusk, G. H., 1998. A 37,500-year pollen record from Lake Malawi and implications for the biogeography of afromontane forests. Journal of Biogeography. 25(3), 479-500. http://www.jstor.org/stable/2846091

Doherty, R. M., Sitch, S., Smith, B., Lewis, S. L., Thornton, P. K., 2010. Implications of future climate and atmospheric CO_2 content for regional biogeochemistry, biogeography and ecosystem services across East Africa. Global Change Biology. 16, 617-640. http://dx.doi.org/10.1111/j.1365-2486.2009.01997.x

Elenga, H., Peyron, O., Bonnefille, R., Jolly, D., Cheddadi, R., Guiot, J., Andrieu, V., Bottema, S., Buchet, G., de Beaulieu, J.-L., Hamilton, A. C., Maley, J., Marchant, R., Perez-Obiol, R., Reille, M., Riollet, G., Scott, L., Straka, H., Taylor, D., Van Compo, E., Vincens, A., Laarif, F., Jonson, H., 2000. Pollen-based biome reconstruction for southern Europe and Africa 18,000 yr BP. Journal of Biogeography. 27, 621-634. http://dx.doi.org/10.1046/j.1365-2699.2000.00430.x

François, L., Utescher, T., Favre, E., Henrot, A.-J., Warnant, P., Micheels, A., Erdei, B., Suc, J.-P., Cheddadi, R., Mosbrugger, V., 2011. Modelling Late Miocene vegetation in Europe: Results of the CARAIB model and comparison with palaeovegetation data. Palaeogeography, Palaeoclimatology, Palaeoecology. 304, 359-378. http://dx.doi.org/10.1016/j.palaeo.2011.01.012

Garcin, Y., Vincens, A., Williamson, D., Guiot, J., Buchet, G., 2006. Wet phases in tropical southern Africa during the last glacial period. Geophysical Research Letters. 33, L07703. http://dx.doi.org/10.1029/2005GL025531

Gerten, D., Schaphoff, S., Haberlandt, U., Lucht, W., Sitch, S., 2004. Terrestrial vegetation and water balance – hydrological evaluation of a dynamic global vegetation model. Journal of Hydrology, 286, 249–270.

http://dx.doi.org/10.1016/j.jhydrol.2003.09.029

Gritti, E. S., Cassignat, C., Flores, O., Bonnefille, R., Chalie, F., Guiot, J., Jolly, D., 2010. Simulated effects of a seasonal precipitation change on the vegetation in tropical Africa. Climate of the Past. 6, 169-178. www.clim-past.net/6/169/2010/

Harris, I., Jones, P.D., Osborn, T.J. and Lister, D.H., 2014. Updated high-resolution grids of monthly climatic observations - the CRU TS3.10 dataset. *International Journal of Climatology*. 34, 623-642. http://dx.doi.org/10.1002/joc.3711

Hély, C., Bremond, L., Alleaume, S., Smith, B., Sykes, M.T., Guiot, J., 2006. Sensitivity of African biomes to changes in the precipitation regime. Global Ecology and Biogeography. 15, 258–270. http://dx.doi.org/10.1111/j.1466-822x.2006.00235.x

Hély, C., Braconnot, P., Watrin, J., Zheng, W., 2009. Climate and vegetation: Simulating the African Humid Period. Comptes Rendus Geoscience. 341, 671-688. http://dx.doi.org/10.1016/j.crte.2009.07.002

Hickler, T., Prentice, I. C., Smith, B., Sykes, M. T., Zaehle S., 2006. Implementing plant hydraulic architecture within the LPJ Dynamic Global Vegetation Model. Global Ecology and Biogeography. 15, 567-577. http://dx.doi.org/10.1111/j.1466-8238.2006.00254.x

Hickler, T., Smith, B., Prentice, I. C., Mjöfors, K., Miller, P., Arneth, A., Sykes, M. T., 2008. CO_2 fertilization in temperate FACE experiments not representative of boreal and tropical forests. Global Change Biology. 14, 1531-1542. doi: 10.1111/j.1365-2486.2008.01598.x

Hickler, T., Vohland, K., Freehan, J., Miller, P. A., Smith, B., Costa, L., Giesecke, T., Fronzek, S., Carter, T. R., Cramer W., Kühn, I., Sykes, M. T., 2012. Projecting the future distribution of European potential natural vegetation zones with a generalized, tree species-based dynamic vegetation model. Global Ecology and Biogeography. 21, 50-63. doi: 10.1111/j.1466-8238.2010.00613.x

Jolly, D., Harrison, S. P., Damnati, B., Bonnefille, R., 1998a. Simulated climate and biomes of Africa during the Late Quaternary: Comparison with pollen and lake status data. Quaternary Science Reviews. 17, 629–657. http://dx.doi.org/10.1016/S0277-3791(98)00015-8

Jolly, D., Prentice, I.C., Bonnefille, R., Ballouche, A., Bengo, M., Brenac, P., Buchet, G., Burney, D., Cazet, J.-P., Cheddadi, R., Edorh, T., Elenga, H., Elmoutaki, S., Guiot, J., Laarif, F., Lamb, H., Lezine, A.-M., Maley, J., Mbenza, M., Peyron, O., Reille, M., Reynaud-Farrera, I., Riollet, G., Ritchie, J.C., Roche, E., Scott, L., Ssemmanda, I., Straka, H., Umer, M., Van Campo, E., Vilimumbalo, S., Vincens, A., Waller, M., 1998b. Biome reconstruction from pollen and plant macrofossil data for Africa and the Arabian peninsula at 0 and 6000 years. Journal of Biogeography. 25, 1007–1027. doi: 10.1046/j.1365-2699.1998.00238.x

Junginger, A., Trauth, M. H., 2013. Hydrological constraints of paleo-Lake Suguta in the Northern Kenya Rift during the African Humid Period (15-5 ka BP). Global and Planetary change. 111, 174-188. http://dx.doi.org/10.1016/j.gloplacha.2013.09.005

Koca, D., Smith, B., Sykes, M.T., 2006. Modelling regional climate change effects on Swedish ecosystems. Climatic Change. 78, 381-406. http://dx.doi.org/10.1007/s10584-005-9030-1

Lebamba, J., Ngomanda, A., Vincens, A., Jolly, D., Favier, C., Elenga, H, Bentaleb, I., 2009. Central African biomes and forest succession stages derived from modern pollen data and plant functional types. Climate of the Past. 5, 403-429. http://dx.doi.org/10.5194/cp-5-403-2009

Mayaux, P., Bartholomé, E., Fritz, S., Belward, A., 2004. A new land-cover map of Africa for the year 2000. Journal of Biogeography. 31, 861-877. doi: 10.1111/j.1365-2699.2004.01073.x

Monserud, R.A., Leemans, R., 1992. The comparison of global vegetation maps. Ecological Modelling. 62**,** 275-293. doi: 10.1016/0304-3800(92)90003-W

Mumbi, C. T., Marchant, R., Hooghiemstra, H., Wooller, M. J., 2008. Late Quaternary vegetation reconstruction from the Eastern Arc Mountains, Tanzania. Quaternary Research. 69, 326-341. http://dx.doi.org/10.1016/j.yqres.2007.10.012

Peyron, O., Jolly, D.,Bonnefille, R., Vincens, A., Guiot, J., 2000. Climate of East Africa 6000 14C Yr B.P. as inferred from pollen data. Quaternary Research. 54, 90–101. http://dx.doi.org/10.1006/qres.2000.2136

Pik, R., 2011. East Africa on the rise. Nature Geoscience. 4, 660-661. http://dx.doi.org/10.1038/ngeo1274

Prentice, I.C., Cramer, W., Harrison, S.P., Leemans, R., Monserud, R.A., Solomon, A.M., 1992. A global biome model based on plant physiology and dominance, soil properties and climate. Journal of Biogeography. 19, 117–134. http://dx.doi.org/10.2307/2845499

Prentice, I.C., Guiot, J., Huntley, B., Jolly, D., Cheddadi, R., 1996. Reconstructing biomes from palaeoecological data: a general method and its application to European pollen data at 0 and 6 ka. Climate Dynamics. 12, 185–194. http://dx.doi.org/10.1007/BF00211617

Prömmel, K., Cubasch, U., Kaspar, F., 2013. A regional climate model study of the impact of tectonic and orbital forcing on African precipitation and vegetation. Palaeogeography, Palaeoclimatology, Palaeoecology 369, 154-162. http://dx.doi.org/10.1016/j.palaeo.2012.10.015

Scheiter, S., Higgins, S. I., 2009. Impacts of climate change on the vegetation of Africa: an adaptive dynamic vegetation modelling approach. Global Change Biology. 15, 2224-2246. doi :10.1111/j.1365-2486.2008.01838.x

Sepulchre, P., Ramstein, G., Fluteau, F., Schuster, M., Tiercelin, J.-J., Brunet, M., 2006. Tectonic uplift and eastern Africa aridification. Science 313, 1419–1423. http://dx.doi.org/10.1126/science.1129158.

Sinninghe Damsté, J. S., Verschuren, D., Ossebaar, J., Blokker, J., van Houten, R., van der Meer, M. T. J., Plessen, B., Schouten, S., 2011. A 25,000-year record of climate-induced changes in lowland vegetation of eastern equatorial Africa revealed by the stable carbon-isotopic composition of fossil plant leaf waxes. Earth and Planetary Science Letters. 302, 236-246. http://dx.doi.org/10.1016/j.epsl.2010.12.025

Sitch, S., Smith, B., Prentice, I.C., Arneth, A., Bondeau, A., Cramer, W., Kaplan, J.O., Levis, S., Lucht, W., Sykes, M.T., Thonicke, K., Venevsky, S., 2003. Evaluation of ecosystem dynamics, plant geography and terrestrial carbon cycling in the LPJ dynamic global vegetation model. Global Change Biology. 9, 161–185. doi: 10.1046/j.1365-2486.2003.00569.x

Smith, B., Prentice, I.C., Sykes, M.T., 2001. Representation of vegetation dynamics in the modelling of terrestrial ecosystems: comparing two contrasting approaches within European climate space. Global Ecology and Biogeography. 10, 621–637. doi:10.1046/j.1466-822X.2001.t01-1-00256.x

Tang, G., Beckage, B., 2010. Projecting the distribution of forests in New England in response to climate change. Diversity and Distributions. 16, 144-158. doi:10.1111/j.1472-4642.2009.00628.x

Tierney, J. E., Russell, J. M., Huang, Y., 2010. A molecular perspective on Late Quaternary climate and vegetation change in the Lake Tanganyika basin, East Africa. Quaternary Science Reviews. 29, 787-800. http://dx.doi.org/10.1016/j.quascirev.2009.11.030

Tierney, J. E., Lewis, S. C., Cook, B. I., LeGrande, A. N., Schmidt, G. A., 2011. Model, proxy and isotopic perspectives on the East African Humid Period. Earth and Planetary Science Letters. 307, 103-112. http://dx.doi.org/10.1016/j.epsl.2011.04.038

Verschuren, D., Sinninghe Damsté, J. S., Moernaut, J., Kristen, I., Blaauw, M., Fagot, M., Haug, G. H., CHALLACEA project members, 2009. Half-precessional dynamics of monsoon rainfall near the East African Equator. Nature. 462, 637-641. http://dx.doi.org/10.1038/nature08520

Vincens, A., Buchet, G., Williamson, D., Taieb, M., 2005. A 23,000 yr pollen record from Lake Rukwa (8º S, SW Tanzania): New data on vegetation dynamics and climate in Central Eastern Africa. Review of Palaeobotany and Palynology. 135, 147-162. http://dx.doi.org/10.1016/j.revpalbo.2005.06.001

Vincens, A., Bremond, L., Brewer, S., Buchet, G., Dussouillez, P., 2006. Modern pollen-based biome reconstructions in East Africa expanded to southern Tanzania. Review of Palaeobotany and Palynology. 140, 187-212. http://dx.doi.org/10.1016/j.revpalbo.2006.04.003

Vincens, A., Buchet, G., Servant, M., and ECOFIT Mbalang collaborators, 2010. Vegetation response to the “African Humid Period” termination in Central Cameroon (7° N) – new pollen insight from Lake Mbalang.

Climate of the Past. 6, 281-2994. http://dx.doi.org/10.5194/cp-6-281-2010

White, F., 1983. The Vegetation of Africa - A descriptive memoir to accompany the Unesco / AETFAT / UNSO vegetation map of Africa. Natural Resources Research Report XX. U. N. Educational, Scientific and Cultural Organization, Paris, France.

Chapter 3:

Modelling vegetation change during Late Cenozoic uplift of the East African plateaus

Abstract

The present-day vegetation in the tropics is mainly characterized by forests worldwide except in tropical East Africa, where forests only occur as patches at the coast and in the uplands. These forest patches result from the peculiar aridity that is linked to the uplift of the region during the Late Cenozoic. The Late Cenozoic vegetation history of East Africa is of particular interest as it has set the scene for the contemporary events in mammal and hominin evolution. In this study, we investigatethe conditions under which these forest patches could have been connected, and a previous continuous forest belt could have extended and fragmented. We apply a dynamic vegetation model with a set of climatic scenarios in which we systematically alter the present-day environmental conditions such that they would be more favourable for a continuous forest belt in tropical East Africa. We consider varying environmental factors, namely temperature, precipitation and atmospheric CO_2 concentrations. Our results show that all of these variables play a significant role in supporting the forest biomes and a continuous forest belt could have occurred under certain combinations of these settings. With our current knowledge of the palaeoenvironmental history of East Africa, it is likely that the region hosted these conditions during the Late Cenozoic. Recent improvements on environmental hypotheses of hominin evolution highlight the role of periods of short and extreme climate variability during the Late Cenozoic specific to East Africa in driving evolution. Our results elucidate how the forest biomes of East Africa can appear and disappear under fluctuating environmental conditions and demonstrate how this climate variability might be recognized on the biosphere level.

3.1 Introduction

The present-day vegetation in the tropics is mainly characterized by forest biomes with tree cover of more than 70 percent worldwide except in tropical East Africa (Hansen et al., 2013). East African forest biomes occur in patches along the coast and in the uplands that are separated from each other and from the central Congolese forests by vast expanses of savanna (White, 1983; Lovett & Wasser, 1993; Fayolle et al., 2014). These forest patches are the result of the geological and climatological history of East Africa (Lovett & Wasser, 1993). In this study, we look into this historical background to investigate the conditions under which a continuous forest belt, a spatial continuation of woody vegetation with closed canopy cover connecting the modern patches along the coast and in the uplands with the central Congolese forests, could have existed, extended and fragmented.

The peculiar aridity of the region and fragmentation of a once continuous forest belt in equatorial East Africa is linked to the rise of the Ethiopian and East African plateaus during the Late Cenozoic (Spiegel et al., 2007; Pik et al., 2008; Wichura et al., 2010). The uplifted topography of the East African Rift System (EARS) acts as a barrier to air movements related to the Atlantic Ocean that are associated with rainfall (Figure. 3.1) and prevent their penetration further eastward (Nicholson, 1996; Sepulchre et al., 2006). Consequently, East Africa receives less precipitation and experiences more seasonality than other parts of the continent at the same latitudes (Nicholson 1996, 2000) and cannot support forest biomes today (Hirota et al., 2011).

The Late Cenozoic palaeovegetation of East Africa is particularly of interest because key speciation and dispersal events in mammals and hominins also took place in East Africa during this period (Potts, 1998). Existence of a continuous forest belt before it was fragmented might have provided migration and dispersal corridors for early hominins (Maslin et al., 2014). Extension and fragmentation of these environments might have influenced their movement, nesting, and hunting practices (Pickering and Bunn, 2007; Sept, 1998; Wheeler, 1994). Therefore understanding the dynamics of East African palaeovegetation is crucial for interpreting the setting in which contemporary evolution events came to pass.

The reconstruction of this period from empirical palaeoenvironmental data is far from complete (Bonnefille, 2010; Jacobs et al., 2010). Fossil flora data provide the only direct evidence of the past extent of biomes but either these proxy localities are rare or records are punctuated by geological processes or they only provide localized information rather than the wider regional patterns (Kingston, 2007; Maslin et al., 2014). Recently, molecular phylogenetic studies of rainforest plant (Davis et al., 2002; Couvreur et al., 2008, Holstein & Renner, 2011) and animal (Tolley et al. 2011; van Velzen et al., 2013) taxa contribute to construct a timetable for the fragmentation of the East African Miocene forests. Yet, resolving the changing patterns exhibited by these forest biomes, together with the environmental drivers of these changes in a spatially extensive way is beyond these approaches. At this point, vegetation modelling can greatly broaden our understanding of the nature and intensity of the forcing factors and the response of the East African vegetation.

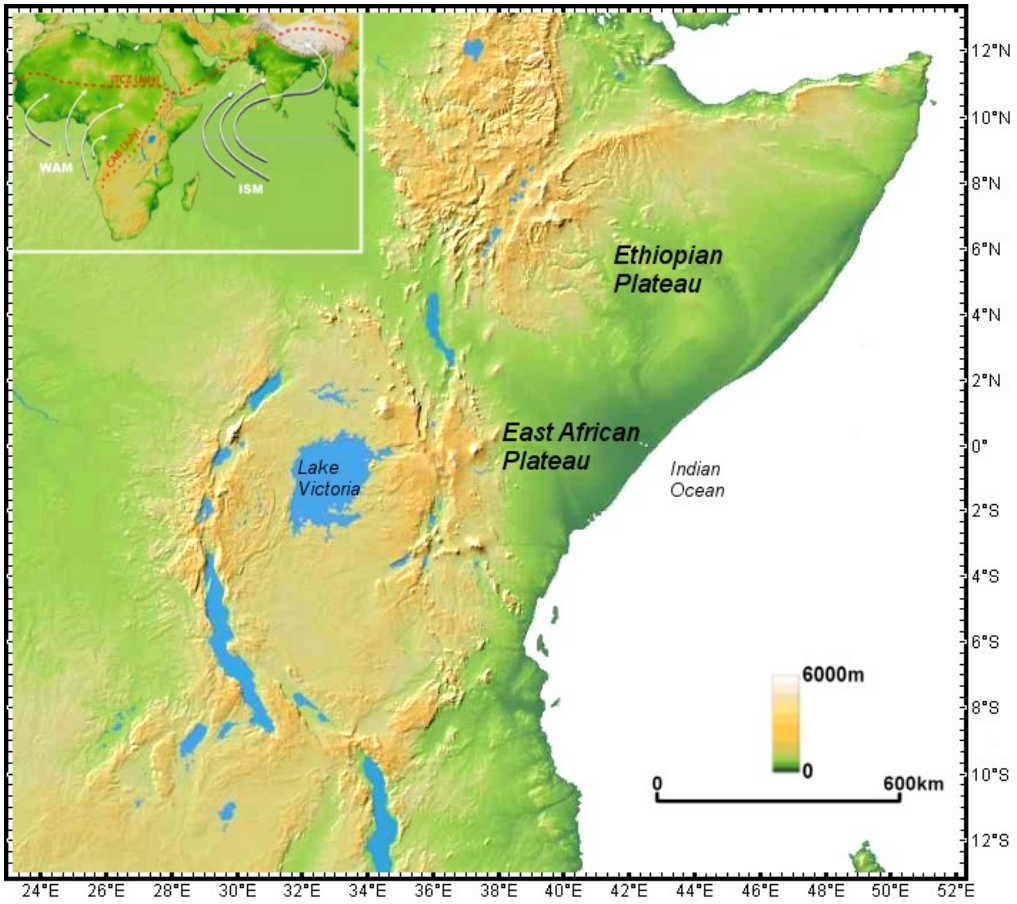

Figure 3.1 Geological and geographical setting of East African Rift System (EARS). Present-day high topography of EARS acts as a barrier in front of the Atlantic originated rainfall system (small- er window on the upper left corner). WAM: West African Monsoon, ISM: Indian Summer Monsoon, ITCZ: Intertropical Convergence Zone, CAB: Congo Air Boundary.

In this study, we applied a dynamic vegetation model (DVM) for East Africa with a set of climatic scenarios that we generated numerically. To produce these scenarios, starting from the present-day setting, we systematically altered the environmental conditions such that they would be more favourable for a continuous forest belt in tropical East Africa. This, so to speak, inverse approach differentiates our study from the previous vegetation modelling studies on East African biomes under the influence of tectonic forcing. Sepulchre et al. (2006), Prömmel et al. (2013) and Sommerfeld et al. (2014) simulated the climate of East Africa with the pre-uplift topography of EARS and then drove DVMs with their climate model outputs to simulate the vegetation. Although this is a valid and very much needed approach, due to the high computational costs of applying climate models, these studies are only available for a very limited number of tectonic and orbital forcing settings so far. Hence, we generated our own climate data following our current knowledge on mechanisms that affected the East African climate during the Late Cenozoic and designed our study accordingly.

To explore the possibility of a Miocene pan-African forest along the equatorial East Africa, we ran a process-based DVM (LPJ-GUESS) for a number of environmental scenarios towards more favourable environments for woody vegetation. In our scenarios: (i) we reduced the elevation of EARS to represent the pre-uplift topography which led to higher temperatures due to lower altitudes; (ii) increased the monthly means of rainfall and wet season length, and (iii) increased the atmospheric CO_2 concentration values. We simulated East African biomes under the combination of these settings.

3.2 Methods

3.2.1 LPJ-GUESS Model

Dynamic vegetation models (DVMs) are widely used tools to reconstruct the palaeovegetation composition and distribution under past climatic conditions and atmospheric CO_2 concentrations (François et al., 2006.; Sepulchre et al., 2006; Prömmel et al., 2010). Here we used the Lund-Potsdam-Jena General Ecosystem Simulator (LPJ-GUESS) in which the ecosystem processes are simulated via

explicit equations (Smith et al., 2001; Sitch et al., 2003, Gerten et al., 2004, Hickler et al., 2012).

In LPJ-GUESS different plant species are aggregated into plant functional types (PFTs), which are characterized by their life-form, morphology, phenology and other biological requirements and limits. LPJ-GUESS gives outputs (e.g. biomass, leaf area index (LAI) etc.) as a mixture of different PFTs, which can later be classified further into biomes according to their bioclimatic and compositional associations. The PFT parameterizations (Table B1-B5) and biome classification rules (Table B6) used are given in Appendix I. Although a comprehensive validation of the LPJ-GUESS model for East Africa is beyond the scope of this study and has been done in a previous study (Fer et al., 2016), the comparison of the simulated present-day biomes (Fig. B2) to a map of observed vegetation and their level of agreement can be seen in the Appendix.

In this study, after distinguishing between steppes, savannas, woodlands, afromontane, tropical seasonal and evergreen forest biomes, we further aggregate afromontane, tropical seasonal and evergreen forests as forest-like biomes, and the remaining biomes as non-forest biomes. A grid cell is classified as a forest biome if total Leaf Area Index (LAI, m^2 of leaves/m^2 of ground) of simulated vegetation is greater than 5.0 and the contribution of woody vegetation (arboreal PFTs) to this total is at least 4.0. A continuous forest belt is then defined as a spatial connection of forested grid cells from coastal forests to the central forests in east-west direction, with a minimum extension of 50 km (one grid cell) in north-south direction. In other words, an individual starting from the Indian coast, could walk uninterrupted to the Atlantic coast under the closed canopy of such a forest belt while the north-south width of this belt never drops below 50 km.

3.2.2 Experimental setup

LPJ-GUESS uses gridded values of topography and climate data, namely temperature, precipitation and cloud cover. All present-day climatic values were obtained from the Climate Research Unit (CRU) monthly time series dataset CRU TS3.20 (Harris et al., 2014), and all the simulations were run at a spatial resolution of 0.5º by 0.5º.

Each scenario is run with the entirety of 111 years of modified (as explained below and in the supplementary material) climate data after a 500 years of spinup phase (in which vegetation and soil develop from bare ground to a state of equilibrium under the given environmental setting). The full set of experimental scenarios analyzed in this study is given in Table 3.1. In addition, under the reduced topography (TOPO50) and 350 ppm setting, we ran a continuous experiment for a thousand years by appending the sequence of scenarios as shown in Table 3.2, in which step by step, either the wet season length is increased by one month or the rainfall amount is increased by 20%. This way we were able to see the continuous effects of increments in precipitation on the vegetation without the specific spinning up phases per scenario.

3.2.2.1 Topography

The timing and magnitude of past developmental stages of the EARS are still matters of investigation (Wichura et al., 2010, 2015). Therefore, we chose two simple and distinct settings to represent the pre-uplifted topography of East Africa: we reduced the elevation to (i) 50% (TOPO50) and (ii) 5% (NORIFT) of its present-day height (the equation provided by Sepulchre et al. (2006) and topographical settings used in this study which can be found in Appendix 1). In our experiments, reduction of topography directly affects the calculation of the new temperature (section 3.2.2.2) values only. However, based on previous climate modelling studies (Sepulchre et al., 2006; Kaspar et al., 2010) we assumed that it was the absence of present-day high topography that increased the precipitation in principle (section 3.2.2.3).

3.2.2.2 Temperature

To calculate the new temperature values with the reduced topography, by treating the present-day temperature values in each grid as a function of its latitude, longitude and present-day elevation, we first calculated the lapse rates (change in temperature per unit change in elevation). Then, by targeting the new elevation datasets (TOPO50 and NORIFT) as described above, we obtained the corresponding temperature values. Since a lower altitude leads to a higher

temperature, temperature values of the NORIFT experiment were higher than the TOPO50 experiment.

3.2.2.3 Precipitation

To define our precipitation scenarios we followed the main findings of the seminal study by Sepulchre et al. (2006) that simulated increased precipitation under reduced topography in East Africa. We applied an increase in precipitation in three different modes: (i) increase in monthly rainfall amounts only, (ii) increase in wet season length only and (iii) increase in both monthly amount and wet season length.

For the first set of experiments considering the increase in precipitation amount only, we systematically increased the amount of present-day precipitation values with the percentages similar to the amounts of Sepulchre et al. (2006) simulated and higher. Although the East African climatic system is quite complex and not every part of the region would have experienced the same type and amount of wetter conditions, we treated the region as a whole for simplicity. In previous climate modelling studies a lowered topography of EARS led to a precipitation increase of 60% with respect to present-day values (Sepulchre et al., 2006; Kaspar et al., 2010). However, during the extreme climate variability periods of the last 10 million years (Maslin and Trauth, 2009), the synergetic effects of tectonic and orbital forcings might result in even higher precipitation. Therefore we included higher percentages of precipitation increase in our scenarios up to 100%. Also, previous climate modelling studies (Sepulchre et al., 2006; Kaspar et al., 2010) gave different amounts of increase in precipitation for different topographical reductions. However, as this study aims at a more complete overview, we applied all precipitation increase scenarios we produced to each of our topographical settings.

Some parts of East Africa receive very little rain today and a percentage increase of these amounts still resulted in very little rainfall in the scenarios we produced. Therefore, in our second set of experiments, we increased the wet season length by adding a wet month to the present-day monthly time series data for every grid. We defined a wet month when the precipitation exceeds 50 mm for that month

following Jacobs and Herendeen (2004). To increase the wet season length, we topped a dry month (<50 mm) of each year with the highest precipitation up to 50 mm. This was to add an extra wet month, and to increase the wet season length for more than one month, we repeated this recurrently (see Table 3.1 for the full set of experiments). For the third set of experiments considering both the increase in precipitation and wet season length, we applied the increases in percentages we used in the 1st set on the 2nd set with increased wet season length (Table 3.1).

3.2.2.4 Cloud cover

As we generated the climate data for our experiments numerically from the present day dataset instead of using outputs of climate models, we also needed to adjust the cloud cover data accordingly. For this, we first fitted a regression between present-day cloud cover values and both its monthly temperature and precipitation time series data in every grid cell. The Beta regression model is suitable for modeling proportions such as cloud cover data (we used the 'betareg' package v3.0-5 from R, Cribari-Neto and Zeileis, 2010). To see how it performed, we first carried out a two-fold cross validation on the present-day values, using the first 50 years as the training sample and the rest as the hold-out sample. The predicted values of the second half were in good agreement with the observed values ($R=0.91$, $p<0.0001$). So, once we generated the modified temperature and precipitation values as described in the previous sections, by using these new temperature and precipitation values as predictors, we computed the modified cloud cover values for each scenario.

3.2.2.5 CO_2 values

The atmospheric CO_2 concentration values (pCO_2) of the Late Cenozoic varied and there is no consensus regarding the estimates of the ancient pCO_2 for the period (Beerling and Royer, 2011). Pagani et al. (1999) showed that pCO_2 stabilized at concentrations between 250 and 320 ppm during the Late Miocene (9 Ma). More recent data suggests pCO_2 of 400-500 ppm during the middle Miocene (Zhang et al., 2013) and of 330-400 ppm during the Pliocene (Seki et al., 2010). Covering the range suggested by previous reconstruction studies, we ran all our

experiments under three different pCO_2 settings to include the effect of pCO_2 on vegetation: 280 (the preindustrial value), 350 and 450 ppm.

Table 3.1 Experimental Setup. Each cell (#70) represents a different scenario with percentages showing the amount of increase in precipitation compared to present-day. We run the LPJ-GUESS model for all these combinations under three different settings of atmospheric CO_2 (pCO_2) concentration (280, 350, 450 ppm), making 210 runs in total. Numbers in the margins show the fraction of simulations (under all three pCO_2 settings) in which a continuous forest belt was simulated. TOPO50: elevation reduced to 50% of its present-day height, NORIFT: reduced to 5% of its present-day height

	TOPO50		NORIFT		
Amount only	+20%		+20%		
	+40%		+40%		
	+60%		+60%		
	+80%		+80%		
	+100%		+100%		6/30
WSL only	+1 wet month		+1 wet month		
	+2 wet months		+2 wet months		
	+3 wet months		+3 wet months		3/30
	+4 wet months		+4 wet months		
	+5 wet months		+5 wet months		
Amount and WSL together	+1 wet month	+20%	+1 wet month	+20%	
		+40%		+40%	
		+60%		+60%	8/30
		+80%		+80%	
		+100%		+100%	
	+2 wet months	+20%	+2 wet months	+20%	
		+40%		+40%	
		+60%		+60%	15/30
		+80%		+80%	
		+100%		+100%	
	+3 wet months	+20%	+3 wet months	+20%	
		+40%		+40%	
		+60%		+60%	20/30
		+80%		+80%	
		+100%		+100%	
	+4 wet months	+20%	+4 wet months	+20%	
		+40%		+40%	
		+60%		+60%	26/30
		+80%		+80%	
		+100%		+100%	
	+5 wet months	+20%	+5 wet months	+20%	
		+40%		+40%	
		+60%		+60%	
		+80%		+80%	29/30
		+100%		+100%	
		65/105		42/105	107/210

3.3 Results

Under our experimental scenarios, a continuous forest belt was simulated in 107 out of 210 runs (Table 3.1 and Figure 3.2). 19, 36, 52 of these 107 were under 280, 250 and 450 ppm of atmospheric CO_2 concentrations (pCO_2); and 65, 42 were under reduced (TOPO50) and removed topography (NORIFT) settings respectively. Three striking points can be deduced from Figure 2 where we give an overview of these results: (i) The number of simulations in which a continuous forest belt was simulated under the TOPO50 setting was significantly higher than the number under the NORIFT setting, (ii) neither an increase of total rainfall amount nor adding wet months produced a continuous forest belt per se in most of the "amount only" or "seasonality only" simulations (smaller circles in the

horizontal and vertical margins of each panel in Figure 3.2), while a combination of these two can easily lead to a continuous belt, and (iii) the higher the pCO_2, the lower the precipitation amount and wet season length threshold for the extension of forest biomes.

Table 3.2. The design of the 1000-year continuous run. All changes in wet season length (WSL) and mean annual precipitation (MAP) are with respect to present-day values. Cells are shaded in accordance with their precipitation amount.

Interval	Change in WSL	Change in MAP
0-100	none	none
100-200	+1	+20%
200-300	+1	+40%
300-400	+2	+40%
400-500	+2	+60%
500-600	+2	+60%
600-700	+2	+40%
700-800	+1	+40%
800-900	+1	+20%
900-1000	none	none

The results from the 1000 yr continuous run are shown in Figure 3.3: As it can be seen from the figure, when a continuous forest is simulated, it occurs at south of 5 ºS. In general, drier (non-forest) biomes are simulated in the northern (eastern) half of the region rather than southern (western) half. Five points were chosen from different parts of the region representing the shifting biomes during this 1000 yr simulation; A (26.8 ºE - 2.8 ºN), B (30.2 ºE - 1.2 ºS), C (36.2 ºE – 0.8 ºS), D (32.8 ºE – 8.8 ºS) and E (36.2 ºE – 10.8 ºS). Site A was always simulated as a forest biome and it is classified as a tropical rainforest in observational vegetation maps today (White, 1983) with a mean annual precipitation (MAP) of 1776 mm/yr which is typical for tropical forest ecosystems of today (~1500 < MAP < 3000 mm $year^{-1}$). The other sites shifted between forest and non-forest biomes as their state in the dry season length and precipitation-evapotranspiration difference space changed. The only intervals where all five of the sites were simulated as a forest biome are between the 400-600 years (only the 400-500 yr interval is mapped on Figure 3.3-b, however it can also be seen from Figure 3.3-a that all

sites have a total woody PFT LAI above 4 during this interval). A continuous forest belt was simulated for the 400-700 yr interval. None of the five points were simulated as a forest biome when the mean annual precipitation - mean annual actual evapotranspiration difference was below 500 mm/yr and when they experienced more than 5 dry months per year.

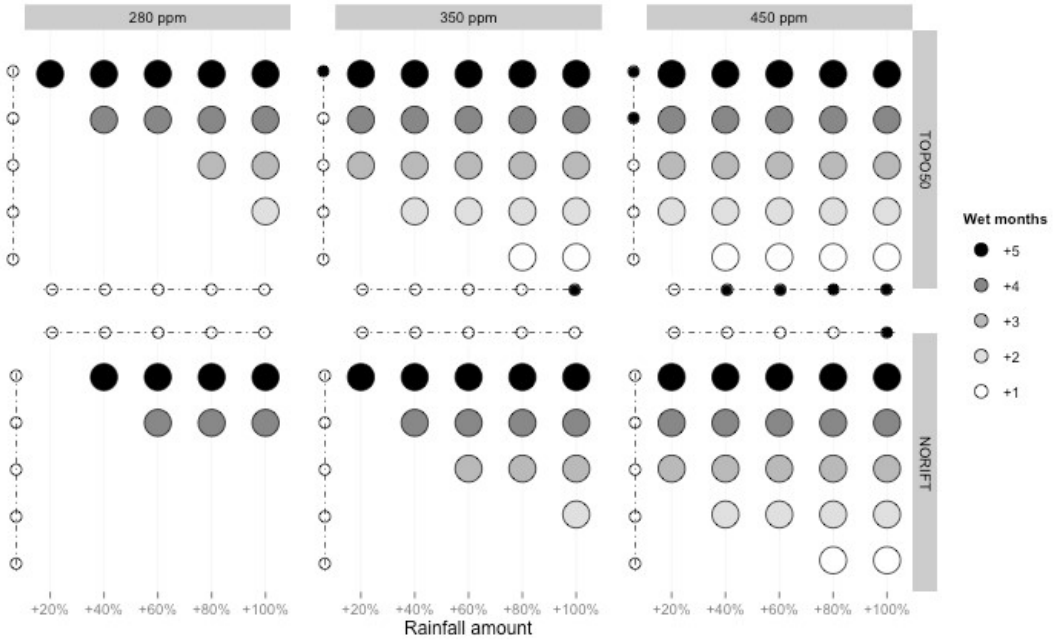

Figure 3.2 Overview of the scenarios under which a continuous forest belt occurs. All combination of settings covered in this study can be seen in the figure. Large circles represent the scenarios in which both seasonality and amount of precipitation changes were applied. A large circle is placed in the corresponding place if a continuous belt was simulated under that particular combination of environmental conditions or the place is left blank if no connection was established. Different shades of large circles represents different number of wet months added in the scenarios as shown by the legend. The small circles in the horizontal and vertical margins of the panels represent the amount only and seasonality only experiments respectively. If a continuous belt is simulated under these, the circle is filled. For example for the NORIFT setting (lower three panels), among the amount only and seasonality only experiments, only 100% increase in rainfall amount under 450 ppm setting resulted in a continuous forest belt.

3.4 Discussion

In this study, by testing a number of scenarios, we explored the spatial dynamics of East African forest biomes under the conditions hypothetically enabled by the absence of the high topography of today. Our results show that, all of the

environmental variables we considered play a significant role in supporting the forest biomes, and certain combinations of these environmental settings can lead to a forest belt in tropical East Africa. Here we discuss our findings in three contexts: (i) the mechanisms behind the vegetation changes that we simulated, (i) the design of the experiments and their meaning for our interpretations, and (iii) comparison of our simulations with the palaeodata.

3.4.1 Simulated vegetation dynamics

3.4.1.1 Temperature and CO_2 interplay

The design of our experiments allowed us to differentiate the effects of each environmental variable we considered. For example, all precipitation and pCO_2 scenarios were run under each of the topographical settings (TOPO50 and NORIFT). Therefore the simulated vegetation under these two settings only differed due to temperature (the lower the topography, the higher the temperature). Thus, we were able to see that all else being equal (i.e., precipitation and pCO_2), woody vegetation cover and the number of simulations in which a continuous forest belt was produced varied with temperature. Our results indicate that the higher temperatures of the NORIFT setting were less favourable for C_3 woody vegetation. Under higher temperatures plants prefer to shut their stomata to reduce water loss via transpiration but this results in lower uptake of CO_2. In C_3 plants the carbon fixation reaction is inefficient as the responsible enzyme (rubisco) also reacts with O_2. This process is called photorespiration, leaving almost half of the CO_2 unutilized (Edwards et al., 2010). Therefore higher temperatures lead to an increased relative photorespiration and a reduced relative net photosynthesis. As this is implemented in LPJ-GUESS likewise (Sitch et al., 2003), other things being equal, net primary productivity (NPP) of the C_3 woody vegetation gets lower with higher temperatures. Moreover, higher temperatures mean higher evaporative demand and, as it can be seen from Figure 3.3-c, the interplay between the total loss of water from the ecosystem (evapotranspiration) and the available precipitation plays a role as to whether or not a biome becomes a forest.

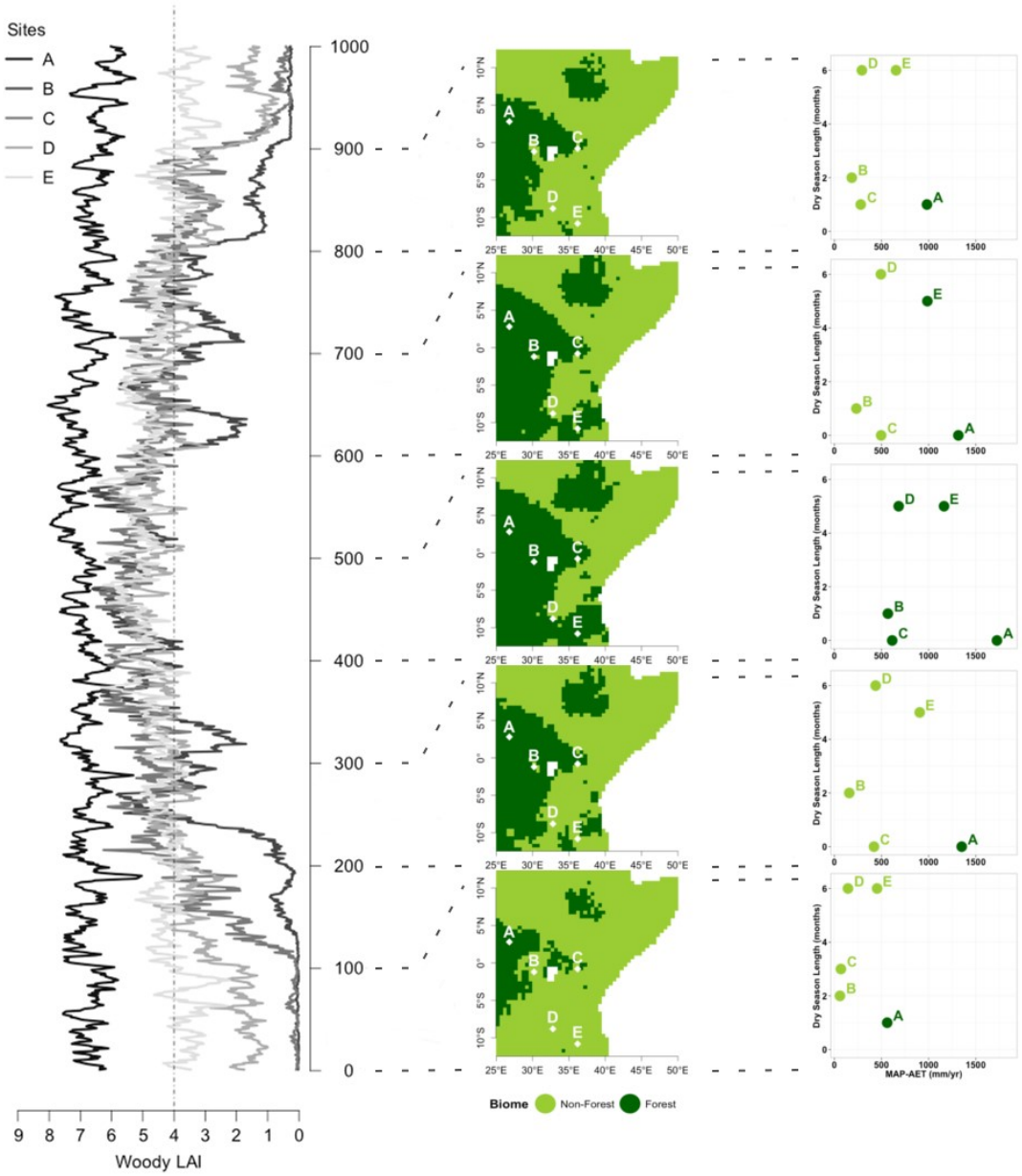

Figure 3.3 The simulated long-term biome dynamics of the continuous experiment under TOPO50 and 350 ppm setting. (a) Total simulated woody Plant Functional Types (PFT) Leaf Area Index (LAI, m2 of leaves/m2 of ground) change in time for the five representative grid points A, B, C, D and E, as shown in (b). The dashed line represents the forest-biome threshold (LAI of woody types N4.0). (b) Biome maps for five 100 year-averaged slices: 0–100, 200–300, 400–500, 600–700 and 800–900 year interval from bottom to top. (c) Climatic conditions and biome classification of the five representative grid points for the time intervals given in (b). Abbreviations: mean annual precipitation (MAP), mean annual actual evapotranspiration (AET). Dry season length is defined as the number of months in a year with b50 mm of rain.

The effect of pCO_2 was overlooked in previous modelling studies that specifically investigated the impact of climatic changes on vegetation under the influence of

different orographic scenarios for East Africa (Sepulchre et al., 2006, Prömmel et al., 2013; Sommerfeld et al., 2014). Our results show impacts of a similar magnitude for pCO_2 and precipitation on vegetation which agree with the strong fertilization effect of CO_2 on woody vegetation as simulated in previous dynamic vegetation modelling studies (François et al., 2006; Hamon et al., 2012). As discussed above, higher temperatures mean less CO_2 uptake and loss in NPP as the stomata tend to shut earlier when water stress is present. Whereas, under higher pCO_2 conditions, faster CO_2 uptake compensates for this, preventing water and NPP losses, lowering the precipitation and wet season length threshold required for the forest biomes. Besides, the predictive performance of LPJ-GUESS under CO_2 enhancement was tested by Hickler et al. (2008). The model was able to reproduce the NPP response of vegetation for temperate forests from where we also have the observation data from the free-air CO_2 enrichment (FACE) experiments, while it was predicting a more than double NPP enhancement in tropical forests from where we do not have such observational data. In our experiments, the increase in NPP due to CO_2 increase only (from 280 ppm to 350 ppm and from 350 ppm to 450 ppm), changes between +20 and +25%. This seems similar with the magnitude quantified in Hamon et al. (2012) for subtropical forests (~ +25%), however the amount of increases in CO_2 in our study (+70 and +100 ppm) is less than the amount of increase in their sensitivity study (+280 ppm). Apart from the differences in the models used in the studies (LPJ-GUESS in ours, CARAIB in Hamon et al., 2012, although both use the same photosynthesis model), we predicted a greater NPP enhancement due to CO_2 increase in tropical forests than Hickler et al. (2008). The photosynthesis model that is implemented within LPJ-GUESS (Farqhuar et al., 1980) represents the effects of pCO_2 and temperature interplay already discussed and was shown to predict a strong temperature dependence of the photosynthetic response on elevated pCO_2 (Long, 1991). However, as we do not have FACE experiments located in the tropics, it is difficult to specify how well this effect is represented in the tropics where temperatures are high. Having said this, as running the simulations under different pCO_2 values results in substantially different outputs, we strongly recommend taking the effect of pCO_2 into consideration when simulating and interpreting the past vegetation. However, it should also be noted that nutrient limitations (e.g. nitrogen) on photosynthetic productivity might

dampen the strong fertilization effect of high pCO_2 (Finzi et al., 2006) and this version of LPJ-GUESS does not include these constraining effects.

3.4.1.2 Amount of precipitation and seasonality

We used three different modes of precipitation increase in our scenarios, therefore, it was possible to distinguish separate and synergetic effects of different modes of precipitation increase on the distribution of the biomes. For example under pCO_2 of 350 ppm and TOPO50 setting, neither 40% increase in precipitation amount nor adding two wet months produced a continuous forest belt per se while a combination of these two resulted in such (Figure 3.2). As it can be seen from our continuous experiment (Figure 3.3) reducing the dry season length resulted in the development and expansion of forest biomes which cannot survive dry periods of more than 5 months. We also note that this was the case under a 350 ppm setting and different pCO_2 could change this threshold (see below). Again when we look at the pCO_2 of 350 ppm and TOPO50 setting, increasing the wet season length by one month and the amount by 60% does not result in a continuous forest belt, while increasing the wet season length by two months and the amount by 40% does (Figure 3.2). When we look at the average monthly rainfall for southern East Africa (SEA; where the connection of the belt occurs when it does) under these scenarios, we see that the former is 147 mm/month and the latter is 132 mm/month. Also, increasing the wet season length by three months and the amount by 20% leads to an average monthly rainfall for SEA of 117 mm/month (even less than +2 wet months and 40% increase), and still a continuous forest belt was simulated. This demonstrates how a similar magnitude of precipitation increase in average rainfall may or may not result in shifts towards forest biomes depending on the length of the dry season and the importance of rainfall seasonality in maintaining tropical African vegetation as highlighted by previous studies (Hely et al., 2006; Vincens et al., 2007, Ivory et al., 2012). This is particularly of relevance when interpreting past climate vegetation. While there are several studies estimating the mean annual precipitation values of the past, studies inferring seasonality from palaeorecords (Vincens et al., 2007; Ivory et al., 2012) are temporally and spatially more scarce and less quantitative making it difficult to construct a comprehensive profile of

seasonality parameters or patterns during the Late Cenozoic in East Africa (Kingston, 2007).

Another remark about the seasonality aspect could be on the choice of a wet month threshold. The threshold that classifies a month as wet or dry differs in previous studies on African vegetation. While Jacobs and Herendeen (2004) chose a >50 mm threshold, Collins et al., (2010) chose a >100 mm threshold to define a wet month. Fontes et al. (1995) introduced another category: they classify a month with a total monthly rainfall between 50 and 100 mm as a sub-dry month, and a month with a total monthly rainfall higher than 100 mm as a wet month. In our study we report our results with a >50 mm threshold to enable comparison with previous palaeoprecipitation estimates, however we ran all our simulations with a >100 mm threshold as well. The distribution of the biomes and number of runs in which a continuous forest belt was simulated when a >100 mm threshold was chosen were similar to the reported results in this study (not shown). This is in agreement with the analysis of Collins et al. (2010) where they found modern-day $\%C_3$ vegetation is correlated more with wet season length than with wet season intensity.

3.4.1.3 Long term vegetation dynamics

Our continuous run of a thousand years, rather than simulating intervals discretely, shows the dynamic shifts in biomes. This experiment reveals two things: First, without the 500 yr spinup phase with the wetter conditions, shifts towards a forest biome happen more slowly. For example, while a hundred years simulation of +2 wet months and a 40% increase in rainfall amount under TOPO50-350 ppm setting (the interval of 300-400 yrs of the total 1000 yrs) results in a continuous forest belt when run separately; it does not when run after 300 years of present-day (100 yr), +1 wet month 20% increase (100 yr), +1 wet month 40% increase (100 yr) precipitation respectively. This is expected as maintaining a forest biome is easier when the ecosystem reaches to a state of equilibrium under a wetter setting (when run separately with the spinup phase) instead of having the same precipitation changes after vegetation and soil passes through drier conditions. For example, the interval of the same scenario towards the end of the experiment (the interval of 600-700 yrs of the total 1000 yrs) produces a continuous forest belt and

slightly more forest biomes compared to its 300-400 yr interval counterpart. Running the same precipitation scenario for the 600-700 yr interval after wetter conditions, mimics a similar situation with the spinup phase. This also agrees with the interpretation of Maslin (2004); if an area is covered with forest and starts to dry out, the ecosystem recycles moisture and maintains the biome as a forest before it shifts to a drier biome (e.g. woodland or savanna), whereas if an area is covered with savanna and starts to get wetter, the climate needs to get much wetter or stay wet for longer before the biome shifts to a forest. Secondly, this experimental run also shows that, given the right set of climatic changes, East African biomes can shift to/from forests on time scales of less than 10^3 years which is also in agreement with previous reports (Hughen et al., 2004).

3.4.2 Scenario selection

3.4.2.1 Topography

We reduced the topography to 50% (TOPO50) and 5% (NORIFT) of its present-day height to represent the past stages of the East African Rift System (EARS). There are still large uncertainties about the timing and magnitude of the uplift in the region (Wichura et al., 2015), and it is difficult to say which setting corresponds to which time in the past. Besides, the propagation of EARS showed a north to south trend in time (Macgregor, 2015), therefore these settings are only simplified representations of the past developmental stages as in previous modelling studies (Sepulchre et al., 2006; Prömmel et al., 2013). However, considering the palaeotopographic constructions so far, we can estimate that our TOPO50 setting in which the East African Plateau is uplifted to ~1,300 m corresponds to Mid- to Late Miocene (after 15 Ma, Wichura et al., 2010, 2015), while NORIFT setting corresponds to the Oligocene (before 25 Ma, Macgregor, 2015). However, these matchings are somewhat of concern in our study as the topographical change was not directly used to force a climate model to simulate changes in atmospheric circulation. Instead, in our numerical experiments we used these topographical changes to calculate new temperature values which would be more likely to occur under reduced topography, as opposed to using present-day temperature values as they are.

3.4.2.2 Temperature

In the tropics temperature is not the main limiting factor for plant distribution but rather plays a role in productivity and is of relevance for plant distribution only at higher elevations (Bonnefille, 2010). Thus, by using two distinct temperature settings associated with reduced topography scenarios, we attempted to include the impact of a change in temperature due to orography on East African vegetation. In our study, we generated the new temperature values statistically through calculation of adiabatic lapse rates. However, temperature changes due to orography can also be influenced by diabatic heating/cooling processes (Ehlers and Poulsen, 2009). To assess how much difference this would make in the interpretation of our scenarios, we compared our statistically calculated TOPO50 temperature values with dynamically computed temperature values from a previous climate modelling study (Prömmel et al., 2013). The tectonic forcing (TECT) experiment in Prömmel et al. (2013) also considers a 50% reduction in topography, therefore presents a good comparison opportunity as a simulated change in temperature due to orography does not necessarily follow an adiabatic lapse rate in a climate model. The comparison of the two (one statistically calculated in this study, TOPO50; the other dynamically computed by Prömmel et al., TECT) climatology temperature data (supplementary material, Figure B2) reveals differences up to 6 °C in some grid cells. The statistical calculation (our TOPO50) led to higher temperature values over the Ethiopian Plateau and the Tanzanian coast compared to the simulated (TECT) temperature, while it returned lower values for most of the remaining areas. To see how this difference translates to the vegetation and affects our interpretations of this study, we ran all the combinations of our TOPO50 setting with TECT temperatures (i.e. other variables kept equal but only simulated values from Prömmel et al. were used as temperature input). The number of simulations in which a continuous forest belt simulated in TECT experiments was slightly lower than TOPO50 (supplementary material, Figure B3), as our TOPO50 temperatures were lower than TECT temperatures in southern East Africa, favouring woody vegetation. However, even in those TECT simulations that were not producing the continuous belt according to the criteria defined in this study, the distribution of biomes was still very similar to its TOPO50 counterparts (not shown). This comparison goes along with our decision to include only two distinct temperature settings to be able to see notable

shifts at the biome level. Nevertheless, we note that when a more temperature sensitive aspect of the environment is under investigation, using only the adiabatic lapse rates to calculate new temperature values due to topographical change may lead to further misestimations.

3.4.2.3 Precipitation

The mechanisms that control East African climate are numerous and have been discussed extensively in previous studies (Nicholson, 1996, 2000; Feakins and deMenocal, 2010; Trauth et al., 2005, 2007, 2009, 2015). In this study, the main mechanism that we assumed to generate a wetter climate in East Africa was the removal (or the reduction) of the tectonic uplift. EARS is such a great geological structure that, by the time it reached its full development, the uplifted topography no longer permitted the rainfall associated with the west African monsoon (WAM) and the Indian Ocean system to penetrate the innermost parts of the region (Nicholson 1996, 2000). Hence, more of the precipitation related air movements could have reached East Africa if the topography were lower then its present day height, resulting in less seasonality due to increased moisture availability. However, this is not the only mechanism that can be associated with our scenarios regarding the Late Cenozoic moisture history of East Africa. Given the geological setting determined by the tectonics, orbital changes also influence the East African climate (Kingston, 2007; Bergner et al., 2009; Feakins and deMenocal, 2010; Trauth et al., 2015). The cyclic variations in the Earth's orbital parameters alter the amount, timing and spatial distribution of received solar radiation, resulting in fluctuations in humidity on time scales of 10^4 to 10^5 yrs (Maslin et al., 2014 and references therein; Trauth et al., 2015 and references therein). For example a wetter climate in East Africa such as those in our scenarios could have occurred during the intervals of extreme climate variability associated with eccentricity and precessional maxima (Trauth et al., 2007). Moreover, there are mechanisms that work on time scales of $<10^3$ yr influencing the East African climate. For example, the changes in northern hemisphere insolation (e.g. a NH insolation maximum during a precession minimum) can alter the pressure gradients in the region. As a result, the Congo Air Boundary, currently blocked by topography, can cross the East African plateaus, bringing

extra moisture from the Congo basin further to the East (Junginger and Trauth, 2013).

3.4.3 Comparison with palaeorecords

In this study, we show that a continuous forest belt could have existed in East Africa under different combinations of environmental settings. Based on our current knowledge of the palaeoenvironmental history of East Africa, it is likely that these conditions prevailed in the region and a continuous forest belt existed during the Late Cenozoic. When considering pCO_2, we acknowledge that there is no agreement on the absolute values of reconstructed pCO_2 (Beerling and Royer, 2011) for the Late Cenozoic. Nevertheless, the estimates of pCO_2 from boron/calcium ratios in foraminifera are between 250-450 ppm over the past 20 Ma, fluctuating around 350 ppm during the Early Pleistocene and Mid-Miocene (Tripati et al., 2009).

Reconstructing the Late Cenozoic environments of East Africa has gained substantial attention in the last decades (Feakins and deMenocal, 2010, and references therein; Maslin et al., 2014, and references therein). However, continuous geological records in space and time are scarce in the region because of the active faulting, erosion, non-deposition processes, and lack of archives outside the rift basins that would accumulate the proxy data. Therefore, given the complexity of the controls on climate and vegetation, it is difficult to extrapolate single records to the whole region for extended time periods. However, both the settings and simulated vegetation in our scenarios are comparable with the palaeorecords. For example, deep and large lakes which existed in the past 10 Myr BP recorded periods of humid conditions in East Africa (Tiercelin and Lezzar, 2002). Borchardt and Trauth (2012) estimated a 25% increase in precipitation during the mid-Holocene (ca. $1.5–0.5 \times 10^4$ yr BP). Although this is a recent humid episode, this magnitude of change also applies to the older ones recorded by the palaeolakes of the past 10 Myr BP. Besides, this +25% change is independent of topographical reduction. Still, a +25% change in precipitation (that results in an average of monthly rainfall of 113 mm/month for SEA) is a comparable amount with our scenario when increasing the wet season length by three months and the

amount of precipitation by 20% (117 mm/month) under which a continuous forest belt was simulated.

Late Oligocene – Early Miocene age palaeobotanical remains from East Africa indicate forest vegetation and show botanical affinities with both Guineo-Congolian and Zambesian communities (Jacobs et al., 2010; Bonnefille, 2010). From the Middle Miocene on, the mixed climatic controls superimposed on the complex topography make the interpretation of the records more difficult. However, evidence dating from 13 to 6 Ma documents biomes from forests to savannas within 10 km of each other suggesting a variety of environments (Jacobs et al., 2010). Palaeobotanical data from Ethiopia, Kenya and Uganda also indicate the presence of evergreen and seasonal forests at different localities, and a peak in tree pollen from a single marine core sample from East Africa dated at 6.8 Ma was interpreted as an expansion of these forest biomes (Bonnefille, 2010). North East African (NEA) vegetation changes over the last 12 Myr were also investigated using plant leaf wax isotopic analysis. Feakins et al. (2013) shows while rainforests were unlikely to have been extensive in NEA, seasonally dry forests which may also reach 100% canopy cover, were a significant component of the regional landscape since the Late Miocene. In our experiments, a considerable expansion of forest biomes and the establishment of a continuous forest belt only occurs south of 5 ºS, and the record by Feakins et al. (2013) is not representative of SEA. However, we also simulated the expansion of forest biomes in NEA. In this study, for simplicity, we did not apply a different amount of increase in precipitation for NEA and SEA, therefore the simulated expansion of forest biomes in NEA would always be overestimated given that the findings (that the increase in precipitation due to lowered topography would be higher in SEA compared to NEA) of previous climate modelling studies are accurate (Sepulchre et al., 2006; Kaspar et al., 2010).

Evidence from the Pliocene reports some occurrence of lowland forest taxa in the EARS, however pollen and palaeobotanical remains from this period is limited due to high oxidation conditions caused by wet-dry cycles (Jacobs et al., 2010; Bonnefille, 2010). Recently synthesized Plio-Pleistocene palaeovegetation data from northern Tanzania (Barboni, 2014), documents drier vegetation from this region in general (since ~4 Ma) with similarities to the present-day vegetation.

Due to design, the distribution of precipitation in our experiments closely follows the present-day distribution. Hence, we simulated less tree cover for the vicinity of northern Tanzania with respect to the more central parts of tropical East Africa (Figure 3-b), not disagreeing with this synthesis. Occurrence of closed woodlands to forests, locally and occasionally, can also be seen from the palaeovegetation records from this region (Barboni, 2014), documenting the wet-dry variability period (~1.9-1.7 Ma) during which East Africa experienced high moisture availability.

Overall, the palaeorecords agree on a variable Late Cenozoic climate and environment in East Africa. Maslin et al. (2012) argue that the arid periods intensified while wet periods remained at a similar level within the progression towards this climate variability. As a result, low-temporal resolution proxy data that are used to interpret the palaeoenvironment for this period might have been affected by time-averaging processes. Therefore it is important to note that such data may not represent the short term variations in the environment given that it could have gone through substantial changes during these periods as demonstrated in the 1000-yr experiment we simulated in this study.

3.5 Conclusion

Extensive compilation of existing palaeoenvironmental records suggest that the East African climate experienced periods of short and extreme climate variability during the Late Cenozoic. Recent improvements on environmental hypotheses of hominin evolution highlight the role of such periods specific to East Africa in driving evolution (Maslin and Trauth, 2009). Our results elucidate how the forest biomes of East Africa could appear and disappear under fluctuating precipitation and pCO_2 values, and demonstrate how this climate variability might be recognized on the biosphere level considering that the distribution of tropical vegetation can vary on short time scales under the right set of climatic changes. The millennial experiment we conducted with a setting that East Africa could actually have experienced during Late Cenozoic uplift of the East African plateaus shows that these changes could occur on the relevant temporal-scales to human evolution. Our findings demonstrate that the discussions on the exact influence of the Late Cenozoic uplift of the East African plateaus on early human

environments would benefit from further contributions from climate and vegetation modelling studies.

3.6 Acknowledgements

This study is a contribution to the NECLIME framework. IF was funded by DAAD, grants to F. J. and German Research Foundation (DFG) Graduate School GRK1364 program (Shaping Earth's Surface in a Variable Environment – Interactions between tectonics, climate and biosphere in the African-Asian monsoonal region). FJ and BT acknowledge the support by the BMBF in the framework of the OPTIMASS project (01LL1302A and 01LL1302B). We thank A. Junginger, H. Wichura and Plant Ecology and Nature Conservation Group of Potsdam University for the inspiring discussions, and K. Prömmel for kindly providing us with their climate model outputs. We appreciate the very helpful comments of the two anonymous reviewers which helped us improve this manuscript to a great extent.

3.7 References

Barboni, D., Vegetation of Northern Tanzania during the Plio-Pleistocene: A synthesis of the paleobotanical evidences from Laetoli, Olduvai, and Peninj hominin sites. Quaternary International, 322-323, 264-276. http://dx.doi.org/10.1016/j.quaint.2014.01.016

Beerling, D.J., Royer, D.L., 2011. Convergent Cenozoic CO_2 history. Nature Geoscience 4, 418-420. http://dx.doi.org/10.1038/ngeo1186

Bergner, A.G.N., Strecker, M.R., Trauth, M.H., Deino, A., Gasse, F., Blisniuk, P., Dühnforth, M., 2009. Tectonic versus climate influences on the evolution of the lakes in the Central Kenya Rift. Quaternary Science Reviews, 28, 2804-2816. doi: 10.1016/j.quascirev.2009.07.008

Bonnefille, R., 2010. Cenozoic vegetation, climate changes and hominid evolution in tropical Africa. Global and Planetary Change 72, 390-411. doi:10.1016/j.gloplacha.2010.01.015

Borchardt, S., Trauth, M.H., 2012. Remotely-sensed evapotranspiration estimates for an improved hydrological modeling of the early Holocene mega-lake Suguta, northern Kenya Rift. Palaeogeography, Palaeoclimatology, Palaeoecology, 361-362, 14-20.

http://dx.doi.org/10.1016/j.palaeo.2012.07.009

Cerling, T. E., 1992. Development of grasslands and savannas in East Africa during the Neogene. Palaeogeography, Palaeoclimatology, Palaeoecology 97, 241-247. doi:10.1016/0031-0182(92)90211-M

Collins, J. A., Schefuss, E., Heslop, D., Mulitza, S., Prange, M., Zabel, M., Tjallingii, R., Dokken, T. M., Huang, E., Mackensen, A., Schulz, M., Tian, J., Zarriess, Wefer, G., 2010. Interhemispheric symmetry of the tropical African rainbelt over the past 23,000 years. Nature Geoscience, 4, 42-45. http://dx.doi.org/10.1038/ngeo1039

Couvreur, T. L. P., Chatrou, L. W., Sosef, M. S. M., Richardon, J. E., 2008. Molecular phylogenetics reveal multiple tertiary vicariance origins of the African rain forest trees. BMC Biology, 6:54. http://dx.doi.org/10.1186/1741-7007-6-54

Cribari-Neto, F., Zeileis, A., 2010. Beta regression in R. Journal of Statistical Software 34-2. http://dx.doi.org/10.18637/jss.v034.i02

Davis, C. C., Bell, C. D., Fritsch, P. T., Matthews, S., 2002. Phylogeny of *Acridocarpus-Brachylophon* (Malpighiaceae): Implications for Tertiary tropical floras and Afroasian biogeography. Evolution 56, 2395-2405.

http://dx.doi.org/10.1554/0014-3820(2002)056[2395:POABMI]2.0.CO;2

Edwards, E.J., Osborne, C.P., Strömberg, C.A.E., Smith, S.A., C4 Grasses Consortium, 2010. The origins of C4 grasslands: integrating evolutionary and ecosystem science. Science 328, 587-591.

http://dx.doi.org/10.1126/science.1177216

Ehlers, T.A., Poulsen, C.J., 2009. Influence of Andean uplift on climate and paleoaltimetry estimates. Earth and Planetary Science Letters 281, 238-248. http://dx.doi.org/10.1016/j.epsl.2009.02.026

Farquhar, G.D., von Caemmerer, S., Berry, J.A., 1980. A biochemical model of photosynthetic CO_2 assimilation in leaves of C_3 plants. Planta, 149, 78–90.

http://dx.doi.org/10.1007/BF00386231

Fayolle, A. Swaine, M. D., Bastin, J.-F., Bourland, N., Comiskey, J. A., Dauby, G., Doucet, J.-L., Gillet, J.-F., Gourlet-Fleury, S., Hardy, O. J., Kirunda, B., Kouamé, F. N., Plumptre, A. J., 2014. Patterns of tree species composition across tropical African forests. Journal of Biogeography 41, 2320-2331. http://dx.doi.org/10.1111/jbi.12382

Feakins, S. J., deMenocal, P.B. 2010. Global and African regional climate during the Cenozoic, Chapter Four. Cenozoic Mammals of Africa. http://dx.doi.org/10.1525/california/9780520257214.003.0004

Feakins, S. J., Levin, N.E., Liddy, H.M., Sieracki, A., Eglington, T. Bonnefille, R., 2013. Northeast African vegetation change over 12 m.y. Geology 41, 295-298.

http://dx.doi.org/10.1130/G33845.1

Fer, I., Tietjen, B., Jeltsch, F., 2016. High-resolution modelling closes the gap between data and model simulations for Mid-

Holocene and present-day biomes of East Africa. Palaeogeography, Palaeoclimatology, Palaeoecology, 444, 144-151.

doi:10.1016/j.palaeo.2015.12.001

Finzi, A.C., Moore D.J.P., DeLucia, E.H., Lichter, J., Hofmockel, K.S., Jackson, R.B., Kim, H.-S., Matamala, R., McCarthy, H.R., Oren, R., Pippen, J.S., Schlesinger, W.H., 2006. Progressive nitrogen limitation of progressive ecosystem processes under elevated CO2 in a warm-temperate forest. Ecology, 87, 15–25.

http://dx.doi.org/10.1890/04-1748

Fontes, J., Gastellu-Etchegorry, J. P., Amram, O., Flouzat, G., 1995. A global phenological model of the African Continent. Ambio, 24, 5. http://www.jstor.org/stable/4314350

François, L., Ghislain, M., Otto, D., Micheels, A., 2006. Late Miocene vegetation reconstruction with the CARAIB model. Palaeogeography, Palaeoclimatology, Palaeoecology 238, 302-320.

http://dx.doi.org/10.1016/j.palaeo.2006.03.034

Gerten, D., Schaphoff, S., Haberlandt, U., Lucht, W., Sitch, S., 2004. Terrestrial vegetation and water balance – hydrological evaluation of a dynamic global vegetation model. Journal of Hydrology 286, 249–270.

http://dx.doi.org/10.1016/j.jhydrol.2003.09.029

Hamon, N., Sepulchre, P., Donnadieu, Y., Henrot, A.-J., François, L., Jaeger, J.-J., Ramstein, G., 2012. Growth of subtropical forests in Miocene Europe: The roles of carbon dioxide and Antarctic ice volume. Geology 40(6):567 http://dx.doi.org/10.1130/G32990.1

Hansen, M. C., Potapov, P. V., Moore, R., Hancher, M., Turubanova, S. A., Tyukavina, A., Thau, D., Stehman, S. V., Goetz, S. J., Loveland, T. R., Kommareddy, A., Egorov, A., Chini, L., Justice, C. O., Townshend, J. R. G., 2013. High-resolution global maps of 21st-Century Forest Cover Change. Science 342, 850-853. http://dx.doi.org/10.1126/science.1244693

Harris, I., Jones, P.D., Osborn, T.J. and Lister, D.H., 2014. Updated high-resolution grids of monthly climatic observations - the CRU TS3.10 dataset. International Journal of Climatology 34, 623-642. http://dx.doi.org/10.1002/joc.3711

Hély, C., Bremond, L., Alleaume, S., Smith, B., Sykes, M.T., Guiot, J., 2006. Sensitivity of African biomes to changes in the precipitation regime. Global Ecology and Biogeography. 15, 258–270. doi:10.1111/j.1466-822x.2006.00235.x

Hickler, T., Smith, B., Prentice, I. C., Mjöfors, K., Miller, P., Arneth, A., Sykes, M. T., 2008. CO_2 fertilization in temperate FACE experiments not representative of boreal and tropical forests. Global Change Biology. 14, 1531-1542. doi:10.1111/j.1365-2486.2008.01598.x

Hickler, T., Vohland, K., Freehan, J., Miller, P. A., Smith, B., Costa, L., Giesecke, T., Fronzek, S., Carter, T. R., Cramer W., Kühn, I., Sykes, M. T., 2012. Projecting the future distribution of European potential natural vegetation zones with a generalized, tree species-based dynamic vegetation model. Global Ecology and Biogeography 21, 50-63. doi: 10.1111/j.1466-8238.2010.00613.x

Hirota, M., Holmgren, M., Van Nes, E. H., Scheffer, M., 2011. Global resilience of tropical forest and savanna to critical transitions. Science 334. http://dx.doi.org/10.1126/science.1210657

Holstein, N., Renner, S.S., 2011. A dated phylogeny and collection records reveal repeated biome shifts in the African genus *Coccinia* (Cucurbitaceae). BMC Evolutionary Biology, 11-28. http://dx.doi.org/10.1186/1471-2148-11-28

Hughen, K., Lehman, S., Southon, J., Overpeck, J., Marchal, O., Herring, C., Turnbull, J., 2004. ^{14}C Activity and global carbon cycle changes over the past 50,000 years. Science 303, 202-207. http://dx.doi.org/10.1126/science.1090300

Ivory, S.J., Lezine, A.-M., Vincens, A., Cohen A.S., 2012. Effect of aridity and rainfall seasonality on vegetation in the southern tropics of East Africa during the Pleistocene/Holocene transition. Quaternary Research 77, 77-86. http://dx.doi.org/10.1016/j.yqres.2011.11.005

Jacobs, B.F., Herendeen, P., 2004. Eocene dry climate and woodland vegetation in tropical Africa reconstructed from fossil leaves from northern Tanzania. Palaeogeography Palaeoclimatology Palaeoecology 213, 115-123.

http://dx.doi.org/10.1016/j.palaeo.2004.07.007

Jacobs, B.F., Pan. A.D., Scotese, C.R., 2010. A review of the Cenozoic vegetation history of Africa. Cenozoic mammals of Africa, Physical and Temporal Setting, California Scholarship Online.doi: 10.1525/california/9780520257214.003.0005

Junginger, A., Trauth, M. H., 2013. Hydrological constraints of paleo-Lake Suguta in the Northern Kenya Rift during the African Humid Period (15-5 ka BP). Global and Planetary change. 111, 174-188. doi: 10.1016/j.gloplacha.2013.09.005

Kaspar, F., Prömmel, K., Cubasch, U., 2010. Impacts of tectonic and orbital forcing on East African climate: a comparison based on global climate model simulations. International Journal of Earth Sciences 99, 1677–1686. http://dx.doi.org/10.1007/s00531-010-0538-x

Kingston, J.D., 2007. Shifting adaptive landscapes: Progress and challenges in reconstructing early hominid environments. American Journal of Physical Anthropology 134, Suppl. 45: 20-58.

http://dx.doi.org/10.1002/ajpa.20733

Long, S.P., 1991. Modification of the response of photosynthetic productivity to rising temperature by atmospheric CO2 concentrations: Has its importance been underestimated? Plant, Cell and Environment, 14, 729–739.

doi:10.1111/j.1365-3040.1991.tb01439.x

Lovett J.C., Wasser S.K., 1993. Biogeography and Ecology of the Rainforests of Eastern Africa. Cambridge: Cambridge University Press.

Macgregor, D., 2015. History of the development of the East African Rift System: A series of interpreted maps through time. Journal of African Earth Sciences 101, 232-252. http://dx.doi.org/10.1016/j.jafrearsci.2014.09.016

Maslin, M.A., 2004, Ecological verses Climatic Thresholds. Science, 306, 2197-2198. http://dx.doi.org/10.1126/science.1107481

Maslin, M.A., Trauth, M.H., 2009. Plio-Pleistocene Eastern African pulsed climate variability and its influence on early human evolution. In: Grine, F.E., Leakey, R.E., Fleagle, J.G. (Eds.), The First Humans–Origins of the Genus Homo. Springer Verlag, Vertebrate Paleobiology and Paleoanthropology Series, pp. 151-158.

Maslin, M.A., Brierley, C.M., Milner, A.M., Shultz, S., Trauth, M.H., Wilson, K.E., 2014. East African climate pulses and early human evolution, commissioned review paper. Quaternary Science Reviews, 101, 1-17. http://dx.doi.org/10.1016/j.quascirev.2014.06.012

Nicholson, S.E., 1996. A review of climate dynamics and climate variability in Eastern Africa. In: Johnson, T.C., Odada, E.O. (Eds.), The Limnology, climatology and caleoclimatology of the East African lakes. Gordon and Breach Publishers, Amsterdam, pp. 25–56.

Nicholson, S.E., 2000. The nature of rainfall variability over Africa on time scales of decades to millenia. Global and Planetary Change 26, 137–158. http://dx.doi.org/10.1016/S0921-8181(00)00040-0

Pagani, M., Freeman, K. H., Arthur, M. A., 1999. Late Miocene atmospheric CO_2 concentrations and the expansion of C_4 grasses. Science 285, 876:879. http://dx.doi.org/10.1126/science.285.5429.876

Pickering, T. R., Bunn, H. T., 2007. The endurance running hypothesis and hunting and scavenging in savanna-woodlands. Journal of Human Evolution 53, 434–438.

http://dx.doi.org/10.1016/j.jhevol.2007.01.012

Pik, R., Marty, B., Carignan, J., Yirgu, G., Ayalew, T., 2008. Timing of East African Rift development in southern Ethiopia: Implication for mantle plume activity and evolution of topography. Geology 36, 161-170.

http://dx.doi.org/10.1130/G24233A.1

Potts, R., 1998. Environmental hypotheses of hominin evolution. American Journal of Physical Anthropology 107, Suppl. 27: 93-136.

Prömmel, K., Cubasch, U., Kaspar, F., 2013. A regional climate model study of the impact of tectonic and orbital forcing on African precipitation and vegetation. Palaeogeography, Palaeoclimatology, Palaeoecology 369, 154-162. http://dx.doi.org/10.1016/j.palaeo.2012.10.015

Seki, O., Foster, G.L., Schmidt, D.N., Mackensen, A., Kawamura, K., Pancost, R.,

2010. Alkenone and boron-based Pliocene pCO_2 records. Earth and Planetary Science Letters 292, 201-211. http://dx.doi.org/10.1016/j.epsl.2010.01.037

Sepulchre, P., Ramstein, G., Fluteau, F., Schuster, M., Tiercelin, J.-J., Brunet, M., 2006. Tectonic uplift and eastern Africa aridification. Science 313, 1419–1423. http://dx.doi.org/10.1126/science.1129158.

Sept, J., 1998. Shadows on a changing landscape: comparing nesting patterns of hominids and chimpanzees since their last common ancestor. American Journal of Primatolology 46, 85–101.

http://dx.doi.org/10.1002/(SICI)1098-2345(1998)46:1<85::AID-AJP7>3.0.CO;2-R

Sitch, S., Smith, B., Prentice, I.C., Arneth, A., Bondeau, A., Cramer, W., Kaplan, J.O., Levis, S., Lucht, W., Sykes, M.T., Thonicke, K., Venevsky, S., 2003. Evaluation of ecosystem dynamics, plant geography and terrestrial carbon cycling in the LPJ dynamic global vegetation model. Global Change Biology. 9, 161–185. doi:10.1046/j.1365-2486.2003.00569.x

Smith, B., Prentice, I.C., Sykes, M.T., 2001. Representation of vegetation dynamics in the modelling of terrestrial ecosystems: comparing two contrasting approaches within European climate space. Global Ecology and Biogeography. 10, 621–637. doi:10.1046/j.1466-822X.2001.t01-1-00256.x

Sommerfeld, A., Prömmel, K., Cubasch, U., 2014. The East African Rift System and the impact of orographic changes on regional climate and resulting aridification. International Journal of Earth Sciences.

http://dx.doi.org/10.1007/s00531-014-1102-x

Spiegel, C., Kohn, B. P., Belton, D. X., Gleadow, A. J. W., 2007. Morphotectonic evolution of the central Kenya rift flanks: Implications for late Cenozoic environmental change in East Africa. Geology 35, 427-430. http://dx.doi.org/10.1130/G23108A.1

Tiercelin, J.J., Lezzar, K.E., 2002. A 300 million years history of rift lakes in Central and East Africa: an updated broad review. In: Odada, E.O., Olago, D.O. (Eds.), The East African Great Lakes: Limnology, Paleolimnology and Biodiversity. Kluwer, Dordrecht, pp. 3e60.

Tolley, K. A., Tilbury, C. R., Measey, G. J., Menegon, M., Branch, W. R., Matthee, C. A., 2011. Ancient forest fragmentation or recent radiation? Testing refugial speciation models in chameleons within an African biodiversity hotspot. Journal of Biogeography 38, 1748-1760.

doi:10.1111/j.1365-2699.2011.02529.x

Trauth, M.H., Maslin, M.A., Deino, A., Strecker, M.R., 2005. Late Cenozoic Moisture History of Eastern Africa. Science 309, 2051-2053. http://dx.doi.org/10.1126/science.1112964

Trauth, M.H., Maslin, M.A., Deino, A., Strecker, M.R., Bergner, A.G.N., Dühnforth, M., 2007. High- and low- latitude forcing of Plio-Pleistocene African climate and human evolution. Journal of Human Evolution 53, 475-486. doi:10.1016/j.jhevol.2006.12.009

Trauth, M.H., Larrasoaña, J.C., Mudelsee, M., 2009. Trends, rhythms and events in Plio-Pleistocene African climate. Quaternaary Science Reviews 28, 399-411.

doi:10.1016/j.quascirev.2008.11.003

Trauth, M.H., Bergner, A.G.N., Foerster, V., Junginger, A., Maslin, M.A., Schaebitz, F., 2015. Episodes of environmental stability and instability in Late Cenozoic lake records of Eastern Africa. Journal of Human Evolution, *in press.*

Tripati, A.K., Roberts, C.D., Eagle, R.A., 2009. Coupling of CO2 and ice sheet stability over major climate transitions of the last 20 million years. Science 326, 1394,

http://dx.doi.org/10.1126/science.1178296

Wheeler, P.E., 1994. The thermoregulatory advantages of heat storage and shade-seeking behaviour to hominids foraging in equatorial savanna environments. Journal of Human Evolution 26, 339–350. http://dx.doi.org/10.1006/jhev.1994.1021

White, F., 1983. The Vegetation of Africa - A descriptive memoir to accompany the Unesco / AETFAT / UNSO vegetation map of Africa. Natural Resources Research Report XX. U. N. Educational, Scientific and Cultural Organization, Paris, France.

Wichura, H., Bousquet, R., Oberhaensli, R., Strecker, M. R., Trauth, M. H., 2010. Evidence for middle Miocene uplift of the East African Plateau. Geology 38, 543-546. http://dx.doi.org/10.1130/G31022.1

Wichura, H., Jacobs, L. L., Lin, A., Polcyn, M. J., Manthi, F. K., Winkler, D. A., Strecker, M. R., Clemens, M., 2015. A 17-My-old whale constrains onset of uplift and climate change in east Africa. Proceedings of the National Academy of Sciences 112,

13:3910-3915.
http://dx.doi.org/10.1073/pnas.1421502112

van Velzen, R., Wahlberg, N., Sosef, M. S. M., Bakker, F. T., 2013. Effects of changing climate on species diversification in tropical forest butterflies of the genus *Cymothoe* (Lepidoptera: Nymphalidae). Biological Journal of the Linnean Society 108, 546-564.

http://dx.doi.org/10.1111/bij.12012

Vincens, A., Garcin, Y., Buchet, G., 2007. Influence of rainfall seasonality on African lowland vegetation during the Late Quaternary: pollen evidence from Lake Masoko, Tanzania. Journal of Biogeography 34, 1274-1288. doi:10.1111/j.1365-2699.2007.01698.x

Zhang, Y. G., Pagani, M., Liu, Z., Bohaty S. M., DeConto R., 2013. A 40-million-year history of atmospheric CO_2. Phil. Trans. R. Soc. A., 371:20130096.
http://dx.doi.org/10.1098/rsta.2013.0096

Chapter 4:

Influence of El Niño-Southern Oscillation regimes on East African vegetation and its future implications under RCP 8.5 warming scenario

Abstract

The El Niño Southern Oscillation (ENSO), is the main driver for the interannual variability in East African rainfall with significant impact on vegetation and agriculture, and dire consequences for food and social security. In this study, we identify and quantify the ENSO contribution to the East African rainfall variability to forecast future East African vegetation response to rainfall variability related to a predicted intensified ENSO. To differentiate the vegetation variability due to ENSO, we removed the ENSO signal from the climate data using Empirical Orthogonal Teleconnections (EOT) analysis. Then, we simulated the ecosystem carbon and water fluxes under the historical climate without components related to ENSO teleconnections. We found ENSO driven patterns in vegetation response and confirmed that EOT analysis can successfully produce coupled tropical Pacific Sea Surface temperature-East African rainfall teleconnection from observed datasets. We further simulated East African vegetation response under future climate change as it is projected by climate models and under future climate change combined with a predicted increased ENSO intensity. Our EOT analysis highlight that climate simulations are still not good at capturing rainfall variability due to ENSO, and as we show here the future vegetation would be different from what is simulated under these climate model outputs lacking accurate ENSO contribution. We simulated considerable differences in East African vegetation growth under the influence of an intensified ENSO regime which will bring further environmental stress to a region with a reduced capacity to adapt effects of global climate change and food security.

4.1 Introduction

The 2010-2011 drought in the Horn of Africa, by some measures the worst drought in 60 years (Nicholson, 2014), is a reminder that rainfall in this politically and socioeconomically vulnerable region can fluctuate dramatically. El Niño Southern Oscillation (ENSO) influence has long been at the center of attention as a driver of this interannual fluctuations in East African rainfall (Indeje et al. 2000, Anyah and Semazzi, 2007, Nicholson, 2015), however, it is still an on-going endeavour to qualify and quantify the future behaviour of ENSO regimes under the predicted future warming (Vecchi & Wittenberg, 2010; Miralles et al., 2014). In this study we aim to identify and quantify the ENSO contribution to the East African rainfall variability in order to increase our understanding on the future response of East African vegetation to rainfall variability related to changing ENSO regimes and climate which can have dire consequences in this region in terms of food and social security.

4.1.1 East African climate

Rainfall in East African climate is primarily controlled by the seasonal passage of the Intertropical Convergence Zone (ITCZ) (Nicholson, 2000). While mean annual precipitation varies from <200 to >2000mm/year (Nicholson, 2000) and dry season length can vary from 0 to >8 months. Interannual variations in the seasonal migration of the East African ITCZ are driven to large extent by the ENSO (Ropelewski and Halpert, 1996) and its related impact through western Indian Ocean sea surface temperature (SST) anomalies (Goddard and Graham, 1999). The effect of ENSO on East African precipitation is diversified. Surface ocean warming in the western Indian Ocean (El Niño) leads to intensification and shifts of the ITCZ, bringing more precipitation to East Africa (Wolff et al., 2011), even through the direct teleconnection through the atmosphere tends to reduce rainfall (La Niña). These regions receive above average rainfall in El Niño years and below average in La Niña years during the OND months (Endris et al., 2013).

4.1.2 East African vegetation

The control ENSO exerts on East African precipitation also manifests itself on the vegetation which is contingent upon the seasonal rainfall. East Africa hosts a variety of biomes ranging from tropical rainforest to desert, however the region is mainly dominated by arid or semi-arid vegetation (Bobe, 2006). The arid and semi-arid vegetation consist of species that can tolerate aridity for several months as a result of the exceedingly seasonal precipitation (Bobe, 2006). Agricultural activities also depends on this strong seasonality as it determines the cropping times (Shisanya et al., 2011). Maize, beans, coffee, tea and wheat are among the important agricultural products of East Africa together with fruit products, and grasses for livestock (FAOSTAT, 2016).

An adaptive management of the limited resources will shape the future severity of climate change impacts on food productivity in this rainfall-reliant setup (Thornton et al., 2014). Therefore, a temporally and spatially extensive understanding of how the ecosystem dynamics in the region will respond to changing climate, and of particular concern to East Africa, to the ENSO regimes is needed. Several studies related the variability in African vegetation to ENSO events (Shisanya et al, 2011; Ivory et al., 2013; Abdi et al., 2016; Detsch et al., 2016). However, the forthcoming of this relationship has been less of a focus, partly due to our imperfect knowledge on the nature of the future ENSO response to changing climate.

4.1.3 ENSO impact on East African vegetation

An opportunity to examine the ENSO – East African vegetation relationship is by means of using predictive tools such as vegetation models which have been successfully applied to determine and forecast regional vegetation dynamics (Moncrieff et al., 2014; Scheiter and Savadogo, 2016) as well as agricultural yields (Waha et al., 2013; Dietrich et al., 2014). In this study, we used the latest climate projections from the Intergovernmental Panel on Climate Change (IPCC) 5th assessment report for Representative Concentration Pathway (RCP) 8.5 scenario, downscaled by the Coordinated Downscaling Experiment (CORDEX) (Nikulin et al., 2012, Endris et al., 2013) to drive such a process-based dynamic

vegetation model, LPJ-GUESS (Lund-Potsdam-Jena general Ecosystem Simulator). To be able to differentiate the vegetation variability due to ENSO, we removed the ENSO signal from the climate data and simulated the vegetation under the historical climate without components related to ENSO teleconnections. In the following sections, we look at the ENSO influence on East African vegetation i) under present conditions, ii) under projected future climate, and iii) under a potentially increased ENSO intensity combined with future climate change. Finally, we discuss the effects of ENSO-related vegetation variability on the carbon and hydrological cycles, and its significance for mitigation efforts in the region.

4.2 Methods

4.2.1 The LPJ-GUESS model

We used the dynamic vegetation model LPJ-GUESS (Lund-Potsdam Jena General Ecosystem Simulator, Smith et al. 2001; Sitch et al. 2003, Gerten et al. 2004), for our study. LPJ-GUESS is a mechanistic model in which ecosystem processes are simulated via explicit equations and is optimised for regional to global applications (Smith et al., 2001; Sitch et al., 2003; Gerten et al., 2004). Vegetation dynamics are simulated as the emergent outcome of growth, reproduction, mortality and competition for resources among woody plant individuals and herbaceous vegetation.

The simulation units in this study are plant functional types (PFTs) distinguished by their growth form, phenology, photosynthetic pathway (C_3 or C_4), bioclimatic limits for establishment and survival and, for woody PFTs, allometry and life history strategy. The simulations of this study were carried out in 'cohort mode,' in which, for woody PFTs, cohorts of individuals recruited in the same patch in a given year are represented by a single average individual, and are thus assumed to retain the same size and form as they grow. A sample instruction file used to run LPJ-GUESS in this study with all the parameters listed can be found under github.com/istfer/ENSOpaper/ins.

Primary production and plant growth follow the approach of LPJ-DGVM (Sitch et al. 2003). Population dynamics (recruitment and mortality) are influenced by available resources and environmental conditions, and depends on demography and the life history characteristics of each PFT (Hickler et al. 2004). Disturbances such as wildfires are simulated based on temperature, fuel load and moisture availability (Thonicke et al. 2001). Litter arising from phenological turnover, mortality and disturbances enters the soil decomposition cycle. Decomposition rates depend on soil temperature and moisture (Sitch et al. 2003). Soil hydrology follows Gerten et al. (2004). A more detailed description of LPJ-GUESS is available in Smith et al. (2001). We used LPJ-GUESS version 2.1 which includes the PFT set and modifications described in Ahlström et al. (2012). LPJ-GUESS has already been successfully applied and validated to match present-day and mid-Holocene biome distributions of East Africa as suggested by data for both periods (Fer et al., 2016).

4.2.2 Datasets Tracking ENSO and regional vegetation

To isolate the ENSO signal contribution to East African precipitation, we conducted an Empirical Orthogonal Teleconnections (EOT) analysis between sea surface temperatures (SSTs) in the tropical pacific ocean and precipitation over East Africa (see section *Identifying the ENSO signal*). For historical extraction (1951-2005), we use monthly National Oceanic and Atmospheric Administration Extended Reconstructed Sea Surface Temperature (NOAA ERSST) V4 dataset (Huang et al., 2014; Liu et al., 2014), available on 2ºx2º global grids as a predictor field. As the response series, we used monthly Climatic Research Unit Time Series (CRU TS) 3.20 dataset (Harris et al., 2014), available on 0.5ºx0.5º global grids.

4.2.2.1 LPJ-GUESS datasets

LPJ-GUESS requires monthly climate (temperature, precipitation, cloud cover), atmospheric CO_2 concentration and soil texture as input data. For historical period (1951-2005), we used monthly CRU TS 3.20 climate data. We chose these years for all historical analysis throughout the study as the historical simulations of CORDEX outputs are available for this period. For future projections (2006-

2100), we used the outputs from the Coordinated Regional Climate Downscaling Experiment (CORDEX) program for the Africa domain. For reporting historical (1951-2005) and future (2006-2100) period, we adhered to the CORDEX division of years for interpretability and reproducibility reasons. For the future scenario, we chose the baseline high emissions Representative Concentration Pathways (RCP) 8.5 scenario under the assumption that climate mitigation targets will not be met (Moss et al., 2010; Riahi et al., 2011). CORDEX, downscaled global climate models (GCMs) by using regional models, and the outputs are available from ESGF-CoG data portal (https://esgf-node.llnl.gov/search/esgf-llnl/). For East African climate, we took the ensemble mean of 9 models for future projections of RCP 8.5 scenario as these are the available, dynamically downscaled climate model outputs by the CORDEX project: CCCma CanESM2, CERFACS CNRM-CM5, QCCCE CSIRO Mk3-6-0, ICHEC EC-EARTH, IPSL CM5A-MR, MIROC5, MPI ESM-LR, NCC NorESM1-M, NOAA GFDL-ESM2M (Full names of the models are given in the Appendix). Instead of working with individual models we decided to drive our simulations with ensemble means as it has been shown to outperform individual models and show a better agreement with data (Endris et al., 2013). RCP 8.5 compatible atmospheric CO_2 values were also used as provided by NOAA – GISS experiment (Nazarenko et al., 2015).

4.2.2.2 Bias correction

To eliminate biases originating from using CRU climate dataset for present and model simulations for future, we subtract the 1951-2005 climatology of downscaled GCM ensemble from the 1951-2100 time series of the ensemble and add the anomalies on CRU 1951-2005 climatology. This way we will able to have a meaningful comparison between CRU-driven and GCM-driven vegetation model outputs while keeping the climate variability from the GCM simulations. We should note here, that this would not change the ENSO signal we will retrieve from the GCM outputs (see next section) because we de-season and work with anomalies of the data field for our EOT analysis.

4.2.2.3 Future Pacific SSTs

For future pacific SSTs, we used outputs from GCM simulations of the same models listed above for RCP 8.5, except ICHEC EC-EARTH which was not available from the data portal at the time. However, these GCM outputs were not downscaled and standardized in terms of spatial resolution (they were all available in monthly time steps in terms of temporal resolution). We created raster files from these outputs and using the "raster-package" (R Core Team, 2015; v2.5-8), we resampled these rasters to brought them to the same spatial resolution as NOAA ERSST V4 dataset, and we took the ensemble mean.

4.2.3 Identifying the ENSO signal

Here we first identify the ENSO signal as a driver for monthly East African precipitation variability over the historical period (1951-2005). To do this we investigate the teleconnectivity between the SSTs in the tropical Pacific Ocean and precipitation over East Africa by using empirical orthogonal teleconnections (EOT). The method is explained by van den Dool et al. (2000) in detail, and Appelhans et al. (2015) implemented the original algorithm in R ('remote' package by Appelhans et al., 2015; R Core Team, 2015). Here, we only briefly present the major steps of the EOT analysis:

4.2.3.1 Empirical Orthogonal Teleconnections (EOTs)

In the EOT analysis, we aim to establish an explanatory relationship between the temporal dynamics of a (predictor) domain and temporal variability of another (response) domain. Such predictor and response domains consist of gridded time series profiles: in this study the gridded monthly SST time series of the tropical pacific as predictor and gridded precipitation time series of East Africa as the response. Then, the first step of EOT analysis is to regress these time series of each predictor domain grid (N_p) against the time series of each response domain grid (N_r) (Appelhans et al., 2015). This will result in a (N_p x N_r) number of regression fits after which we can calculate the sum of coefficients of determination per predictor grid (ending up with N_p sum of coefficients of determination values). Then, the grid with the highest sum will be identified as the

"base point" of the leading mode as it explains the highest portion of the variance in the response domain (Appelhans et al., 2015). The time-series at this base point is referred as the leading teleconnection, or hereafter as the first EOT.

4.2.3.2 Screening for ENSO signal

We applied the EOT method on de-seasoned and de-noised data fields in order to retrieve a low frequency signal such as ENSO: here we used the SSTs in the tropical pacific ocean as predictor and precipitation over East Africa as response. Then we proceeded to calculate the SSTs modes that are most affecting for East African rainfall variability. We found the 1st EOT to be the ENSO signal. We compared this EOT with Nino3.4 index to see whether we were able to isolate the ENSO signal. The commented code used for all methods is publicly available on Github (github.com/istfer/ENSOpaper).

Before moving on to identifying future pacific sea surface temperature – East African precipitation interactions, we applied the same extraction to historical GCM outputs (simulations) to see whether we can identify a similar relationship from GCM products. Finally, we prepared the model drivers with the modified ENSO signal we identified from the future simulations (see next section) and ran the model with these datasets (here we focused on precipitation data only, while precipitation varies in these simulations and the others -temperature- were kept as they were in the climate datasets: present – CRU TS 3.2, future – CORDEX ensemble de-biased using CRU as explained above).

4.2.4 Removing and intensifying the ENSO signal

In order to investigate the contribution of the ENSO signal to East African precipitation, we removed the ENSO signal and explored the rainfall pattern with and without ENSO contribution as well as the resulting vegetation changes calculated by LPJ-GUESS. We used the "remote" package which specifically implements the EOT analysis and keeps track of calculated values in a structured workflow: The rainfall we are left with after removing the first EOT mode (which we identified as the ENSO signal) becomes the rainfall behaviour without ENSO contribution (within the 'remote' package, this calculation of the residuals is

automatically available after the calculation of the EOT modes). Therefore, if we take the difference between these residuals and the initial de-seasoned and de-noised data, this will give us the amount that we need to subtract from the raw data field to obtain the rainfall behaviour without ENSO contribution. The steps are explained below as pseudocode:

i) Deseason and denoise the response and predictor fields.

$EA_{r,\ ds,\ dns}$: East African precipitation (response domain). Subscripts indicate raw, deseasoned, deseasoned and denoised respectively.

$PAC_{r,\ ds,\ dns}$: Tropical Pacific Ocean Sea Surface Temperatures (SSTs) (predictor domain). Subscripts indicate raw, deseasoned, deseasoned and denoised respectively.

$$EA_{ds} = \text{deseason}(EA_r) \quad PAC_{ds} = \text{deseason}(PAC_r) \tag{1}$$

$$EA_{dns} = \text{denoise}(EA_{ds}) \quad PAC_{dns} = \text{denoise}(PAC_{ds}) \tag{2}$$

ii) Conduct Empirical Orthogonal Teleconnection (EOT) analysis:

$$EOT_{modes} \leftarrow EOT(EA_{dns} \sim PAC_{dns}) \tag{3}$$

Here the EOT_{modes} object can be thought as a list that stores both the time series of the modes, the reduced fields obtained after the removal of each mode, slopes and intercepts of the fields (for more details see Appelhans et al., 2015).

iii) Calculate the difference (*Diff*) between the de-seasoned, de-noised data (EA_{dns}) and the rainfall behaviour without ENSO contribution from the information that is already stored in the resulting EOT_{modes} object (ENSO signal is the first mode, therefore the rainfall behaviour we are left without ENSO will be the $EA_{modes,\ rr1}$ where subscript *rr1* indicating "response residual" after the removal of the first EOT mode:

$$Diff = EA_{dns} - EA_{modes,\ rr1} \tag{4}$$

iv) If we subtract this difference from the initial raw response field (EA_r), we will obtain the East African precipitation without ENSO contribution ($EA_{r,\ woENSO}$):

$$EA_{r,\ woENSO} = EA_r - Diff \tag{5}$$

v) As EOT analysis is basically a regression analysis, we can also obtain the ENSO contribution (*Diff*) from the regression equation as shown below (which will become handy when we insert back the intensified ENSO signal):

$$Diff = EOT_{modes,\ eot\_1} * EOT_{modes,ri\_1} - EOT_{modes,\ rs\_1} \tag{6}$$

Here $EOT_{modes,\ eot\_1}$, EOT_{modes,ri_1} and $EOT_{modes,\ rs\_1}$ refer to the EOT time series of the 1st mode (the ENSO signal), intercept of and slope of the response field calculated for the 1st mode (Appelhans et al., 2015).

vii) Then, it is possible to modify the future ENSO signal ($EOT_{modes,\ eot\_m}$) obtained from EOT analysis on simulation datasets, re-calculate its contribution to the East African rainfall ($Diff_{new}$) and add this amount back on the precipitation data without ENSO signal ($EA_{r,\ woENSO}$) to obtain new precipitation amounts ($EA_{r,\ new}$) due to new signal. We can later use this $EA_{r,\ new}$ as the future precipitation input to our vegetation model to drive future simulations.

$$Diff_{new} = EOT_{modes,\ eot\_m} * EOT_{modes,ri\_1} - EOT_{modes,\ rs\_1} \tag{7}$$

$$EA_{r,\ new} = EA_{r,\ woENSO} + Diff_{new} \tag{8}$$

Here it is noticable that slope(s) and intercept(s) would also have been different if the ENSO signal was changes ($EOT_{modes,\ eot\_m}$). However, this simplification is adequate for experiments in this paper. Moreover, we used the intercept and slope we retrieved from the EOT analysis on observational datasets while re-calculating the new difference ($Diff_{new}$) due to intensified ENSO signal. Because the East African rainfall patterns explained by Tropical Pacific SSTs in the GCM simulations are different from observations (Figure C1 and C2). By using slopes and intercepts obtained from the observational data we were also able to preserve the more accurate patterns in rainfall differences.

viii) Finally, we obtained the modified ENSO signal ($EOT_{modes,\ eot\_m}$) in Eq. (7) by detrending (fitting a LOWESS smoother and removing it from the signal) and multiplying the ENSO signal we extracted from the future simulations (deseasoned and denoised GCM simulations for East African rainfall – EA_{dns_ftr} - and Tropical Pacific SSTs - PAC_{dns_ftr} -) with a coefficient (k = 3) such that the peaks of the new signal would be as strong as the observed anomalies (± 2.5 °C, Figure 4.1 and C3). For the code of this step see IdentifyModifyFutureENSO.R script at github.com/istfer/ENSOpaper.

$$EOT_{modes\_ftr} \leftarrow EOT(EA_{dns\_ftr} \sim PAC_{dns,\ ftr}) \quad (9)$$

$$EOT_{modes,\ eot\_m} \leftarrow k \times \text{detrend}(EOT_{modes\_ftr,\ eot\_1}) \quad (10)$$

4.3 Results

4.3.1 EOT analysis – extracting the ENSO signal

We compared the first EOT mode extracted after de-seasoning and de-noising the fields as explained by Appelhans et al. (2015) to the Nino-3.4 index recorded (Figure 4.1). The high correlation between the two (R = 0.90) confirms that we were able to extract the ENSO signal by conducting the EOT analysis. On the predictor domain (Tropical Pacific SSTs), the Nino-3.4 region found to be the area which explains the most variance in the response domain (East African precipitation) as expected (Figure C1). The time series of the first EOT explains 0.85% of the rainfall variability over the analyzed period here (1951-2005). This small amount is not surprising, because East African precipitation follows a strong seasonal pattern following the position of the Intertropical Convergence Zone (ITCZ) within the year. Therefore, seasonality alone explains most of the variability in East African rainfall. In addition, due to the complex topographical setting of the region, local conditions play a major role in the variation of the rainfall. Still, when we de-season and de-noise the raw data fields to identify low-frequency signals such as ENSO, the ENSO signal emerged as the most important teleconnection between tropical pacific SST anomalies and East African precipitation.

Having successfully extracted the ENSO signal from the observation datasets, we applied the same procedure with the outputs of the climate models. We used an ensemble of SSTs from 8 GCM outputs as the predictor field and an ensemble of rainfall from 9 GCMs downscaled by CORDEX as the response domain. The comparison between the calculated first EOT time series to the Nino-3.4 index observed was much poorer (R=0.19) (Figure 4.1) which indicates that GCMs are not capturing the coupled Pacific SST – East African rainfall teleconnection. Another striking feature that can be observed in Figure 4.1 is the smoothness of the time series of the 1st mode calculated from the EOT analysis on ensembles of climate model outputs when compared to the recorded index and the calculated ENSO signal from the observation datasets. In other words, the ENSO signal retrieved from the EOT analysis on the climate model outputs is nowhere near strong as the others. According to this signal obtained from the simulation datasets, the only ENSO events that happened during 1951-2005 period were in the "weak" category (Figure 4.1). Finally, the calculated patterns were different than the EOT analysis on observed datasets (the corresponding figure is given in the Appenix, Figure C2): The areas where the sum of the coefficients of determination were the highest were again situated around Nino 3.4 region but closer to the Nino 4 region this time (Figure C2 – left panel). Spatially, the north-eastern and central parts of the response domain are the most explained whereas previously it was more centralized around the coastal equatorial parts of the region (Figure C2 – right panel).

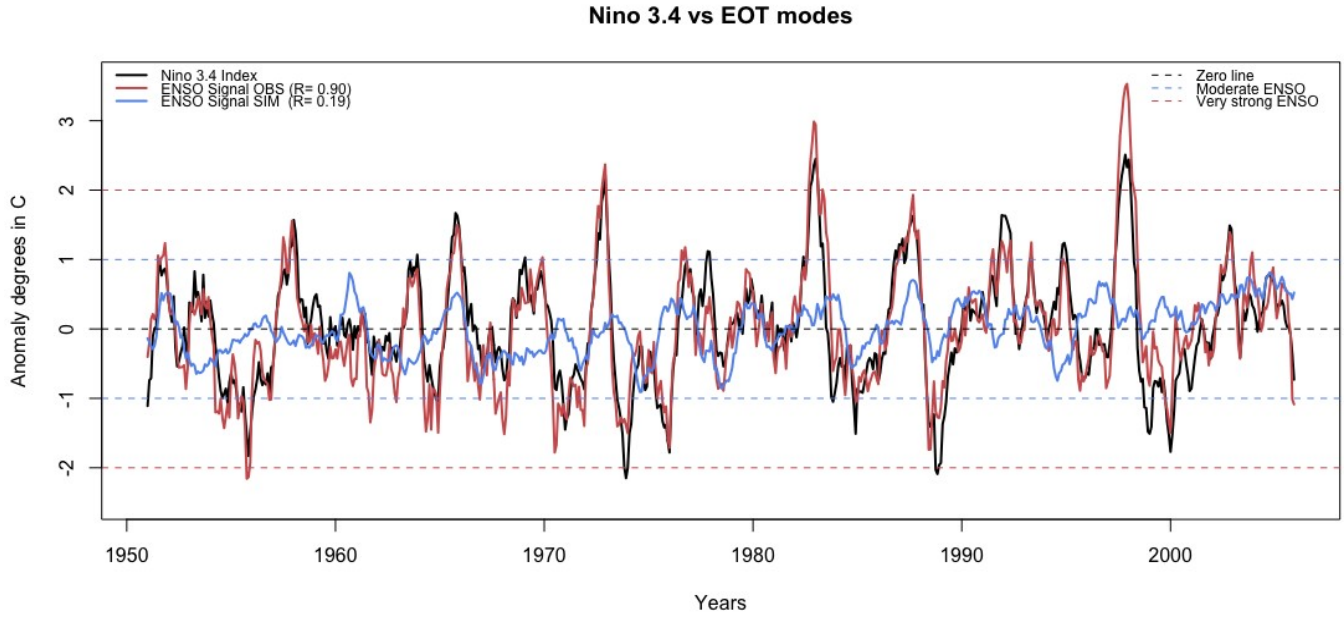

Figure 4.1. The comparison between Nino 3.4 Index recorded by NOAA (black line), time series of the 1st mode obtained from the EOT analysis on observed CRU-NOAA datasets (red), and time series of the 1st mode obtained from the EOT analysis on ensembles of the climate model simulations (blue). Black dashed line: Zero line. Blue dashed lines ± 1.0° anomaly thresholds for categorizing moderate ENSO events. Red dashed lines: ± 2.0° anomaly thresholds for categorizing very strong ENSO events.

4.3.2 Historical simulations with and without the ENSO signal

After calculating the ENSO signal, we removed the amount due to ENSO from the East African precipitation (CRU precipitation), and simulated East African vegetation using both datasets (CRU_{normal} and $CRU_{without\_ENSO}$) to see its effect on vegetation. As it can clearly be seen from Figure 1, impact of ENSO signal is not the same everywhere on the East African domain, which means removing ENSO signal would have differential effects on the rainfall amount. Regional maps of rainfall anomalies for the strongest three El Niño (1972, 1982, 1999) and La Niña (1973, 1975, 1988) events between 1951-2005 period are given in Figure 4.2. Here we show what the rainfall would be if there were not any influence by the Pacific SSTs particularly during these three years. Especially the coastal Kenya and Tanzania experience a strong change in the amount of rainfall they receive:

During the El Niño periods, these parts of East Africa receive up to 200 mm yr^{-1} more rain other than they would receive, while they receive ~100 mm yr^{-1} less rain during the La Niña years. The impact is the opposite for western part of Ethiopia : receiving ~200 mm yr^{-1} less rainfall during El Niño years, while ~100 mm yr^{-1} more during La Niña years. To provide a closer look to the impacts of ENSO related variability on vegetation, we report the results on vegetation simulations within the two transects where we see the strongest impacts over these two oppositely behaving, coastal and northwestern, regions (Figure. 4.2).

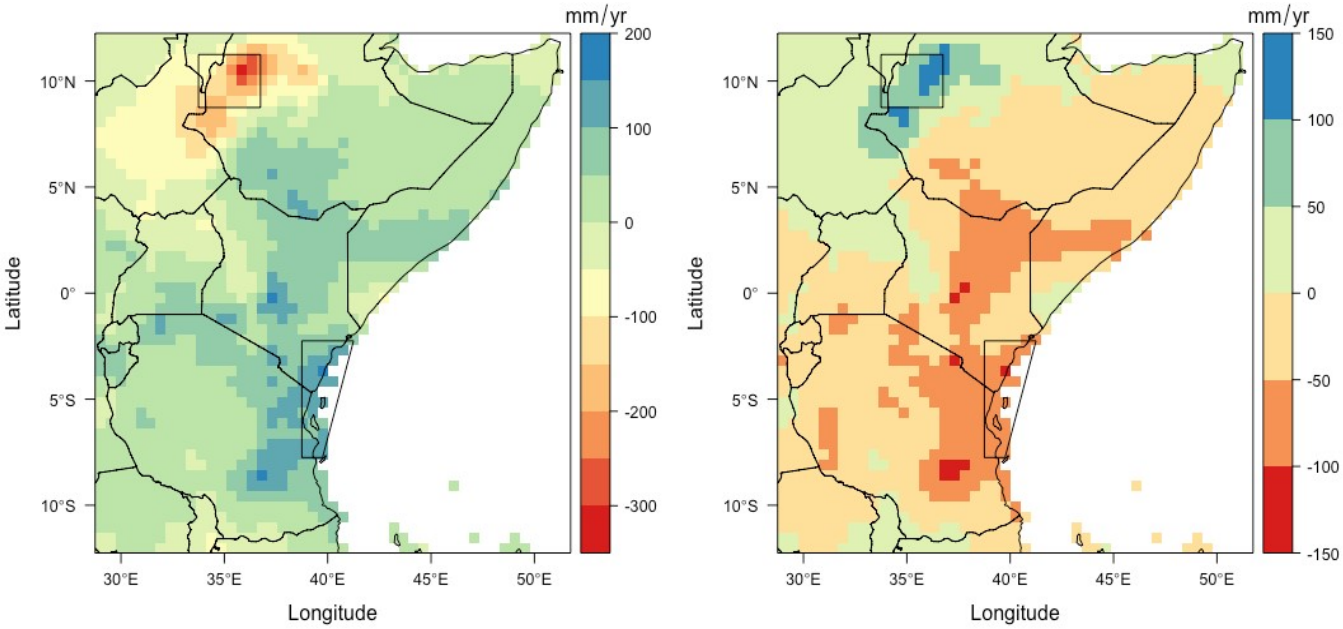

Figure 4.2. Regional maps of anomalies (mm yr^{-1}) for the strongest three (1972, 1982, 1997) El Niño (left) and (1973, 1975, 1988) La Niña (right) events between 1951-2005 period (anomalies were calculated by subtracting precipitation without ENSO contribution from precipitation with ENSO contribution). Northern inner and southern coastal transects chosen for reporting results on vegetation simulations.

We drove the dynamic vegetation model once with CRU dataset as is and once with CRU dataset with removed ENSO contribution. Results are reported for the previously mentioned north and south sites in Figure 4.3 and Table 4.1. Outputs from the northern-inner part show more variability within the chosen grid-cells for this region. Indeed, this region is on the western edge of Ethiopian Plateau, with a transition of biomes from mountainous forests to woodlands and savannas (Fer et al., 2016). As the rainfall patterns in relation to ENSO signal was the opposite between these regions (Figure 4.2), we expect to see that the response of these

regions to the removal of the ENSO signal to be opposite, and this is indeed what we see in Figure 4.3: While outputs such as net primary productivity (NPP), net ecosystem exchange (NEE), soil evapotranspiration (EVAP) and surface runoff (RUNOFF) for northern site were less than otherwise they would be for El Nino events, they would be higher La Nina events. And the opposite behaviour is true for the southern site.

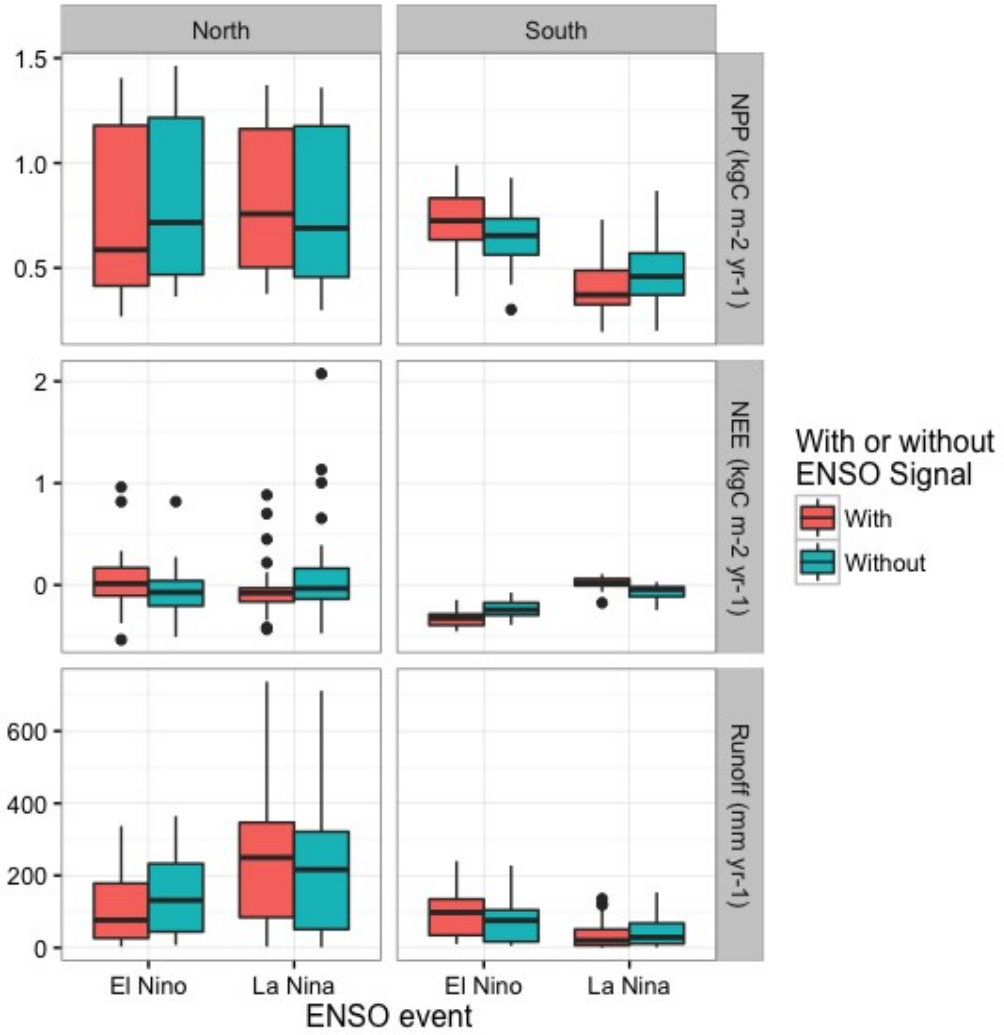

Figure 4.3. Carbon and water fluxes from north and south transects, simulated under climate with and without ENSO contribution, for the strongest three (1972, 1982, 1997) El Niño and (1973, 1975, 1988) La Niña events between 1951-2005 period. Top panel: Net Primary Productivity (NPP). Middle: Net Ecosystem Exchange (NEE). Bottom: Total runoff. Locations of the northern-inner and southern-coastal sites are given in Figure 2.

In order to test whether the difference between the vegetation simulated under climate with ENSO contribution, and the vegetation simulated under climate with

removed ENSO contribution, we conducted a paired t-test on the outputs. The results (Table 4.1) show that except NEE for northern sites, all differences between the vegetation simulated with and without ENSO impact were significant. In summary, ENSO contribution is significantly affecting the East African vegetation and we would expect different vegetation if there were no ENSO events.

Table 4.1. Paired t-test results to test whether there is a significant difference in the vegetation simulations that are driven with and without ENSO contributions for the three strongest ENSO events during the historical period (1951-2005) and with and without intensified ENSO signal for the strongest ENSO events during the future period (2006-2100). Grey highlighted cells indicate insignificant differences according to p=0.05 threshold. Significant p-values indicate rejection of the H_0 in favor of the alternative, that is true difference in means is not equal to 0. p: p-value, md: mean of the differences

NPP: Net Primary Productivity, NEE: Net Ecosystem Exchange, RUNOFF: Surface runoff). Location of North (N) and South (S) sites are shown on Figure 2.

		NPP ($kgC\ m^{-2}\ yr^{-1}$)		RUNOFF ($mm\ yr^{-1}$)		RUNOFF ($mm\ yr^{-1}$)	
		El Niño	La Niña	El Niño	La Niña	El Niño	La Niña
Historical	**N**	p < 0.05 md: -0.056	p < 0.05 md: 0.035	p = 0.089	p = 0.1	p < 0.05 md: -41.35	p < 0.05 md: 22.21
	S	p < 0.05 md: 0.084	p < 0.05 md: -0.074	p < 0.05 md: -0.088	p < 0.05 md: 0.087	p < 0.05 md: 19.41	p < 0.05 md: -10.74
Future	**N**	p < 0.05 md: -0.052	p < 0.05 md: 0.033	p = 0.93	p = 0.58	p < 0.05 md: -10.91	p < 0.05 md: 46.97
	S	p < 0.05 md: 0.049	p < 0.05 md: -0.101	p < 0.05 md: -0.113	p < 0.05 md: 0.173	p < 0.05 md: 5.66	p = 0.06

4.3.3 Future simulations with and without the intensified ENSO signal

We conducted the same paired t-test for the north and south sites for the future simulations (Table 4.1). In the northern site where intensified signal leads to less (more) NPP during El Niño (La Niña) years, the mean difference is -52 (+32.6) gC m^{-2} yr^{-1} between the vegetation simulated under future climate with and without intensified ENSO signal. In the southern site where intensified signal leads to more (less) NPP during El Niño (La Niña) years, the mean difference is +49.1 (-101.1) gC m^{-2} yr^{-1} between the vegetation simulated under future climate with and without intensified ENSO signal. While the mean differences for NEE were not significant at the northern site, southern site stores 112.7 (173.1) gC m^{-2} yr^{-1} more (less) carbon under the intensified ENSO scenario during the El Niño (La Niña) years.

Another noteworthy output is that, the northern site has a lot more runoff during the La Niña years under the intensified ENSO scenario. This is especially clear on Figure 4.4 where spatial patterns of the differences in the simulated future vegetation under RCP 8.5 scenario with and without intensified ENSO are shown. The opposite behaviour of the northern parts of East Africa under El Niño vs. La Niña conditions can also be observed on NPP and RUNOFF figures, wheres for NEE differences a particular pattern is not emergent. This is mainly because NEE values can themselves be negative (flux to ecosystem) and positive (release to atmosphere).

The opposite temporal behaviours of the northern and southern transects are also clear in Figure 4.5 which shows the time series of the differences between simulated NPP, NEE and RUNOFF under climate drivers with and without intensified ENSO signal. In line with the characterized behaviours above, we simulated higher (lower) NPP for the southern transect (red line) for the El Nino (La Nina) years under the intensified scenario, whereas the opposite is true for the northern transect (black line). The higher amplitude of RUNOFF difference for the northern transect is notable in the bottom panel (Figure 4.5).

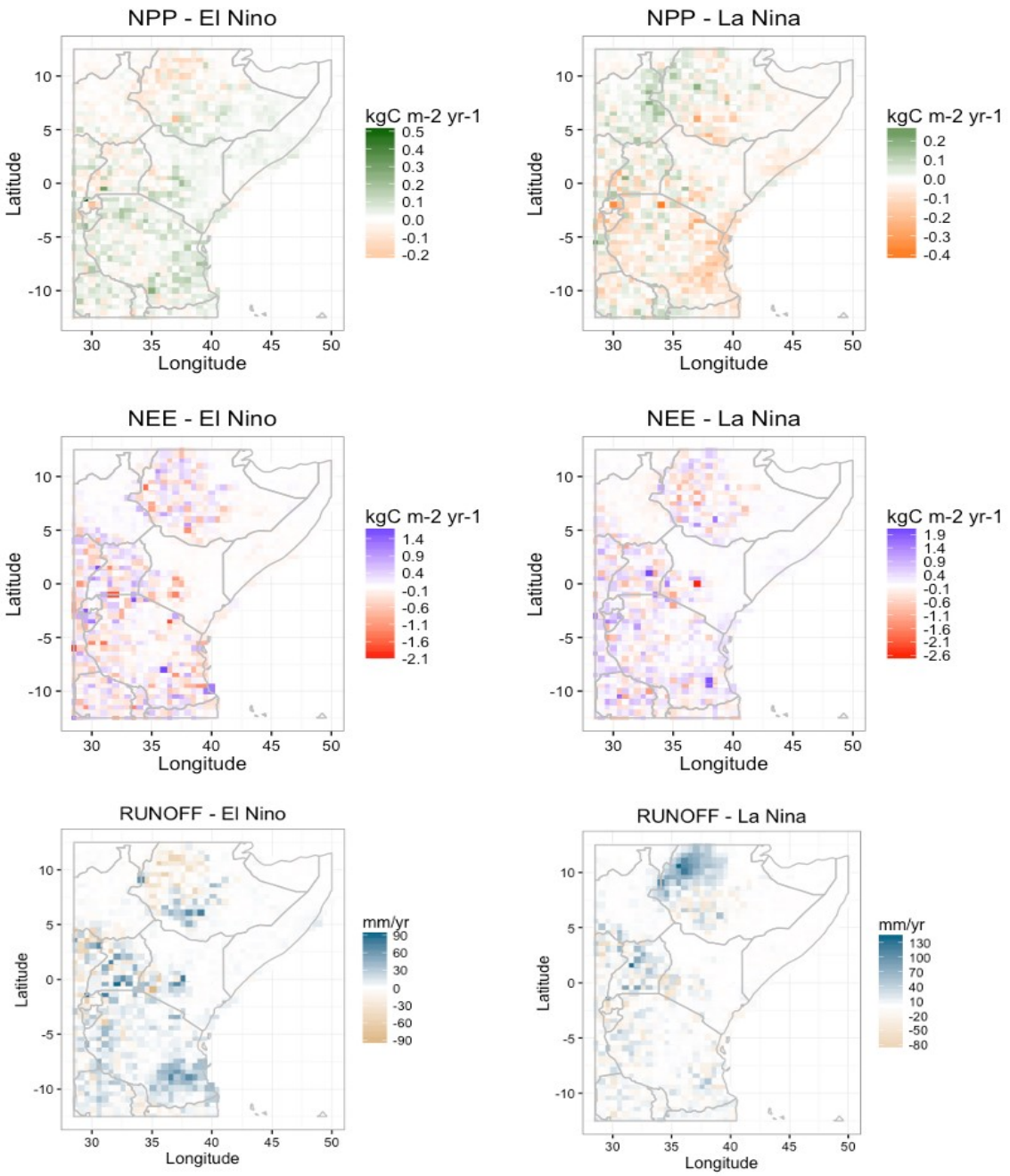

Figure 4.4. Simulated future differences in the NPP, NEE and RUNOFF between with and without intensified ENSO runs. (Left) Mean differences for the strong El Nino years (≥ + 1.5°C) (2025, 2026, 2077) were calculated by subtracting the GCM-ensemble driven simulations without modification from the GCM-ensemble driven future simulations with intensified ENSO signal. (Right) Same for strong future La Nina events (≤ – 1.5°C) (2039, 2049, 2084).

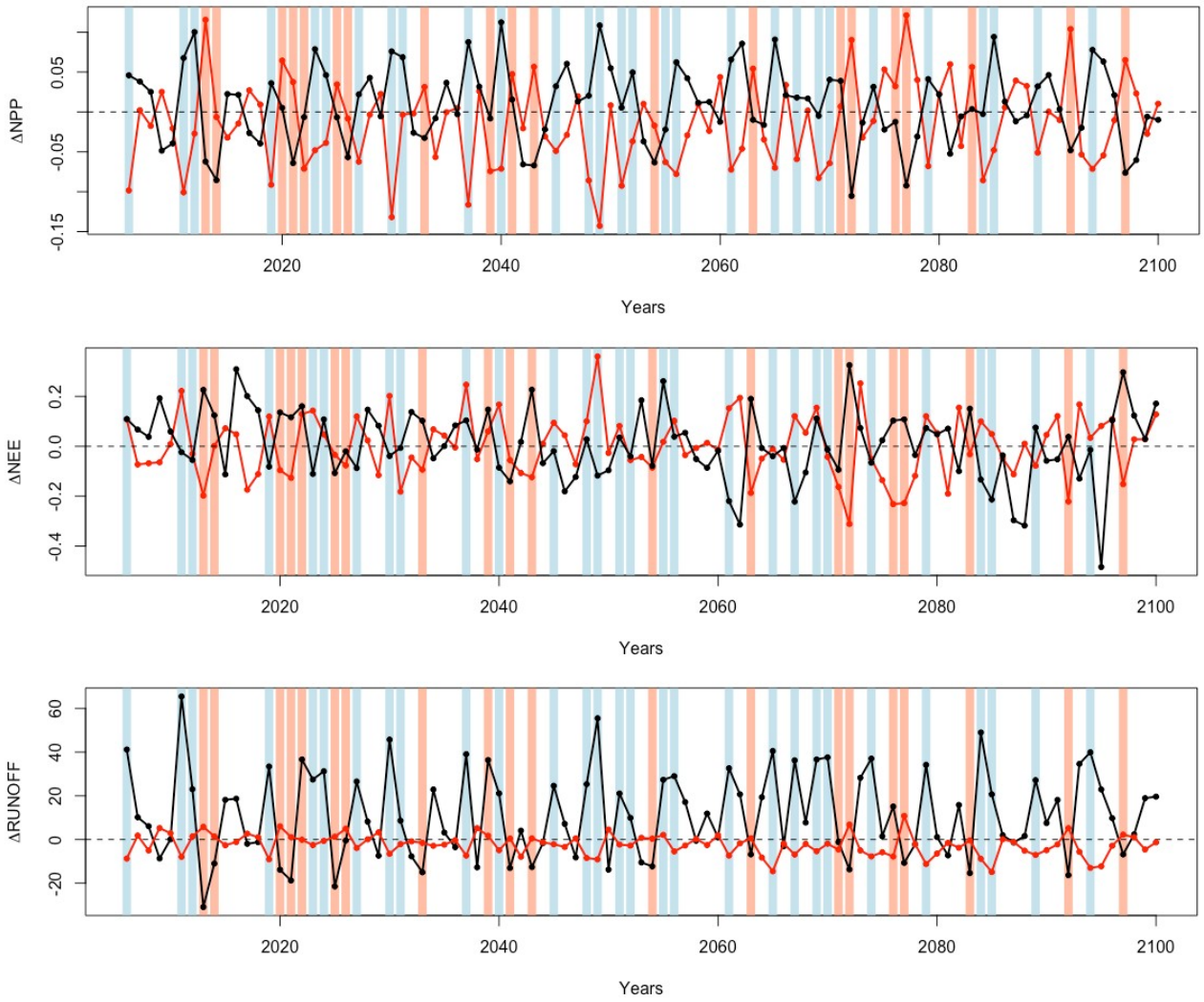

Figure 4.5. Temporal differences in the NPP, NEE and RUNOFF according to future simulations with and without intensified ENSO contribution (Δ = With_Intensification - Without_Intensification). Black line: Northern transect, Red line: southern transect. Vertical blue lines: All moderate (< -1.0° C) La Nina years identified for the future period (2006-2100), Vertical pink lines: Moderate (> 1.0° C) El Nino years. The units are same as Figure 4.

4.4 Discussion

4.4.1 Identifying and intensifying the ENSO Signal

East African rainfall variability and especially contribution of the ENSO was investigated before (Indeje et al., 2000; Schreck and Semazzi, 2004). Here we used a different method, Empirical Orthogonal Teleconnections (EOT) analysis to quantitatively calculate the ENSO contribution and found the spatial correlation patterns over the East Africa region to be in agreement with previous studies who independently looked at Pacific SST drivers for East African precipitation (Anyah

and Semazzi, 2007). The ENSO signal identified through this method was also showing strong correlation with NOAA Nino3.4 index, which means EOT method was a suitable choice for our analysis.

Using the EOT method, we presented a relatively conservative estimate of ENSO variability in East African rainfall, because we considered the direct Tropical Pacific teleconnection only. However, there are accompanying changes: ENSO events are linked to Indian Ocean Dipole, which more directly influences EA rainfall (Black et al., 2003). It has been suggested that subsequent to ENSO triggering, internal Indian Ocean dynamics could take over. More specifically, East African rainfall increases as the western Indian Ocean gets warmer which is often associated with ENSO forcing. However, warmer western Indian Ocean can weaken the rains when it interacts with southeasterly atmospheric circulations (Schreck and Semazzi, 2004). The exact relationship and discrepancies between IOD and ENSO behaviours are yet to be revealed (Lim et al. 2016). Still, we found that the ENSO-East Africa connection to be robust as previous studies (Indeje et al., 2000; Anyah and Semazzi, 2007) and did not delve into IOD relationship. Also, we were motivated by the previous studies that have identified ENSO influence to be important in dryland vegetation dynamics (Ahlström et al., 2015; Abdi et al., 2016). Hence, we focused on reporting more comparable results with those. Another factor that could affect our estimations is atmospheric latency. In our analysis, we did not consider any time lags for the tropical pacific SST anomalies and East African precipitation teleconnection, but a time lag can be expected due to atmospheric circulation processes, and the influence of SST anomalies might not develop instantaneously. Therefore if we account for this time lag, we might explain even more of the rainfall variance. For a more comprehensive study of SST influences on East African rainfall see Appelhans and Nauss (2016).

The EOT method, which is shown here to be effective on the historical observations, produced different East African rainfall variability patterns due to Pacific SSTs when GCM outputs were used. Also the ENSO signal retrieved was much weaker than the one extracted from the observation datasets in terms of both ENSO event strength and the match (correlation) with the Nino 3.4 index. As a preliminary investigation (not shown), we conducted the EOT analysis across

mixture of observed-simulated datasets: Pacific $SSTs_{observed}$ (NOAA ERSST) - East African $precipitation_{simulated}$ (CORDEX), and Pacific $SSTs_{simulated}$ (GCMs) - East African $precipitation_{obsrved}$ (CRU). The ENSO signal retrieved from the Pacific $SSTs_{observed}$ - East African $precipitation_{simulated}$ pair was a better match with Nino 3.4 index than the one extracted from the simulated-simulated pair but still worse than the one extracted from observed-observed dataset pair, whereas ENSO signal retrieved from the Pacific $SSTs_{simulated}$ - East African $precipitation_{obsrved}$ pair was not a better match to Nino 3.4 index than the one extracted from the simulated-simulated pair. This quick test indicated that the GCM simulated Tropical Pacific SSTs are the main source of the poor teleconnection identified from the simulated-simulated pair and a dynamic downscaling of the tropical Pacific SSTs might improve the ocean-atmosphere coupled teleconnection. However, more formal tests are needed to conclude on this matter, which was beyond the scope of this study.

4.4.2 Present-day simulations

Despite the fact that our estimation of ENSO contribution to the East African interannual rainfall variability was conservative, the precipitation difference between with and without ENSO contribution was equivalent to one or even two rainy months for some of the grid cells. These regions already receive a small amount of rainfall and even minor differences are critical for agricultural food production and the productivity of the natural ecosystem that sustains a large biodiversity. We found up to 0.1 kgC m^{-2} yr^{-1} mean difference in NPP in the southern parts of the region solely due to ENSO contribution.

We found that ENSO influence on net ecosystem exchange is also prominent in the semi-arid ecosystems of East Africa. Especially, in southern-coastal parts, ecosystem releases more to the atmosphere during La Nina events whereas it would store more carbon otherwise. This would also have implications on global carbon cycle as it has previously been found that regional response of semi-arid ecosystems, mainly occupying low latitudes, play an important role in determining the trend in CO_2 uptake by terrestrial ecosystems (Ahlström et al. 2015). For instance, La Nina events are associated with large carbon sinks in Australian semi-arid ecosystems due to increased precipitation and 2011 anomaly

in global carbon sink was mainly attributed to the response of Australian ecosystems (Poulter et al., 2014). While semi-arid ecosystems of East Africa might play a smaller role than Australian ones (simply due to the difference in the area they cover), it would still influence the magnitude and trend of the global carbon sink by terrestrial ecosystems. Furthermore, Forzieri et al. (2017) report the importance of the interplay between vegetation cover (in terms of Leaf Area Index, LAI) and surface biophysics, finding an amplification of their relationship under extreme warm-dry and cold-wet years. Here we found that the ENSO contribution impacts the temporal LAI variability in East Africa considerably (Figure C5), presenting a good example of such temporal variations that can play significant roles in modulating key vegetation-climate interactions. According to the analysis by Forzieri et al. (2017), the magnitudes of differences we found in our study due to accounting for an intensified ENSO signal are influential on the surface energy balance components such as longwave outgoing radiation, latent heat flux and sensible heat flux. Our findings reiterate the importance of considering ENSO contribution in carbon and energy budget calculations for any region that is influenced by ENSO variability.

Here we also report ENSO influence on surface runoff as excess runoff response causes problems in East Africa. In this region, Rift Valley Fever (RVF) and Malaria outbreaks are threatening the livelihood of the society and these vector-borne diseases are transmitted by mosquitoes who breed in flooded low-lying habitats (Meegan and Bailey, 1989, Kovats et al., 2003, Hope and Thomson, 2008). For example, a major RVF outbreak during late 1997 to early 1998 has been linked to the heavy and prolonged rains that are associated with 1997-98 El Nino event (Trenberth, 1998), in agreement with our results where we found that the southern coastal site experiences higher runoff during El Nino events than otherwise it would do.

Another important ecological factor to be considered for East African vegetation dynamics is fire. The fire occurrence in LPJ-GUESS depends on the atmospheric temperature values, and moisture and litter availability. Therefore, although we did not calibrate LPJ-GUESS fire parameters for East Africa or explicitly changed fire regimes under any of the scenarios, the model simulated the changes in fire behaviour due to different environmental states implicitly. More specifically, for

the southern coastal part, a higher mean expected return time of fire was simulated during the El Nino years for simulations with ENSO contribution than without due to higher moisture availability during ENSO years for this region (not shown). For the same site, the opposite was true for La Nina years, and the whole behaviour was reversed for the northern site. A more sophisticated fire – ENSO – vegetation interplay can be further investigated using models that have an individual level representation of fire response such as aDGVM2 (Scheiter, Langan and Higgins, 2013).

In this study, we did not further calibrate the LPJ-GUESS PFT parameters as it has been calibrated and validated for the region by previous studies (Doherty et al., 2010, Fer et al., 2016). It is possible that these point estimate values do not capture the uncertainties associated with the PFT parameters. However, previous studies have shown LPJ-GUESS parameters to be robust (Zaehle et al., 2005; Doherty et al., 2010). Besides, as we used the same set of parameters for all runs, the discrepancies simulated with and without ENSO contribution would still hold. As LPJ-GUESS spins up from bare ground, we also do not expect much uncertainty influencing the model predictions with and without ENSO contribtuion due to initial conditions. On the other hand, we expect the driver uncertainty to dominate the uncertainty around model predictions. However, that is exactly what we aimed at to quantify in this study as being discussed in the following sections.

4.4.3 Scenario selection and future simulations

In the results for the future simulations, the total surface runoff and NPP responses were considerably underestimated. Under the intensified ENSO scenario, an excessive amount of runoff is simulated for the northern parts during La Nina years and for the southern parts during El Nino years, which would exacerbate the disease events in the region. Likewise, the simulated low amounts of runoff for the northern parts during El Nino years indicate drought events in this parts of the region. This effect can also be seen in the simulated NPP responses which reduces considerably for the northern parts during El Nino years. Furthermore, the amounts we calculated here agree well with previous studies

showing changes in NPP supply associated with ENSO events in sub-Saharan African drylands (Abdi et al., 2016).

The regions identified to be impacted by ENSO the most, are also the regions that currently undergo the highest woody vegetation decrease and human population increase in East Africa according to the analysis by Brandt et al. (2017). In our future simulations, we simulated increase in woody vegetation LAI due to climate change (Figure A4) in those regions of East Africa. It requires further analysis to say whether this anthropogenic reduction in woody vegetation could be met by future climate and atmospheric CO_2 related increase. However, it reinforces the essentiality of accounting for ENSO influence as independent analyses show increasing stress over this region.

In this study, we chose RCP8.5 as our future warming scenario for two reasons: i) we aimed to follow the current trajectory which is pointing beyond RCP 8.5 scenario given the observed trends (Sanford et al., 2014), ii) we intended to capture the furthest range presented by RCPs as that is the extent to be considered for the assessment of ecosystem responses and mitigation efforts. However, we found that the ENSO signal as identified by the EOT method to be very weak in the GCM outputs and for the future simulations we intensified the ENSO signal such that very strong ENSO years can also be experienced as it is the real-world case. It could be argued that we did not even applied an extra intensification due to RCP8.5, and this discrepancy would hold regardless of the future scenario. Considering that we are expected to experience even stronger ENSO events in the future than today (Cai et al., 2013) we could have intensified this signal even more. However, our results with this realistic intensification already shows the importance of capturing atmosphere-ocean teleconnections in climate simulations for reliable future simulations of the ecosystems. We simulated large differences in future ecosystem responses under our 'intensified' ENSO scenario, as large as the differences we calculated for the present-day with and without ENSO simulations. In other words, if we were to predict vegetation response to future climate change by using GCM outputs as they are, it would be as if simulating the present-day vegetation with climate data without any ENSO contribution.

Apart from the temporal and strength mismatch, the GCM simulations are also

producing different spatial patterns for tropical Pacific SST-East African rainfall teleconnection. Therefore, in our modification we chose to correct for this spatial pattern by using the relationships we obtained from the observed datasets as this correction did not influence the temporal behavior and the peakiness of the ENSO signal retrieved from the GCM simulations. As a result, our findings can be compared for present day patterns directly.

Another finding in our study regarding the spatial patterns was that, while the region that explains the most variability in East African rainfall is closer to the Nino-3.4 region in our historical analysis, it shifts towards the Nino-4 region in the EOT analysis with GCM outputs. In our methodology the coupling of tropical Pacific Sea Surface temperature-East African rainfall variability emerges from the data, and this shift in the influence region agrees well with previous studies that identify an increase in the intensity of Central-Pacific (CP) ENSO in the future from GCM outputs (Kim and Yu, 2012). While CP ENSO is thought to be forced by changes in the atmospheric circulation, mechanism for Eastern-Pacific ENSO is rather associated with thermocline variations in the oceanic circulation (Yu, Kao and Lee, 2010), and the seasonal impacts produced by these two types of ENSO could differ. For example, wetter patterns of EP El Nino events in East Africa might not occur under CP El Nino events and, CP La Nina events could induce drier conditions in the southern parts of the region than EP La Nina events (Wiedermann et al. 2017) which could result in prolongated drought events for the East Africa region. Future work with further discrimination of CP-EP event types could help better anticipate the ecosystem responses to such seasonal extremes.

4.5 Conclusion

In this study, we translated the lack of ability of GCMs to account for ENSO teleconnections into quantified discrepancies in terms of ecosystem responses. We investigated the relationship between interannual East African rainfall variability and ENSO events using Empirical Orthogonal Teleconnection (EOT) analysis, and found a robust connection from observational datasets in agreement with previous studies, while confirming that GCM outputs are still not reliable for capturing this pertinent rainfall variability due to ENSO. While the strength of this relationship is not homogeneous among the region, and the patterns of vegetation

response presented opposite characteristics in the northern and southern areas, ENSO influence on East African vegetation and in return its carbon and hydrological fluxes was apparent. The simulated vegetation responses showed non-negligible differences under climate with and without stronger ENSO signal in relevance to mitigation efforts for future climate change. We conclude that the future vegetation would be different from what is simulated under these climate model outputs lacking accurate ENSO contribution to the degree of ignoring the ENSO influence altogether. Comparably with findings from previous studies linking vegetation-climate interactions, we discussed the importance of accounting for this influence which can bring further environmental stress to East Africa. Overall, our results highlight that more robust projections on coupled atmosphere-ocean teleconnections can help reducing large uncertainties of the future magnitude and sign of carbon sink provided by terrestrial ecosystems by improving our understanding on the vegetation response.

4.6 Acknowledgements

IF was funded by DAAD, grants to F. J. and German Research Foundation (DFG) Graduate School GRK1364 program (Shaping Earth's Surface in a Variable Environment – Interactions between tectonics, climate and biosphere in the African-Asian monsoonal region). FJ and BT acknowledge the support by the BMBF in the framework of the OPTIMASS project (01LL1302A and 01LL1302B). We thank Plant Ecology and Nature Conservation Group of Potsdam University for the inspiring discussions, and Dr. Appelhans for helpful discussions on the EOT method. We are grateful for the Biogeosciences' editor and the two anonymous reviewers for their comments and suggestions that helped us improve this manuscript to a great extent.

4.7 References

Abdi, A. M., Vrieling, A., Yengoh, G. T., Anyamba, A., Seaquist, J. W., Ummenhofer, C. C., Ardö, J., 2016, The El Nino - La Nina cycle and recent trends in supply and demand of net primary productivity in African drylands, Climatic Change, 138:111-125. dx.doi.org/10.1007/s10584-016-1730-1

Ahlström, A., Schurgers, G., Arneth, A., Smith, B, 2012. Robustness and uncertainty in terrestrial ecosystem carbon response to CMIP5 climate change projections. Environmental Research Letters, 7(4), dx.doi.org/10.1088/1748-9326/7/4/044008

Ahlström, A., Raupach, M. R., Schurgers, G., Smith, B., Arneth, A., Jung, M.,Reichstein, M., Canadell, J. G., Friedlingstein, P., Jain, A. K., Kato, E., Poulter, P., Sitch, S., Stocker, B. D., Viovy, N., Wang, Y. P., Wiltshire, A., Zaehle, S., Zeng, N., 2015, The dominant role of semi-arid ecosystems in the trend and variability of the land CO_2 sink, Science, 348(6237), 895-899. dx.doi.org/10.1126/science.aaa1668

Anyah, R.O., Semazzi, F.H.M., 2007, Variability of East African rainfall based on multiyear RegCM3 simulations, International Journal of Climatology, 27, 357-371. dx.doi.org/10.1002/joc.1401

Appelhans, T., Detsch, F., Nauss, T., 2015, remote: Empirical orthogonal teleconnections in R, Journal of Statistical Software, 65-10. https://www.jstatsoft.org/article/view/v065i10

Appelhans, T., Nauss, T., 2016, Spatial patterns of sea surface temperature influences on East African precipitation as revealed by empirical orthogonal teleconnections, Frontiers in Earth Science, dx.doi.org/10.3389/feart.2016.00003

Bobe, R., 2006, The evolution of arid systems in eastern Africa, Journal of Arid Environments, 66(3), 564-584. dx.doi.org/10.1016/j.jaridenv.2006.01.010

Brandt, M., Rasmussen, K., Penuelas, J., Tian, F., Schurgers, G., Verger, A., Mertz, O., Palmer, J. R. B., Fensholt, R., 2017, Human population growth offsets climate-driven increase in woody vegetation in sub-Saharan Africa, Nature Ecology & Evolution. dx.doi.org/10.1038/s41559-017-0081

Detsch, F., Otte, I., Appelhans, T., Hemp, A., Nauss, T., 2016, Seasonal and long-term vegetation dynamics from 1-km GIMMS-based NDVI time series at Mt. Kilimanjaro, Tanzania. Remote Sensing of Environment, 178, 70-83. http://dx.doi.org/10.1016/j.rse.2016.03.007

Dietrich, J. P., Schmitz, C., Lotze-Campen, H., Popp, A., Müller, C., 2014, Forecasting technological change in agriculture – An endogenous implementation on global land use model, Technological Forecasting & Societal Change, 81, 236-249 http://dx.doi.org/10.1016/j.techfore.2013.02.003

Doherty, R. M., Sitch, S., Smith, B., Lewis, S. L., Thornton, P. K., 2010, Implications of future climate and atmospheric CO_2 content for regional biogeochemistry, biogeography and ecosystem services across East Africa, Global Change Biology, 16, 617-640, dx.doi.org/10.1111/j.1365-2486.2009.01997.x

Endris, H. S., Omondi, P., Jain, S., Lennard, C., Hewitson, B., Chang'a, L., Awange, J.L., Dosio, A., Ketiem, P., Nikulin, G., Panitz, H. J., Büchner, M., Stordal, F., Tazalika, L., 2013, Assessment of the performance of CORDEX regional climate models in simulating eastern Africa rainfall, Journal of Climate. 26 (21): pp. 8453-8475, http://dx.doi.org/10.1175/JCLI-D-12-00708.1

FAO (Food and Agriculture Organization of the United Nations). 2016. FAOSTAT http://faostat.fao.org.

Fer, I., Tietjen, B., Jeltsch, F., 2015. High-resolution modelling closes the gap between data and model simulations for Mid-Holocene and present-day biomes of East Africa. Palaeogeography, Palaeoclimatology, Palaeoecology, 444, 144-151. http://dx.doi.org/10.1016/j.palaeo.2015.12.001

Forzieri, G., Alkama, R., Miralles, D. G., Cescatti, A., 2017, Satellites reveal contrasting responses of regional climate to the widespread greening of Earth, Science, 356:6343, 1180-1184, http://dx.doi.org/10.1126/science.aal1727

Gerten, D., Schaphoff, S., Haberlandt, U., Lucht, W., Sitch, S., 2004. Terrestrial vegetation and water balance – hydrological evaluation of a dynamic global vegetation model. Journal of Hydrology, 286, 249–270. http://dx.doi.org/10.1016/j.jhydrol.2003.09.029

Goddard, L., Graham, N. G., 1999, Importance of the Indian Ocean for simulating rainfall anomalies over eastern and southern Africa, Journal of Geophysical Research, 104, 19099-19116, dx.doi.org/10.1029/1999JD900326

Harris, I., Jones, P.D., Osborn, T.J., Lister, D.H., 2014, Updated high-resolution grids of monthly climatic observations - the CRU TS3.10 dataset, International Journal of Climatology. 34, 623-642. http://dx.doi.org/10.1002/joc.3711

Hickler, T., Smith, B., Sykes, M.T., Davis, M. B., Sugita, S., Walker, K., 2004, Using a generalized vegetation dynamics in Northeastern USA, Ecology, 86(2), 519-530, dx.doi.org/10.1890/02-0344

Hope, L.K., Thomson, M.C., 2008, Climate and Infectious diseases. Seasonal forecasts, climatic change and human health, Springer 31-70 http://dx.doi.org/10.1007/978-1-4020-6877-5_3

Huang, B., V.F. Banzon, E. Freeman, J. Lawrimore, W. Liu, T.C. Peterson, T.M. Smith, P.W. Thorne, S.D. Woodruff, H.-M. Zhang, 2014, Extended Reconstructed Sea Surface Temperature version 4 (ERSST.v4): Part I. Upgrades and intercomparisons. *Journal of Climate*, http://dx.doi.org/10.1175/JCLI-D-14-00006.1

Indeje, M., Semazzi, F. H. M., Ogallo, L. J., 2000, ENSO Signals in East African Rainfall Seasons, International Journal of Climatology, 20, 19-46(2000), dx.doi.org/10.1002/(SICI)1097-0088(200001)20:1<19::AID-JOC449>3.0.CO;2-0

Ivory, S. J., Russell, J., Cohen, A. S., 2013, In the hot seat: Insolation, ENSO, and vegetation in the African tropics, Journal of Geophysical Research: Biogeosciences, 118, 1347-1358, dx.doi.org/10.1002/jgrg.20115

Kim, S. T., Yu, J-Y, 2012, The two types of ENSO in CMIP5 models, Geophysical Research Letters, 39:11. dx.doi.org/10.1029/2012GL052006

Kovates, R.S., Bouma, M.J., Hajat, S., Worrall, E., Haines, A., 2013, El Niño and health, Lancet, 362(9394), 1481-9, dx.doi.org/10.1016/S0140-6736(03)14695-8

Lim, E-P, Hendon, H. H., Zhao, M., Yin, Y., 2016, Inter-decadal variations in the linkages between ENSO, the IOD and south-eastern Australia springtime rainfall in the past 30 years. Climate Dynamics. dx.doi.org/10.1007/s00382-016-3328-8

Liu, W., Huang, B. , Thorne, P.W. , Banzon, V.F. , Zhang, H.-M. , Freeman, E., Lawrimore, J., Peterson, T.C. , Smith, T.M., Woodruff, S.D., 2014: Extended Reconstructed Sea Surface Temperature version 4 (ERSST.v4): Part II. Parametric and structural uncertainty estimations. Journal of Climate. dx.doi.org/10.1175/JCLI-D-14-00007.1

Meegan, J. M., C. L. Bailey, 1989, Rift Valley fever. The Arbo Viruses: Epidemiology and Ecology, T. P. Monath, Ed., Vol. IV, CRC Press, 51–76.

Miralles, D. G., van den Berg, M. J., Gash, J. H., Parinussa, R. M., de Jeu, R. A. M., Beck, H. E., Holmes, T. R. H., Jimenez, C., Verhoest, N. E. C., Dorigo, W. A., Teuling, A. J., Dolman, A. J., 2014, El Nino - La Nina cycle and recent trends in continental evaporation, Nature Climate Change, 4, 122-126. dx.doi.org/10.1038/nclimate2068

Moncrieff, G.R., Scheiter, S., Bond, W.J., Higgins, S.I., 2014, Increasing atmospheric CO2 overrides the historical legacy of multiple stable biome states in Africa, New Phytologist, 201(3), 908-915. dx.doi.org/10.1111/nph.12551

Moss, R. H., Edmonds J. A., Hibbard, K. A., Manning, M. R., Rose, S.K., van Vuuren D. P., Carter, T. R., Emori, S., Kainuma, M., Kram, T., Meehl, G. A., Mithcell, J. F. B., Nakicenovic, N., Raihai, K., Smith, S. J., Stouffer, R. J., Thomson, A. M., Weyant, J. P., Willbanks, T. J., 2010, The next generation of scenarios for climate change research and assessment. Nature, 463:747–756, dx.doi.org/10.1038/nature08823

Nazarenko, L., Schmidt, G.A., Miller, R.L., Tausnev, N., Kelley, M., Ruedy, R., Russell, G.L., Aleinov, I., Bauer, M., Bauer, S., Bleck, R., Canuto, M., Cheng, Y., Clune, T. L., Del Genio, A. D., Faluvegi, G., Hansen, J. E., Healy, R. J., Kiang, N. Y., Koch, D., Lacis, A. A., LeGrande, A. N., Lerner, J., Lo, K. K., Menon, S., Oinas, V., Perlwitz, J. P., Puma, M. J., Rind, D., Romanou, A., Sato, M., Shindell, D. T., Sun, S., Tsigaridis, K., Unger, N., Voulgarakis, A., Yao, M.-S., Zhang, J., 2015: Future climate change under RCP emission scenarios with GISS ModelE2.

J. Adv. Model. Earth Syst., **7**(1), 244-267, dx.doi.org/10.1002/2014MS000403

Nicholson, S.E., 2000. The nature of rainfall variability over Africa on time scales of decades to millenia. Global and Planetary Change 26, 137–158. http://dx.doi.org/10.1016/S0921-8181(00)00040-0

Nicholson, S.E., 2014, A detailed look at the recent drought situation in the Greater Horn of Africa, *Journal of Arid Environments*, 103, 71-79. dx.doi.org/10.1016/j.jaridenv.2013.12.003

Nicholson, S. E., 2015, Long-term variability of the East African 'short-rains' and its links to large-scale factors, International Journal of Climatology, 35(13), 3979-3990. http://dx.doi.org/10.1002/joc.4259

Nikulin, G., Jones, C., Giorgi, F., Asrar, G., Büchner, M., Cerezo-Mota, R., Christensen, O., Deque, M., Fernandez, J., Hänsler, A., van Meijgaard, E., Samuelsson, P. Sylla, M. B., Sushama, L., 2012, Precipitation climatology in an ensemble of CORDEX-Africa regional climate simulations, American Meteorological Society, 25, 6058-6078. dx.doi.org/10.1175/JCLI-D-11-00375.1

Poulter, B., Frank, D., Ciais, P., Myneni, R. B., Andela, N., Bi, J., Broquet, G., Canadell, J. G., Chevallier, F., Liu, Y. Y., Running, S. W., Sitch, S., van der Werf, G., 2014, Contribution of semi-arid ecosystems to interannual variability of global carbon cycle, Nature, 509, 600-603, dx.doi.org/10.1038/nature13376

R Core Team (2015). R: A Language and Environment for Statistical Computing. R Foundation for Statistical Computing, Vienna, Austria. URL http://www.R-project.org/

Riahi, K., Rao, S., Krey, V., Cho, C., Chirkov, V., Fischer, G., Kindermann, G., Nakicenovic, N., Rafaj, P., 2011, RCP 8.5 – A scenario of comparatively high greenhouse gas emissions. Climatic Change, 109:22. dx.doi.org/10.1007/s10584-011-0149-y

Ropelewski, C.F., Halpert, M.S., 1996, Quantifying Southern Oscillation-rainfall relationships, *Journal of Climate*, 9, 1043-1059. dx.doi.org/10.1175/1520-0442(1996)009<1043:QSOPR>2.0.CO;2

Sanford. T., Frumhoff, P. C., Luers, A., Gulledge, J., 2014, The climate policy narrative for a dangeroously warming world. Nature Climate Change, 4, 164-166. dx.doi.org/10.1038/nclimate2148

Scheiter, S., Langan, L., Higgins, S. I., Next-generation dynamic global vegetation models: learning from community ecology. New Phytologist, 198(3), 957-969. dx.doi.org/10.1111/nph.12210

Scheiter, S., Savadogo, S., 2016, Ecosystem management can mitigate vegetation shifts induced by climate change in West Africa, Ecological Modelling, 332, 19-27, http://dx.doi.org/10.1016/j.ecolmodel.2016.03.022

Schreck, C. J, Semazzi, F. H. M., 2004, Variability of the recent climate of East Africa, International Journal of Climatology, 24:681-701, dx.doi.org/10.1002/joc.1019

Shisanya, C. A., Recha, C., Anyamba, A., 2011, Rainfall variability and its impact on Normalized Difference Vegetation Index in arid and semi-arid lands of Kenya, International Journal of Geosciences, 2, 36-47. dx.doi.org/10.4236/ijg.2011.21004

Sitch, S., Smith, B., Prentice, I.C., Arneth, A., Bondeau, A., Cramer, W., Kaplan, J.O., Levis, S., Lucht, W., Sykes, M.T., Thonicke, K., Venevsky, S., 2003. Evaluation of ecosystem dynamics, plant geography and terrestrial carbon cycling in the LPJ dynamic global vegetation model. Global Change Biology. 9, 161–185. http://dx.doi.org/10.1046/j.1365-2486.2003.00569.x

Smith, B., Prentice, I.C., Sykes, M.T., 2001. Representation of vegetation dynamics in the modelling of terrestrial ecosystems: comparing two contrasting approaches within European climate space. Global Ecology and Biogeography. 10, 621–637. http://dx.doi.org/10.1046/j.1466-822X.2001.t01-1-00256.x

Thonicke, K., Venevsky, S., Sitch, S., Cramer, W., 2001, The role of fire disturbance for global vegetation dynamics: coupling fire into a dynamic vegetation model, Global Ecology and Biogeography, 10(6), 661-67. dx.doi.org/10.1046/j.1466-822X.2001.00175.x

Thornton, P.K., Ericksen, P.J., Herrero, M., Challinor, A.J., 2014, Climate variability and vulnerability to climate change: a review, *Global Change Biology*, 20, 33-13-3328. dx.doi.org/10.1111/gcb.12581

Trenberth, K. E., 1998, Forecasts of the development of the 1997- 98 El Niño event. *CLIVAR Exchanges,* Vol. 3, No. 2/3, 4–14. http://www.cgd.ucar.edu/cas/papers/clivar98_Santiago

van den Dool, H.M., Saha, S., Johansson, A., 2000, Empirical orthogonal teleconnections, *Journal of Climate*, 13 (8), 1421-1435. dx.doi.org/10.1175/1520-0442(2000)013<1421:EOT>2.0.CO;2

Vecchi, G. A., Wittenberg, A. T., 2010, El Nino and our future climate: where do we stand?, WIREs Climate Change, 1(1), 260-270, dx.doi.org/10.1002/wcc.33

Waha, K., Müller, C., Bondeau, A., Dietrich, J.P., Kurukulasuriya, P., Heinke, J., Lotze-Campen, H., 2013, Adaptation to climate change through he choice of cropping system and sowing date in sub-Saharan Africa, Global Environmental Change, 23, 130-143. http://dx.doi.org/10.1016/j.gloenvcha.2012.11.001

Wiedermann, M., Siegmund, J. F., Donges, F. J., Kurths, J., Donner,. R. V., 2017, Differential imprints of distinct ENSO flavors in global extreme precipitation patterns, Geophysical Research Letters, in review. https://arxiv.org/pdf/1702.00218.pdf

Wolff, C., Haug, G.H., Timmermann, A., Damste, J.S.S, Brauer, A., Sigman, D.M., Cane, M.A., Verschuren, D., 2011, Reduced interannual rainfall variability in East Africa during the Last Ice Age, *Science*, 333, 743. dx.doi.org/10.1126/science.1203724

Yu, J-Y., Kao, H-Y., Lee, T., 2010, Subtropics-Related interannual sea surface temperature variability in the Central Equatorial Pacific, American Meteorologica Society, 23, dx.doi.org/10.1175/2010JCLI3171.1

Zaehle, S., Sitch, S., Smith, S., Hatterman, F., 2005, Effects of parameter uncertainties on the modeling of terrestrial biosphere dynamics, Global Biogeochemical Cycles, 19:3, dx.doi.org/10.1029/2004GB002395

Chapter 5: Discussion and Conclusion

5.1 Transient dynamics of East African vegetation

The primary aim of this dissertation was to better understand the transient dynamics of East African vegetation through mechanistic process-based dynamic vegetation model (DVM) simulations. This approach was needed to study past, present and future responses of East African vegetation to environmental changes mainly for two reasons: 1) DVMs are proper means of studying such questions: vegetation models are essentially the collection of what we know about these natural systems, i.e. they embody our hypotheses of how terrestrial ecosystems work. This dissertation not only tested these hypotheses and theories for the under-studied East African ecosystems, but also used them for interpreting past changes and providing robust future projections. 2) DVMs are scaffolds: While studying East African vegetation is important for the various reasons that are stated throughout this dissertation, both current observations and palaeo-proxies are fragmentary from the region. Whereas DVMs can bring pieces of information from different sources together and reconcile them as demonstrated in chapters of this dissertation.

5.1.1 Simulating East African vegetation

DVMs are actively being develop and improved, as the one (LPJ-GUESS) used in this study. The number of DVMs increase incessantly. So do the data. However, projections of future ecosystem responses still show substantial disagreements between models (Friedlingstein et al., 2014). One main source of these disagreements is the gap in our understanding of tropical ecosystems. Both tropical forests and tropical drylands (ranging from dry sub-humid to hyper-arid lands) are less well-studied than their temperate counterparts. However, these ecosystems cycle a significant amount of terrestrial carbon, and they host a remarkable portion of global biodiversity. Thus, it is not unexpected to have disagreements in model predictions that have different representations of tropical ecosystems in their underlying processes.

To begin with, current vegetation models typically use more plant functional types (PFTs) to describe temperate biomes than tropical ones despite the much higher diversity in these biomes. In this dissertation, I used six PFTs to represent tropical African vegetation (excluding the montane cold-types) which is higher than previous applications of LPJ-GUESS (Hely et al., 2006; Doherty et al., 2010). This provided better comparison to both vegetation maps and the pollen data. However, the parameterization of these PFTs could be improved. Especially, the C4 grass hydraulic and photosynthetic properties are not very well informed due to scantness of direct measurements. Besides, the fact that there is only a single C4 and C3 grass type (note that in this dissertation I used a cold-type and a warm-type C3 grass, but still only the warm C3 type was representative for lowland biomes) is not consistent with the functional diversity of thousands of grass species. For instance, a first diversification that could be thought of is a distinction between wetter and drier types of C4 grasses for representing Andropogoneae and Chloridoideae lineages respectively, as these are expected to show different responses to climate change (Still et al., 2014). Another missing or inadequately represented functional type in DVMs are the shrubs. Shrubs are typical functional forms in semi-arid ecosystems such as savannas and are common in East Africa. They have different allometries and physiological responses than trees. While in theory it is possible to define as many PFTs as one wants, the parameterization of such PFTs require quality measurements of plant traits. With advancement of plant trait databases such as TRY (Kattge et al, 2011), PFT parameterization is getting easier, more empirical and more justified. Having multiple grass and shrub functional types could have improved the model-data agreement and influenced future predictions in this study as well.

Likewise, important ecological and physiological processes still need further development in these models for tropical biomes, considering the magnitude of stocks and fluxes in these ecosystems. For example, multiple nutrient limitations on photosynthesis might be important for pedictions in tropical biomes, whereas it is mostly not accounted for by ecosystem models (Norby et al., 2017). The version of LPJ-GUESS in this study does not include neither nitrogen (N) or phosphorus (P) limitation, however, a newer version of the model now represents plant and soil N dynamics and shown to improve model predictions (Smith et al., 2014). C-N-P interactions could be particularly important to consider while

simulating topical biomes because similarly, the response of model parameters associated with the acclimation of photosynthesis to temperature and CO_2 concentration are less understood for tropical biomes. Both this dissertation and previous studies showed very high sensitivity of tropical biomes to elevated CO_2 concentration (Hickler et al., 2008), but this sensitivity could be dampened or even exacerbated by nutrient availability in these biomes. The representation of the interplay between C-N-P interactions, effect of fire on nutrient availability and precipitation in tropical biomes is constantly being improved, however, direct field measurements, long-term monitoring and manipulative experiments are needed from the region.

5.1.2 Synthesis

However limited, LPJ-GUESS version used in this study, with its current implementations and PFT set, successfully reproduced the overall vegetation patterns in East Africa and provided valuable insights regarding its past and future dynamics. Chapter 2 focused on exhaustive validation of the model in the region not only for present but also for the past. Driving the model with spatially downscaled climate data increased model agreement with both vegetation maps and pollen data. Increased agreement with pollen data with higher spatial-resolution model outputs was expected as pollen data provides relatively localized vegetation signals. Whereas, increased agreement with potential natural vegetation map was rather surprising because higher spatial-resolution meant a lot more possibilities for disagreeing grid cells between the vegetation map and the model output. This is especially the case for East Africa with large transitional areas around the rift topography. Not reduced, and even increased agreement indicate that the statistical downscaling of climate data applied in this study was successful and could be used in future studies. Chapter 2 also showed that Holocene vegetation changes in East Africa were driven by both the annual precipitation and the seasonality of this precipitation. Chapter 3 investigated the sensitivity of East African biomes to precipitation amount and seasonality in a retrospective context, and identified transition points in climate space and time. Chapter 4 assessed the contribution of climate variability due to ENSO on East African vegetation and quantified the future uncertainties associated to this variability. In the light of these studies, I have reached the following conclusions:

1) Dynamic vegetation models can provide a more spatially and temporally complete understanding of East African vegetation dynamics until enough data can be collected in sufficient quantity and quality from the region. Even then, DVMs can continue to help us test competing hypotheses and scenarios against observations. Furthermore, they can be used in making forecasts based upon these refined theories and eventually inform policy decisions.

2) Previously established site-level climate sensitivities of vegetation scales up to regional-level in East Africa. In addition to amount of change in precipitation, the status of a biome in the climate space (e.g. the total amount it receives and the seasonality of this precipitation) is also a key factor in biome shifts in East Africa. The drivers of dynamics in drier biomes (savannas and woodlands) and wetter biomes (mixed forests and evergreen forests) can differ even while they are undergoing through same environmental changes.

3) A greener East Africa and multiple reconnection/disconnection events of forest biomes are highly likely in the Late Cenozoic with implications on human and mammal evolution and migration. Furthermore, the shifts from denser to more open vegetation, and vice versa, are shown to be possible to occur on much shorter time scales that are relevant to human evolution than previously thought.

4) As East African vegetation has evolved under high climate variability, it is more resilient to environmental stress than its counterparts around the tropics. However, in some areas these biomes are already at the edge of their tipping points. Future climate and land-use change pressures can accelerate degradation of their ecosystem services and should be addressed in mitigation decisions.

5) Global change research still needs much improved representations of non-linear interactions in earth system processes both in ecosystem and climate models. Until then, potential discrepancies should be quantified

through numerical experiments and accounted for in future predictions. Especially ENSO events have a non-negligible influence on East African vegetation, and on other dryland ecosystems around the world which in return have a dominant role on global carbon cycle trend and variability.

5.2 Future steps

Overall, each component of this dissertation helped to fill both knowledge and methodology gaps in understanding East African vegetation dynamics, as well as to provide ancillary data for related studies such as palaeohydrology and palaeontology. Use of DVMs proved to be successful and helpful in simulating past, present and future of East African vegetation in essence. However, in addition to aforementioned potential improvable areas in vegetation modeling, further research and method development needs became apparent along the way to improve this workflow as a whole.

5.2.1 Studying the palaeovegetation

Fossil pollen, without a doubt, can give important information regarding past vegetation and has been widely used in palaeoecology since the development of optical microscopes. Whereas, methods for quantification of this information is relatively new (Prentice et al., 1996). Expert interpretation through comparative analyses is still the most common way of reconstructing palaeovegetation from pollen data in the literature. In this dissertation, I used the most quantitative and unbiased method accessible to me at the time. Despite that, I often needed to appeal to expert opinion on PFT assignments and biome classification thresholds for which there were no strictly defined rules to follow. This was not unexpected because it is well-known that there are uncertainties regarding the palaeovegetation information recorded by the pollen data. As a result, there is room for a certain level of flexibility in interpretation of the pollen data. Furthermore, there are also no strict rules regarding the classification of DVM outputs into biomes that are comparable to the biomes reconstructed from the pollen data. Ultimately, a more direct, quantitative and formal comparison between pollen and dynamic vegetation models is needed. Dynamic vegetation

models already, mostly, incorporate mechanistic and quantitative representations of ecosystem processes. A more unbiased and formal way of comparing model outputs to pollen data could be obtained through statistical modeling of the pollen data that makes the information extracted from the pollen data directly comparable to model outputs with quantified uncertainties around this information (Paciorek and McLachlan, 2009). For example, instead of biomizing the pollen records according to arbitrary rules, we can reconstruct the above ground biomass from pollen data through statistical models of allometric equations of species or genera. Above ground biomass is a state variable that is directly comparable to model outputs. Also, now this biomass estimation can have a confidence interval that can be accounted for while calculating the model-data mismatch.

A formal and quantitative model-data comparison brings further opportunities. If we can calculate the mismatch between model and data (likelihood) at a time point, we can inform model predictions with data. For example, we can start the model from a point in the past until we have information from pollen data. At the time point from which we have data, we can compare the state predicted by the model to the state reconstructed from the data and accordingly adjust model states as suggested by the data. Then we can run the model forward until we have another data point in time and re-adjust model states according to data, and so on. We can repeat this as many times as we have data points for. This framework is called data assimilation (Dubinkina et al., 2011). This is an ideal way of reconstructing the palaeovegetation (or palaeoclimate) because it borrows strengths of both the data and the model: data inform the patterns of the model states, whereas the model explains the mechanisms behind patterns suggested by the data. This framework is not only possible for fossil pollen data, but for any proxy as long as information about a state variable corresponding to a model output could be inferred from the proxy. It also has the flexibility to assimilate multiple types of data at the same time.

5.2.2 Model uncertainty

Estimations from the proxy data that we compare model outputs to have uncertainties, but the model outputs have uncertainties too. There are multiple sources of these uncertainties: First, no model perfectly captures the reality, so

model process error is one source. Second, the drivers are another source of uncertainty. The climate data that we feed into the models as inputs are also uncertain. This could be due to measurement errors, or natural variability if we are considering the observed climate. If we are considering the simulated climate data, the climate models have their own process errors and other uncertainty sources. Even for the same future or past scenario, there can be multiple realizations of the climate. Third, it is a common practice (as in this dissertation) to treat the PFT parameters as point values. However, there again can be measurement errors or natural variability to these parameters. Some model processes can be sensitive to these parameters and could give different results under slightly different values. Therefore, it is a better practice to propagate these uncertainties into model outputs while conducting simulation experiments with DVMs. This could be achieved by running model ensembles with multiple combinations of drivers and parameter values (and initial conditions if used). The result would be a spread of model predictions which would capture our imperfect knowledge of the system. Although this approach would increase uncertainty associated with our model predictions, it is better to account for these uncertainties, than being over-confident and biased.

Once the driver / parameter / initial condition uncertainties are propagated to model outputs, one can start working towards reducing these uncertainties. Process error could be reduced in time with betterment of our theoretical understanding as knowledge accumulate, but it does not necessarily asymptote to zero. Whereas more rigorous and numerous measurements and observations can help reduce driver and parameter uncertainties. For example, after determining that model outputs are sensitive to a certain parameter, or a certain parameter is too uncertain (e.g. can take values within a very wide interval due to little information), or both, we can design experiments or field campaigns for collecting more measurements and observations on that trait to constrain the parameter. Sometimes, it might not be possible to obtain direct measurements due to high cost-benefit ratio or due the nature of the parameter at hand. In that case, other existing datasets that corresponds to model outputs, such as eddy flux data, can be used in indirect calibration of model parameters (Figure 5.1, Hartig et al., 2012). In Bayesian model calibration frameworks, we can constrain model parameters through Markov Chain Monte Carlo algorithms by repeatedly comparing model

outputs to data. Such frameworks help us to reduce parameter uncertainties and the associated uncertainties in the model predictions (Hartig et al., 2012). This could be especially valuable for regions like East Africa where remotely sensed data can also be utilized.

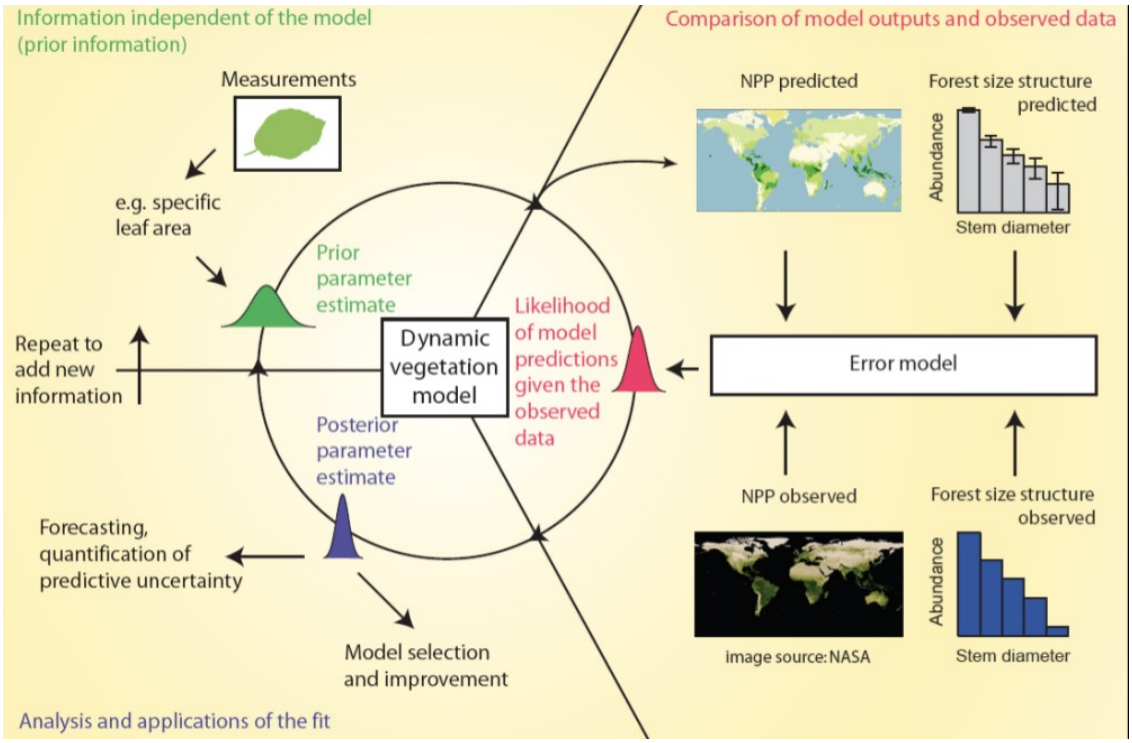

Figure 5.1 Indirect (inverse) parameterization of dynamic vegetation models (figure from Hartig et al., 2012). When there is no or few measurements that we can directly map to model parameters, we can use indirect parameterization to adjust model parameters such that model-data agreement improves. This can be achieved through Bayesian calibration frameworks.

To sum up, future efforts in modeling East African vegetation will benefit from quantification of uncertainties in more formal ways. There is certainly a need for more observational and experimental data from East Africa on parameters and processes. In the meantime, recent developments in Bayesian calibration methods could help improving models and global change research altogether.

5.3 References

Doherty, R. M., Sitch, S., Smith, B., Lewis, S. L., Thornton, P. K., 2010. Implications of future climate and atmospheric CO_2 content for regional biogeochemistry, biogeography and ecosystem services across East Africa. Global Change Biology. 16, 617-640. doi: 10.1111/j.1365- 2486.2009.01997.x

Dubinkina, S., Goosse, H., Yoann, S-D, Crespin, E., Crucifix, M., 2011, Testing a particle filter to reconstruct climate changes over the past centuries, International Journal of Bifurcation and Chaos, 21(12), 3611-3618.

Friedlingstein, P., M. Meinshausen, V.K. Arora, C.D. Jones, A. Anav, S.K. Liddicoat, and R. Knutti, 2014, Uncertainties in CMIP5 Climate Projections due to Carbon Cycle Feedbacks. J. Climate, **27**, 511–526, doi:10.1175/JCLI-D-12-00579.1

Hartig, F., Dyke, J., Hickler, T., Higgins, S. I., O'Hara, R.B., Scheiter, S., Huth, A., 2012, Connecting dynamic vegetation models to data – an inverse perspective, Journal of Biogeography, 39, 2240-2252, doi: 10.1111/j.1365-2699.2012.02745.x

Hély, C., Bremond, L., Alleaume, S., Smith, B., Sykes, M.T., Guiot, J., 2006. Sensitivity of African biomes to changes in the precipitation regime. Global Ecology and Biogeography. 15, 258 – 270. doi: 10.1111/j.1466-822x.2006.00235.x

Hickler, T., Smith, B., Prentice, I. C., K., Miller, P., Arneth, A., Sykes, M. T., 2008. CO_2 fertilization in temperate FACE experiments not representative of boreal and tropical forests. Global Change Biology. 14, 1531-1542.

doi: 10.1111/j.1365-2486.2008.01598.x

Kattge J, S Díaz, S Lavorel, IC Prentice, P Leadley, G Bönisch, E Garnier, M Westoby, PB Reich, IJ Wright, et al. (2011) TRY – a global database of plant traits. Global Change Biology 17:2905–2935. doi: 10.1111/j.1365-2486.2011.02451.x

Norby, R.J., Gu, L., Haworth, I.C, Jensen, A.M., Turner, B. L., Walker, A.P., Warren, J.M., Weston, D. J., Xu, C., Winter, K., 2017, Informing models through empirical relationships between foliar phosphorus, nitrogen and photosynthesis across diverse woody species in tropical forests of Panama, NewPhytologist, doi:10.1111/nph.14319

Paciorek, C., McLachlan, J. S., 2009, Mapping ancient forests: Bayesian inference for spatio-temporal trends in forest composition using fossil pollen proxy record, J Am Stat Assoc, 104(486), 608-622, doi:10.1198/jasa.2009.0026

Prentice, I.C., Guiot, J., Huntley, B., Jolly, D., Cheddadi, R., 1996. Reconstructing biomes from palaeoecological data: a general method and its application to European pollen data at 0 and 6 ka. Climate Dynamics. 12, 185–194.

http://dx.doi.org/10.1007/BF00211617

Smith, B., Warlind, D., Arneth, A., Hickler, T., Leadley, P., Siltberg, J., Zaehle,S., 2014, Implications of incorporating N cycling and N limitations on primary production in an individual-based dynamic vegetation model, Bioegosciences, 11, 2027-2054.

Still, C.J., Griffith, D., Edwards, E., Forrestel, E., Lehmann, C., Anderson, M., Craine, J., Pau, S., Osborne, C., 2014, Expanding the range of plant functional diversity represented in global vegetation models: Towards lineage-based plant functional types, AGU Fall Meeting.

Appendix A

Table A1. Pollen sites from which data were compiled for comparison with the LPJ-GUESS simulation results.

	Site name	Latitude	Longitude	Altitude	Number of ^{14}C dates	Number of pollen samples	Upper age (cal yr BP)	Lower age (cal yr BP)
1	Abernethy	56.233	-3.717	221	7	49	5950	14720
2	Achit-Nur	49.500	90.600	1453	4	20	2240	14750
3	Akulinin Exposure P1282	47.117	138.550	20	6	29	610	44890
4	Akuvaara	69.125	27.683	170	5	33	0	11680
5	Alut Lake	60.137	152.313	480	25	117	1130	31540
6	Ampoix	48.167	2.933	1015	5	120	1720	12280
7	Åntu sinijarv	59.133	26.326	95	9	54	-30	14810
8	Aronde	49.463	2.691	50	3	46	0	14190
9	Asbotorpsjon	58.417	13.833	280	9	35	9240	17220
10	Baberzo	63.375	37.517	138	3	11	510	13580
11	Baidara	68.850	66.900	30	10	67	4430	17190
12	Ballinloghig	52.400	-10.300	84	11	68	1220	13110
13	Bebrukas Lake (core 5)	54.090	24.120	149	14	50	150	15400
14	Belle lake	52.183	-7.033	33	8	49	6030	14650
15	Berelyekh River, Indigirka Lowland	70.583	145.000	20	4	37	8610	46350
16	Bergakyllen	57.167	16.150	73	5	28	7170	23500
17	Bezdonnoe	62.033	32.757	121	3	53	470	13780
18	Black Sea southwest	42.184	28.917	0	3	22	1820	15150
19	Blavasstjonn	64.917	11.667	92	4	36	80	11960
20	Bledowo Lake	52.550	20.670	78	4	294	60	13300
21	Blomoy	60.533	4.883	36	4	18	6070	15440
22	Bludlivaya River	69.067	148.400	100	3	3	25640	42200
23	Bolotnyii Stream	42.850	132.783	4	4	16	29150	43000
24	Bugristoe	58.250	85.167	100	5	67	4240	12230
25	Cam Loch	58.083	-5.000	130	7	37	11300	16200
26	Chabada (central Yakutia)	61.983	129.367	290	5	62	190	9280
27	Chernikhovo	53.420	26.430	52	4	52	2070	16860
28	Chistic	57.335	33.000	205	4	34	3040	8780
29	Circle	59.803	-151.158	300	3	52	30	15120
30	Cororion	53.200	-4.100	83	11	156	120	11120
31	Cregganmore	54.250	-0.960	60	3	66	3680	16170
32	Daba-Nur	48.200	98.794	2465	6	25	1930	13480
33	Derput	57.033	124.117	700	6	52	500	12520
34	Dikikh Olyenyeii Lake Exposure	67.800	-178.800	300	5	48	40730	44970
35	Domsvatnet	70.317	31.033	120	5	37	270	11530
36	Elgennya	62.100	-149.000	1040	6	52	0	18760
37	Elikchan 4 Lake	60.750	151.883	810	16	126	90	46820
38	Ermistu	58.367	13.967	17	5	85	4460	11580
39	Etivlik Lake	68.133	-156.033	631	4	23	90	18040

	Site name	Latitude	Longitude	Altitude	Number of ^{14}C dates	Number of pollen samples	Upper age (cal yr BP)	Lower age (cal yr BP)
40	Frengstadsetra	62.567	10.133	790	5	31	4380	10650
41	Glendalough	53.000	-6.333	130	5	150	-50	12600
42	Goluboye	61.117	152.267	810	13	41	180	11050
43	Grasvatn	63.700	8.700	45	8	45	230	14640
44	Grosses Überling Schattseit-Moor:	47.167	13.900	1750	5	65	0	17960
45	Gun-Nur	50.250	106.600	600	7	36	70	11890
46	Gytgykai Lake	63.167	175.000	102	9	68	0	21740
47	Harding Lake	64.444	-146.908	218	4	41	60	28990
48	Hawks Tor	50.533	-4.600	229	5	35	12400	15420
49	Hidden Lake	63.940	-144.658	372	5	33	30	20480
50	Hockham Mere	52.500	0.833	33	23	163	1490	14720
51	Hopseidet	70.833	27.717	225	4	53	-40	13010
52	Hoton Nur	48.667	88.300	2083	6	37	270	28270
53	Ifjord	70.433	27.633	317	4	93	0	14050
54	Jack London lake	62.167	149.500	820	7	60	330	20850
55	Joe Lake	66.767	-157.217	183	18	87	-30	46940
56	Kaarkotinlampi	61.147	25.867	104	5	37	220	13530
57	Kaiyak Lake	68.150	-161.417	190	7	53	2770	40500
58	Kansjon	57.633	14.533	308	12	45	80	15540
59	Karasieozerskoe	56.767	60.750	230	3	31	350	9150
60	Khomustakh Lake	63.820	121.620	120	9	72	3820	13340
61	Krechet	64.617	158.355	32	16	46	450	47090
62	Krugloye	66.367	37.583	140	6	17	2400	12750
63	Kupena	41.983	24.333	1300	6	31	670	15120
64	Lac Long Inferieur	44.058	7.450	2093	12	71	1440	17750
65	Lago d'Ajo	43.050	-6.150	1570	6	78	130	24980
66	Lago di Martignano	42.117	12.333	200	8	68	0	14000
67	Laguna de la Roya	42.217	-6.767	1608	6	72	360	16170
68	Lake Boguda	63.667	123.250	120	7	58	1330	11340
69	Lake Sambosjon	57.133	12.417	35	15	111	980	11290
70	Lake Shabla-Ezeretz	43.833	28.850	1	9	39	390	8830
71	Lake Skrzetuszewskie	52.550	17.361	109	7	83	370	12570
72	Lake Solso	56.133	8.633	41	34	66	640	10430
73	Le Fourneau	48.444	-0.192	–	10	74	100	23950
74	Lednica	52.557	17.390	109	9	84	520	10800
75	Liivjarve Bog	59.217	27.583	46	7	64	170	10660
76	Lilla Gloppsjon	59.804	14.628	198	11	86	0	11140
77	Liten Cappesjavri	71.074	25.368	41	16	72	70	13910
78	Lobsigensee	47.032	7.299	514	10	83	50	11180
79	Loch Maree	57.083	-5.483	60	6	57	50	10790
80	Loch Sionascaig	58.061	-5.175	74	7	148	680	12790
81	Lochan coir a' Ghobhainn	57.183	-6.300	82	4	21	8770	13140
82	Loras	45.664	5.244	410	6	136	540	21560
83	Luganskoe	43.733	40.692	2428	3	28	280	7680
84	Maksimkin Yar	58.333	88.167	150	4	48	200	9190
85	Mire Pelisoo	58.467	22.383	33	5	57	140	10240
86	Mokre louky (South)	48.833	14.833	425	5	82	3160	11230

	Site name	Latitude	Longitude	Altitude	Number of ^{14}C dates	Number of pollen samples	Upper age (cal yr BP)	Lower age (cal yr BP)
87	Lago Grande di Monticchio	40.944	15.600	1326	****	496	60	101500
88	Mukkavaara	68.917	21.000	535	9	56	700	11970
89	Nedre Madbergagolen	58.600	12.167	138	9	13	11760	13420
90	Niechorze	54.000	15.050	5	9	52	3360	15430
91	Nigula	58.000	24.667	55	11	60	740	8780
92	Nizhnevartovskoye	61.250	77.000	55	14	33	180	10120
93	Notsel	51.554	4.769	5	4	62	11310	15410
94	Nulsaveito	67.533	70.167	57	5	30	5830	8720
95	Oltush Lake	51.697	23.957	158	8	42	530	11670
96	Over Kobbkrokvatnet	70.699	29.295	–	13	69	60	13670
97	OverGunnarsfjorden	71.038	28.169	78	13	117	-40	13180
98	Ozerki	50.417	80.467	107	10	48	0	15110
99	Padule	44.297	10.215	1187	7	69	20	12330
100	Pashennoe	49.370	75.400	871	12	34	0	10610
101	Petropavlovka	58.333	82.500	100	5	66	670	10730
102	Pickletillem	56.400	-2.900	21	11	29	10940	14720
103	Place du Commerce	47.214	-1.556	7	7	40	5860	9010
104	Plesheevo Lake	56.750	38.500	148	2	101	2770	90360
105	Ptichje	66.350	30.567	120	2	29	400	10280
106	Pur-Taz	66.700	79.733	50	5	70	4540	11050
107	Puscizna Rekowianska	49.483	19.817	656	8	76	0	10399
108	Puyuk Lake	63.500	-162.200	15	2	38	60	20090
109	Quintanar de la Sierra	42.033	-3.017	1470	20	82	0	17420
110	Ranger Lake	67.147	-153.650	820	8	60	0	42170
111	Rebel Lake	67.417	-149.800	914	3	45	0	19410
112	Rezabinec	49.250	14.117	369	9	34	0	13330
113	Rotsee	47.076	8.326	419	11	128	0	13290
114	Roztoki core 14A	49.717	21.583	230	2	25	13130	14570
115	Rugozero	64.083	32.633	140	2	37	480	11250
116	Saint Julien de Ratz	45.350	5.267	650	4	156	790	17540
117	Shombashuo	65.117	32.633	100	2	28	180	15590
118	Skaidejavri	70.001	27.867	183	5	100	0	11060
119	Skvarran	57.200	16.150	86	6	31	9510	17740
120	Slopiec	50.783	20.783	248	11	68	40	12280
121	Sluggan Moss	54.933	-6.300	52	40	115	60	14100
122	Smorordinovoye Lake	64.767	141.100	798	11	76	110	27180
123	Starniki	50.270	26.050	198	10	30	470	13610
124	Sudoble Lake	54.033	28.100	165	8	61	170	13750
125	Suollakh	57.050	123.850	–	8	51	2770	13250
126	Suovalampi	69.583	28.833	104	5	34	260	12050
127	Syrjalansuo	61.217	28.117	83	6	81	0	16430
128	Taloye Lake	61.017	152.333	750	7	36	2520	10810
129	Tarnawa Wyzna	49.100	22.833	670	8	63	2100	14500
130	Tarnowiec	49.700	21.617	22	9	62	110	17190
131	Tiinkdhul Lake	66.583	-143.150	189	7	56	350	21560
132	Tomtabaken	57.483	14.467	303	14	43	6400	15460
133	Toppeladugard	55.600	13.367	35	3	40	12750	13270
134	Tourves	43.500	5.900	298	8	117	3650	15270

	Site name	Latitude	Longitude	Altitude	Number of ^{14}C dates	Number of pollen samples	Upper age (cal yr BP)	Lower age (cal yr BP)
135	Trollvatnet	69.875	23.467	188	5	34	2020	14930
136	Tschokljovo Marsh	42.367	22.083	870	6	30	250	9100
137	Tsuolbmajavri	68.692	22.083	526	14	146	20	12920
138	Uddelermeer	52.237	5.762	26	4	100	10940	13850
139	Ust'Mashevskoe	56.317	57.883	220	5	51	20	9320
140	Vallee de la Voise	48.417	1.750	–	5	62	460	10500
141	Vallon de Provence	44.391	6.404	2075	6	83	3010	12210
142	Vernerovice	50.100	16.250	450	9	38	0	13560
143	Vingolen	57.133	15.950	104	6	32	9550	13730
144	Vohma Mire	59.050	27.333	46	14	50	530	8780
145	Wachel-3	53.038	8.036	17	7	104	20	8800
146	Wien Lake	64.333	-151.267	305	9	43	0	14960
147	Wrangel Island	71.167	-179.750	200	18	31	9490	14040
148	Yenicaga	40.783	32.033	–	5	55	3310	15250
149	Ylimysneva	62.133	22.867	172	4	51	-30	9640
150	Zalozhsty	49.750	25.450	320	15	24	160	9950
151	Zaruckoe	63.900	36.250	20	5	64	440	9940
152	Zirbenwaldmoor	46.858	11.025	2150	7	66	970	10110
153	Zsombo Swamp	46.361	19.994	92	2	54	80	15720

Table A2 Reclassification of the White's Vegetation Map (White, 1983) classes which are present in the study area into new classes that are comparable with LPJ-GUESS' simulated biomes.

No.	White's Class Name	New class
1	Lowland rain forest	Evergreen Forest
2	Rain forest: drier types	Seasonal Forest
4	Transitional rain forest	Seasonal Forest
8	Swamp forest	Evergreen Forest
11	Mosaic of lowland rain forest and secondary grassland	Seasonal Forest
12	Mosaic of lowland rain forest, woodland and secondary grassland	Seasonal Forest
16	East African coastal mosaic	Woodland
17	Mixture of Afromontane and lowland species	Woodland
19	Undifferentiated montane vegetation	Afromontane
25	Wetter woodland	Woodland
26	Drier woodland	Woodland
27	Woodland	Woodland
28	Woodland and scrub woodland	Woodland
29	Undifferentiated woodland	Woodland
31	Mosaic of woodland and secondary grassland	Woodland
35	Transition from woodland to wooded grassland	Savanna
37	Secondary wooded grassland	Savanna
38	Evergreen and semi-evergreen bushland and thicket	Woodland
40	Deciduous thicket	Savanna
42	Deciduous thicket	Savanna
43	Wooded grassland and deciduous bushland	Savanna
45	Mosaic of evergreen bushland and secondary wooded grassland	Savanna
54	Semi-desert grassland and shrubland	Steppe
59	Wooded edaphic grassland	Savanna
60	Grassland and wooded grassland	Savanna
61	Grassland and wooded grassland	Savanna
62	Grassland and wooded grassland	Savanna
63	Grassland and wooded grassland	Savanna
64	Grassland and wooded grassland	Savanna
65	Altimontane, afroalpine	Afroalpine
67	Desert	Desert
68	Desert	Desert
71	Regs, hamadas, wadis	Steppe
75	Herbaceous swamp and aquatic vegetation	Water/Masked out
76	Halophytic vegetation	Water/Masket out
77	Mangrove	Evergreen Forest
81	Water	Masked out

Table A3.2 Reclassification of the GLC2000 (Mayaux *et al*., 2004) classes which are present in the study area into new classes that are comparable with LPJ-GUESS' simulated biomes.

No.	GLC2000 Class Name	New class
1	Closed evergreen lowland forest	Evergreen Forest
3	Submontane forest	Seasonal Forest
4	Montane forest	Afromontane
6	Mangrove	Seasonal Forest
7	Mosaic forest/croplands	Masked out
8	Mosaic forest/savanna	Seasonal Forest
9	Closed deciduous forest	Seasonal Forest
10	Deciduous woodland	Woodland
11	Deciduous shrubland with sparse trees	Woodland
12	Open deciduous shrubland	Savanna
13	Closed grassland	Savanna
14	Open grassland with sparse shrubs	Savanna
15	Open grassland	Savanna
16	Sparse grassland	Steppe
17	Swamp bushland and grassland	Water/Masked out
18	Croplands	Masked out
19	Croplands with open woody vegetation	Masked out
20	Irrigated croplands	Masked out
22	Sandy desert and dunes	Desert
23	Stony desert	Desert
24	Bare rock	Desert
25	Salt hardpans	Desert
26	Inland waters	Water/Masked out
27	Cities	Masked out

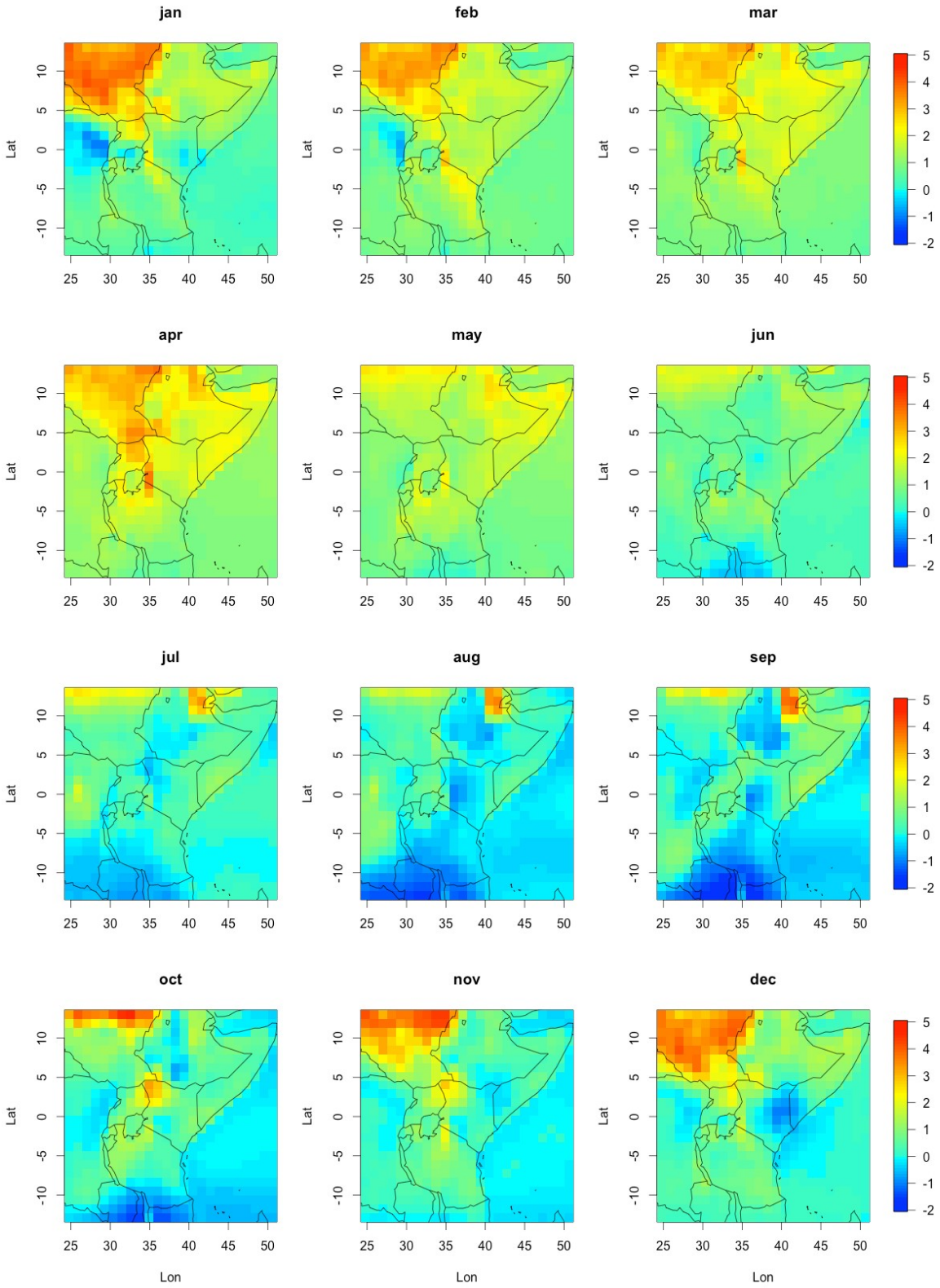

Figure A1 Monthly anomaly maps for temperature climatology (Bosmans et al., 2012) (Present-day minus mid-Holocene, the values shown are in ºC/month).

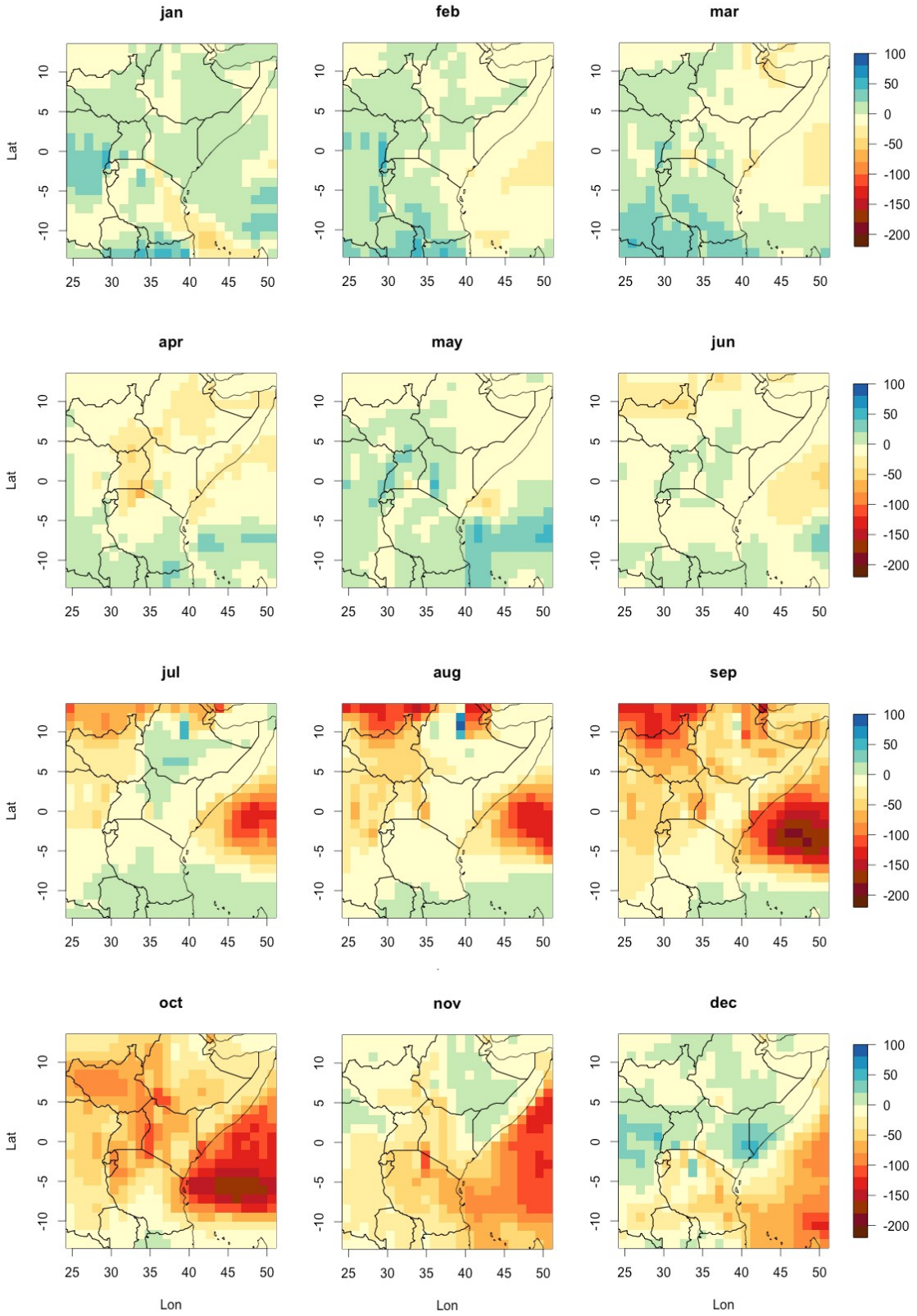

Figure A2 Monthly anomaly maps for precipitation climatology (Bosmans et al., 2012) (Present-day minus mid-Holocene, the values shown are in mm/month).

Table A4 Logistic regression results. Each biome name in the corner of the table represents the mid-Holocene (MH) biome of the sites (i.e. sites that were steppe biomes in Mid-Holocene either shifted to desert biomes in present-day (PD) or remained a steppe). We applied a logistic regression analysis to assess which environmental variables explain whether the biome remains the same or shifts to another.

shift: categories of shift - towards a more open/closed vegetation or remained same from MH to PD
pre_diff: % change in MAP from Mid-Holocene to Present-day.
pre_mh: Mid-Holocene MAP
R package: rms(), function: lrm()

STEPPE	shift~	LR chi2	Pr(> chi2)	Pseudo-R2	C-index	AIC
pre_diff		3.73	0.0536	0.054	0.581	115.0031
pre_mh		29.98	<0.0001	0.383	0.830	88.7459
pre_diff + pre_mh		47.46	<0.0001	0.558	0.910	73.26969

SAVANNA	shift~	LR chi2	Pr(> chi2)	Pseudo-R2	C-index	AIC
pre_diff		3416.14	<0.0001	0.534	0.899	5913.557
pre_mh		2224.97	<0.0001	0.379	0.870	7104.727
pre_diff + pre_mh		7113.87	<0.0001	0.872	0.774	2217.827

WOODLAND	shift~	LR chi2	Pr(> chi2)	Pseudo-R2	C-index	AIC
pre_diff		2234.80	<0.0001	0.454	0.847	5621.293
pre_mh		32.54	<0.0001	0.008	0.620	7823.55
pre_diff + pre_mh		3749.68	<0.0001	0.665	0.952	4108.412

S. FOREST	shift~	LR chi2	Pr(> chi2)	Pseudo-R2	C-index	AIC
pre_diff		77.68	<0.0001	0.046	0.616	4158.323
pre_mh		338.28	<0.0001	0.185	0.751	3897.726
pre_diff + pre_mh		1618.43	<0.0001	0.648	0.897	2619.574

E. FOREST	shift~	LR chi2	Pr(> chi2)	Pseudo-R2	C-index	AIC
pre_diff		295.56	<0.0001	0.233	0.763	2135.574
pre_mh		370.34	<0.0001	0.284	0.795	2060.801
pre_diff + pre_mh		1026.59	<0.0001	0.634	0.908	1406.553

Appendix B

Parameters used in LPJ-GUESS simulations[1]

Table B1 Global parameters

Parameter	Value	Parameter	Value
vegmode	"cohort"	ifdisturb	1
nyear_spinup	500	ifbgestab	1
ifdailynpp	0	ifsme	1
ifdailydecomp	0	ifstochestab	1
ifcalcsla	1	ifstochmort	1
iffire	1	ifcdebt	1
npatch	30	ifsmoothgreffmort	1
patcharea	1000	ifdroughtlimitedestab	1
estinterval	5	ifrainonwetdaysonly	0
distinterval	100	ifspeciesspecificwateruptake	0

nyear	Number of years for which to run simulation.
ifdailynpp	Whether to calculate NPP daily (1) or monthly (0).
ifdailydecomp	Whether to calculate soil respiration daily (1) or monthly (0).
ifcalcsla	Whether to calculate SLA from leaf longevity (1) or not (0).
iffire	Whether to implement fire (1) or not (0).
npatch	Number of replicate patches to simulate.
patcharea	Patch area (m^2).
estinterval	Years between establishment events in cohort mode.
distinterval	Average return time for generic patch-destroying disturbances (yr).
ifdisturb	Whether generic patch-destroying disturbances enabled (1) or not (0).
ifbgestab	Whether background establishment enabled (1) or not (0).
ifsme	Whether spatial mass effect enabled (1) or not (0).
ifstochestab	Whether establishment stochastic (1) or not (0).
ifstochmort	Whether mortality stochastic (1) or not (0).
ifcdebt	Whether C debt (storage between years) permitted (1) or not (0).
ifsmoothgreffmort	Whether to vary mort_greff smoothly with growth efficiency (1) or to use the standard step-function (0)
ifdroughtlimitedestab	Whether establishment is limited by drought (1) or not (0).
ifrainonwetdaysonly	Whether to rain on wet days only (1), or to rain a bit every day (0)
ifspeciesspecificwateruptake	Whether there is species specific water uptake (1) or not (0)

[1] Presented as in Allen et al., 2010.

Table B2 Parameters common to all PFTs

Parameter	Value
lambda_max	0.8
reprfrac	0.1
k_chilla	0
Photosynthetic pathway	C3 for all except C4G

lambda_max	Non-water-stressed ratio of intercellular to ambient CO_2 partial pressure.
reprfrac	Fraction of NPP allocated to reproduction.
k_chilla	Constant in equation for budburst chilling time requirement.

Table B3 Parameters common to groups of PFTs defined by their life form

Parameter	Trees	Grasses
lifeform	"tree"	“grass”
ltor_max	1	0.5
cton_leaf	29	29
cton_root	29	29
cton_sap	330	–
kest_repr	200	–
kest_bg	0.1	–
kest_pres	1	–

ltor_max	Non-water-stressed leaf : fine root mass ratio.
cton_leaf	Leaf C : N mass ratio.
cton_root	Fine root C : N mass ratio.
cton_sap	Sapwood C : N mass ratio.
kest_repr	Constant in equation for tree establishment rate.
kest_bg	Constant in equation for tree establishment rate.
kest_pres	Constant in equation for tree establishment rate.

Table B4 Parameters related to shade tolerance

Parameter	Shade Tolerant	Shade Intolerant
greff_min	0.04	0.08
alphar	2	10
parff_min	125000 (incl. Grasses)	250000

greff_min	Threshold for growth suppression mortality (kgC m^{-2}leaf yr^{-1}).
alphar	Shape parameter for recruitment – juvenile growth rate relationship.
parff_min	Minimum forest floor PAR for grass growth/tree establishment (J m^{-2} day^{-1}).

Table B5 Parameters per plant functional types (PFTs)

	MBS	MNE	TeBS	TeBE	TeNE	TrBE	TrIBE	TrBR	TrIBR	C3CG	C3WG	C4G
Form	W	W	W	W	W	W	W	W	W	H	H	H
Phenology	S	S	S	E	E	E	E	R	R	A	A	A
Leaf long.	0.5	2	0.5	2	2	2	2	0.5	0.5	1	1	1
Turn. leaf	1	0.5	1	1	0.25	0.5	0.5	1	1	1	1	1
Root dist.	70/30	60/40	70/30	70/30	60/40	80/20	60/40	80/20	50/50	90/10	80/20	80/20
Turn. root	0.7	0.7	1	1	0.25	0.7	0.7	1	1	0.7	0.7	0.7
Shade tol.	T	T	T	T	T	T	I	T	I	-	-	-
Resp_C	1.2	1.2	1.2	1.2	1.2	0.15	0.15	0.15	0.15	1.0	1.0	0.5
ptemp_min	-4	-4	-4	-4	-4	2	2	2	2	-5	0	6
ptemp_low	15	15	15	20	20	22	24	22	24	5	10	30
ptemp_high	25	25	25	30	30	30	32	30	32	25	30	45
ptemp_max	38	38	38	42	42	55	55	55	55	38	55	55
gmin	0.5	0.3	0.5	0.5	0.3	0.5	0.5	0.5	0.5	0.5	0.5	0.5
Turn. sap	0.05	0.05	0.05	0.05	0.05	0.05	0.1	0.05	0.1	-	-	-
emax	5	5	5	5	5	7	7	7	7	5	5	7
est_max	0.05	0.05	0.05	0.05	0.05	0.05	0.2	0.05	0.2	1	1	1
phengdd5ramp	150	0	200	0	0	0	0	0	0	0	100	100
tcmin_surv	-32.5	-32.5	-17	3	-2	15.5	15.5	15.5	15.5	-1000	-1000	15.5
tcmin_est	-32.5	-32.5	-17	3	-2	15.5	15.5	15.5	15.5	-1000	-1000	15.5
tcmax_est	10	10	18.5	18.5	20	1000	1000	1000	1000	15.5	1000	1000
twmin_est	-1000	-1000	-1000	-1000	-1000	-1000	-1000	-1000	-1000	-1000	-1000	-1000
gdd5min_est	350	600	1200	1200	1200	0	0	0	0	0	0	0
wscal_min	0	0	0	0	0	0	0	0.1	0.1	0.1	0.1	0.2
drought_tol	0.3	0.2	0.3	0.1	0.08	0.15	0.1	0.15	0.1	0.01	0.01	0.01
fire_resist	0.12	0.12	0.12	0.3	0.5	0.15	0.25	0.15	0.35	0.5	0.5	0.5
litterme	0.3	0.3	0.35	0.35	0.35	0.1	0.1	0.1	0.1	0.1	0.35	0.1

MBS: Mountainous Broad-leaved Summergreen

MNE: Mountainous Needle-leaved Evergreen

TeBS: Temperate Broad-leaved Summergreen

TeBE: Temperate Broad-leaved Evergreen

TeNE: Temperate Needle-leaved Evergreen

Tr(I)BE: Tropical Shade (In-)Tolerant Broad-leaved Evergreen

Tr(I)BR: Tropical Shade (In-)Tolerant Broad-leaved Raingreen

C3CG: C3 (Cold) Grasses

C3WG: C3 (Warm) Grasses

C4G: C4 Grasses

Form	W=Woody; H = Herbaceous.
Phenology	Phenology – S = summergreen; E = evergreen; A = any.
Leaf long.	Leaf longevity in years.
Turn. leaf	Leaf turnover (proportion per year).
Root dist.	Proportions of roots in upper 50cm of soil and below. (%)
Turn. root	Fine root turnover (proportion per year).
Shade tol.	Shade tolerance – I = Shade intolerant; T = Shade tolerant;
Resp_C	Respiration coefficient
pstemp_min	Minimum temperature limit for photosynthesis (°C)
pstemp_low	Minimum temperature of optimal range limit for photosynthesis (°C)
pstemp_high	Maximum temperature of optimal range limit for photosynthesis (°C)
pstemp_max	Maximum temperature limit for photosynthesis (°C)
gmin	Canopy conductance not associated with photosynthesis (mm s^{-1})
turn. sap	Sapwood turnover (proportion per year)
emax	Maximum evapotranspiration rate (mm day^{-1}).
est_max	Maximum sapling establishment rate (individual m^{-2} yr^{-1})
phengdd5ramp	Growing degree days on 5°C base to attain full leaf cover.
tcmin_surv	Minimum 20-yr coldest month mean temperature for survival (°C).
tcmin_est	Minimum 20-yr coldest month mean temperature for establishment (°C).
tcmax_est	Maximum 20-yr coldest month mean temperature for establishment (°C).
twmin_est	Minimum warmest month mean temperature for survival (°C).
gdd5min_est	Minimum growing degree days above 5°C for establishment.
wscal_min	Water stress threshold for leaf abscission.
drought_tol	Drought tolerance (1 = intolerant; 0 = tolerant)
fire_resist	Fire resistance (proportion surviving fire).
litterme	Litter moisture flammability threshold (fraction of AWC).

Biome Classification rules

Table B6 Biome classification rules. Rules are based on total leaf area index (LAI) and proportions of LAIs of different plant functional types (PFT) and **are applied in the given order** to classify the model outputs into biomes. XERO=Afroalpine, WAMF=Afromontane, TEFO=Tropical Evergreen Forest, TSFO=Tropical Seasonal Forest, WOOD=Woodland, SAVA=Savanna, STEP=Steppe, MNE=Mountainous Needle-leaved Evergreen, MBS=Mountainous Broad-leaved Summergreen, C3CG=Cold C3 Grass, TeNE=Temperate Needle-leaved Evergreen, TeBE=Temperate Broad-leaved Evergreen, TrBE=Tropical (Shade-tolerant) Broad-leaved Evergreen.

Rules	Biome
(1): If (MNE LAI >0.01 or MBS LAI > 0.01) and C3CG LAI > 2.0	XERO
(2): If TeNE LAI > 0.01 or TeBE LAI > 0.1 TeBS LAI > 0.1	WAMF
(3): If Tot. LAI >= 6.0 and woody LAI >=5.0 and TrBE is the dominant PFT	TEFO
(5): If Tot. LAI > 5.0 and woody LAI> =4.0	TSFO
(5): If Tot. LAI > 2.5 and woody LAI> =1.5	WOOD
(6): If Tot. LAI > 0.5 and woody LAI > 0	SAVA
(7): If Tot. LAI >= 0.1	STEP
(8): If Tot. LAI < 0.1	Bare Soil

Generation of new datasets:

Topographical settings

EXP_topo = (CTL_topography – Hlim)*C + Hlim (Sepulchre et al., 2006)

EXP_topo : Experimental topography

CTL_topography: Control (present-day) topography

Hlim : Altitude threshold = 200 meters

C : Reduction coefficient = 0.5 for TOPO50, 0.05 for NORIFT settings used in this study.

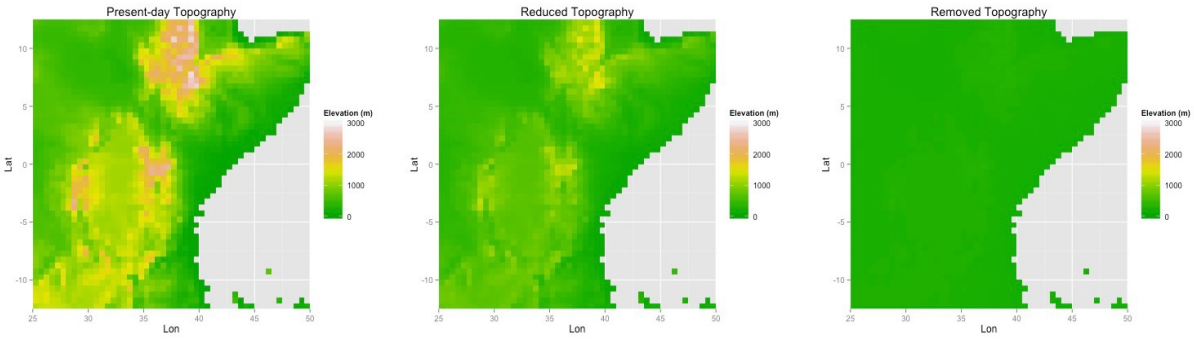

(a) **(b)** **(c)**

Figure B1 Topographical settings used in this study. Topography is reduced to (b) 50% (TOPO50, reduced topography) and (c) 5% (NORIFT, removed topography) of the (a) present-day height.

Temperature:

1. We first fitted a linear regression on the present-day values, that treats the present-day temperature values in each grid as a function of its latitude, longitude and present-day elevation.

$T_{present} \sim Lat + Lon + Elv_{present}$

2. Then, by targeting the new elevation datasets (TOPO50 and NORIFT) as described above, we obtained the new temperature values:

$T_{topo50} \leftarrow predict(Lat + Lon + Elv_{topo50})$
$T_{norift} \leftarrow predict(Lat + Lon + Elv_{norift})$

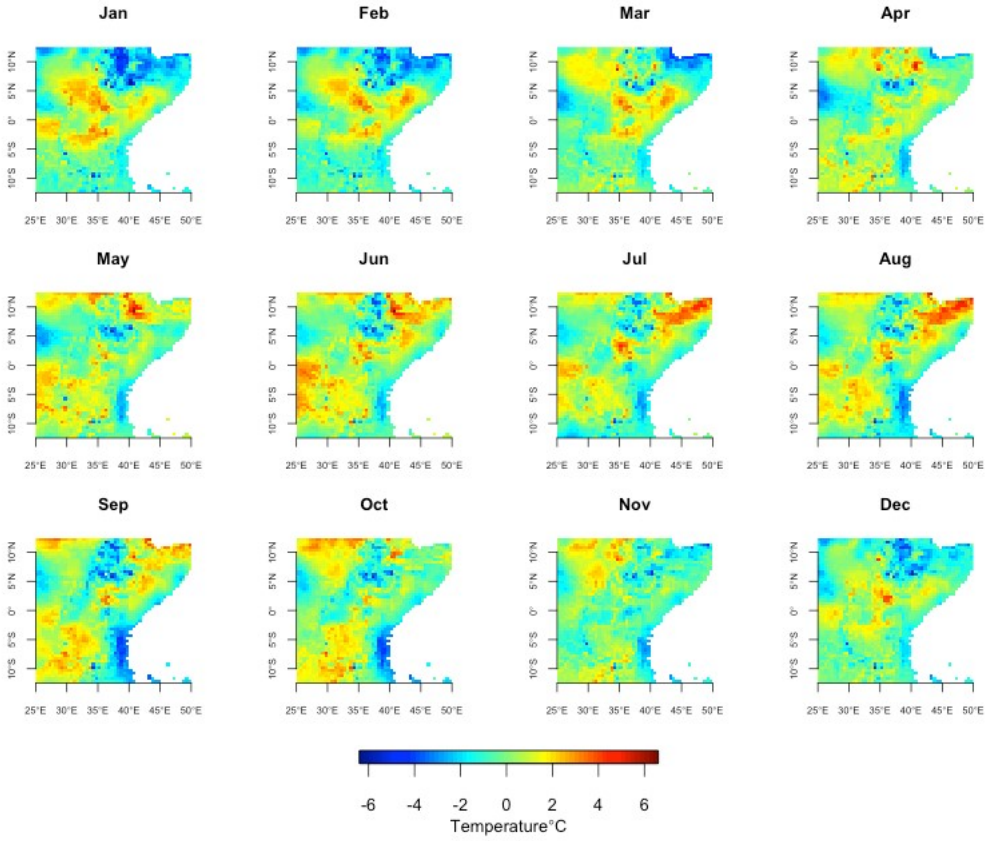

Figure B2 Comparison of the two, one statistically calculated in this study, TOPO50; the other dynamically computed by Prömmel et al. (2013) TECT, climatology temperature data. Anomalies shown are TECT-TOPO50 differences.

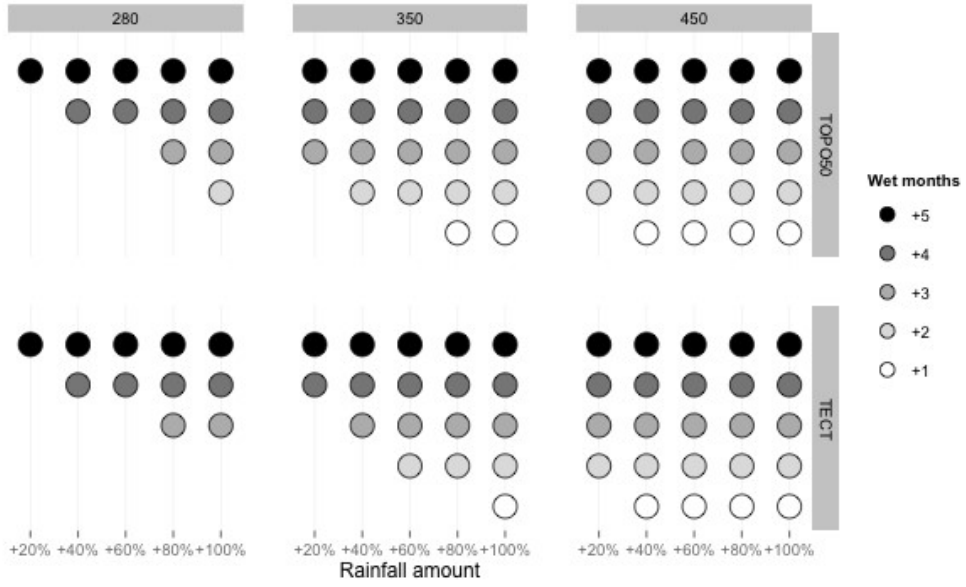

Figure B3 Comparison of the simulations in which a continuous forest belt simulated under TOPO50 and TECT temperatures. Large circles represent the scenarios in which both seasonality and amount of precipitation changes were applied. A large circle is placed in the corresponding place if a continuous belt was simulated under that particular combination of environmental conditions or left blank if no connection was established. Different shades of large circles represents different number of wet months added in the scenarios.

Precipitation:

i) increase in monthly rainfall amounts only:

$P_{20} \leftarrow P_{present} + P_{present}$ x 20/100

The same applies for 40% and other percentages of increase.

(ii) increase in wet season length only:

1. Look at all 12 months of each year
2. Choose the months with precipitation <50 mm
3. Top the month with the highest precipitation, among those filtered in Step 2, up to 50 mm
4. Repeat to add more than one wet month

(iii) increase in both monthly amount and wet season length:

P_{S1}: Present day precipitation with one wet month added (to each year).

$P_{S1\_20} \leftarrow P_{S1} + P_{S1}$ x 20/100

The same applies for scenarios with more than one wet month added and other percentages of increase.

Cloud Cover:

C, T and P being monthly gridded time series cloud cover, temperature and precipitation data respectively:

1. We first fitted a (beta) regression on the present-day values:

$C_{present} \sim T_{present} + P_{present}$

2. Once the new set of temperature and precipitation values for each setting is generated as above, we computed the modified cloud cover data by using these new T and P values as regressor variables of the fitted equation.

$C_{topo50\_S1} \leftarrow predict(T_{topo50} + P_{S1})$

T_{topo50}: new temperature values for Topo50 topographical setting

P_{S1} : new precipitation values for +1 wet season

...

$C_{norift\_S1\_20} \leftarrow predict(T_{norift} + P_{S1\_20})$

T_{norift}: new temperature values for NORIFT topographical setting

P_{S1_20} : new precipitation values for +1 wet season and 20% increase

Comparison of the simulated present-day biomes to an observed vegetation map

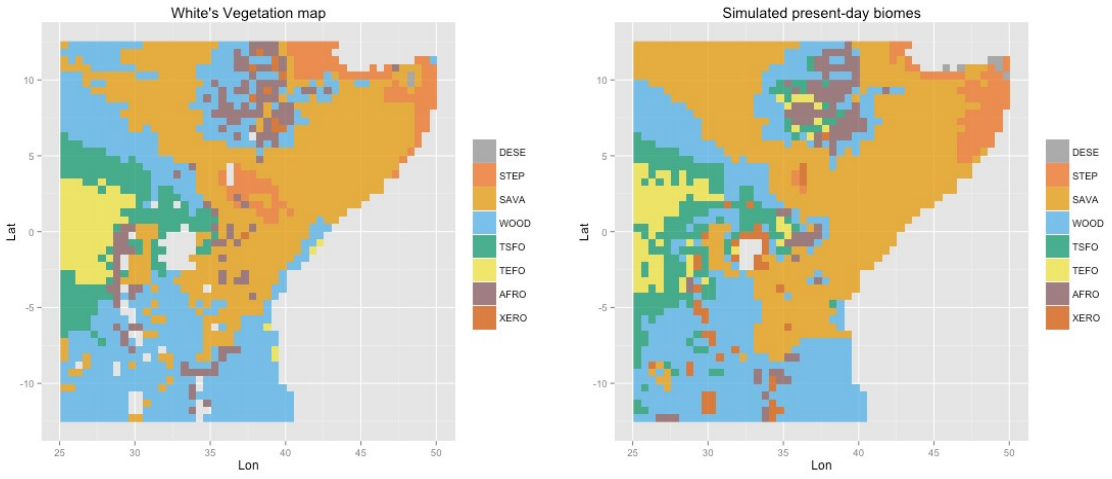

(a) (b)

Figure B4 Biome distributions of East Africa. a) White's vegetation map, b) Present-day biomes simulated by LPJ-GUESS. Each color represents a different biome whereas white areas represents the masked-out water bodies.

XERO=Afroalpine, WAMF=Afromontane, TEFO=Tropical Evergreen Forest, TSFO=Tropical Seasonal Forest, WOOD=Woodland, SAVA=Savanna, STEP=Steppe, DESE=Desert

Table B7 Accuracy assessments between simulated map and vegetation map. KIA = Kappa Index of agreement per biome; κ = Generalized Kappa value, α = the proportion of correctly classified cells; # = number of grid cells to compare (without the masked out cells). Levels of agreement: <0.4 poor, 0.4-0.55 fair, 0.55-0.7 good, 0.7-0.85 very good, >0.85 excellent (Monserud and Leemans,1992).

	LPJ-GUESS vs. White's map (0.5º x 0.5º)	
Biomes	KIA	
Bare Soil	0	
Steppe	0.47	
Savanna	0.65	
Woodland	0.62	
Seasonal F.	0.49	
Evergreen F.	0.51	
Afromontane	0.53	
Afroalpine	0	
Overall	α	κ
	0.70	0.59
#	1812	

Allen, J. R. M., Hickler, T., Singarayer, J. S., Sykes, M. T., Valdes, P. J., Huntley, B., 2010. Last Glacial vegetation of northern Eurasia. Quaternary Science Reviews 29, 2604-2618. http://dx.doi.org/10.1016/j.quascirev.2010.05.031

Fer, I., Tietjen, B., Jeltsch, F., 2015. High-resolution modelling closes the gap between data and model simulations for Mid-Holocene and present-day biomes of East Africa. (*In review)*

Monserud, R.A., Leemans, R., 1992. The comparison of global vegetation maps. Ecological Modelling. 62**,** 275-293. http://dx.doi.org/10.1016/0304-3800(92)90003-W

Prömmel, K., Cubasch, U., Kaspar, F., 2013. A regional climate model study of the impact of tectonic and orbital forcing on African precipitation and vegetation. Palaeogeography, Palaeoclimatology, Palaeoecology 369, 154-162. http://dx.doi.org/10.1016/j.palaeo.2012.10.015

Sepulchre, P., Ramstein, G., Fluteau, F., Schuster, M., Tiercelin, J.-J., Brunet, M., 2006. Tectonic uplift and eastern Africa aridification. Science 313, 1419–1423. http://dx.doi.org/10.1126/science.1129158.

Appendix C

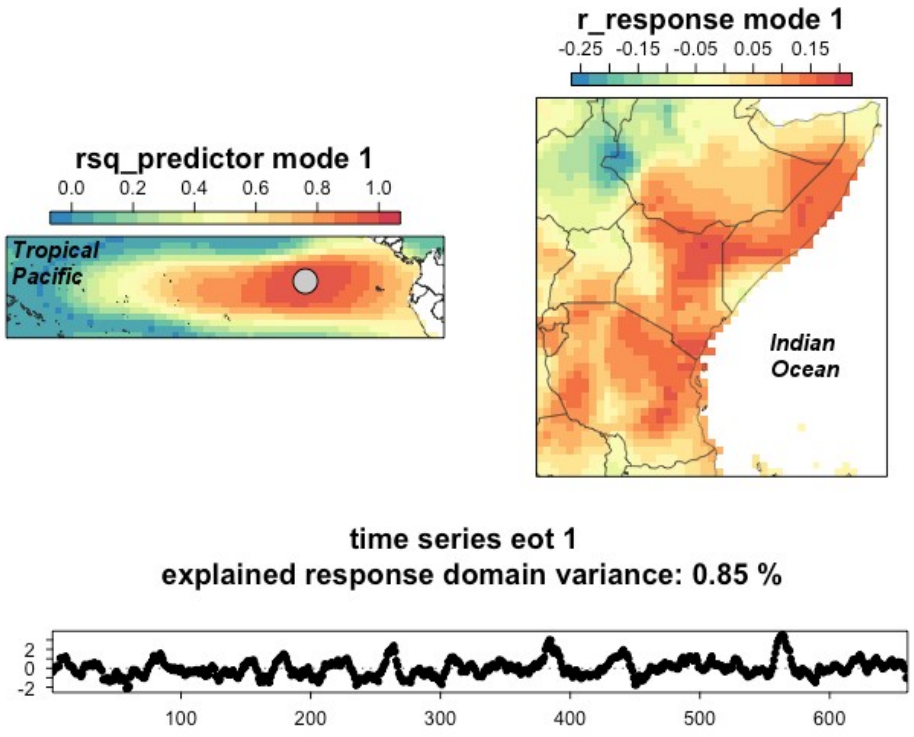

Figure C1. Coupled ocean-atmosphere teleconnection between Pacific Sea Surface Temperatures and East African Rainfall retrieved from historical observations. (Upper Left) The coefficients of determination for the predictor field highlights that the Nino-3.4 region explains the variance in the response domain the most. (Upper Right) Correlation coefficients of the each pixel of the East Africa (response) domain shows that spatially the coastal parts and a north-western area is being explained by the predictor field. (Bottom panel) Time series of Tropical Pacific SST anomalies at the base point (the gray circle in the upper left panel) of the first mode as ENSO signal.

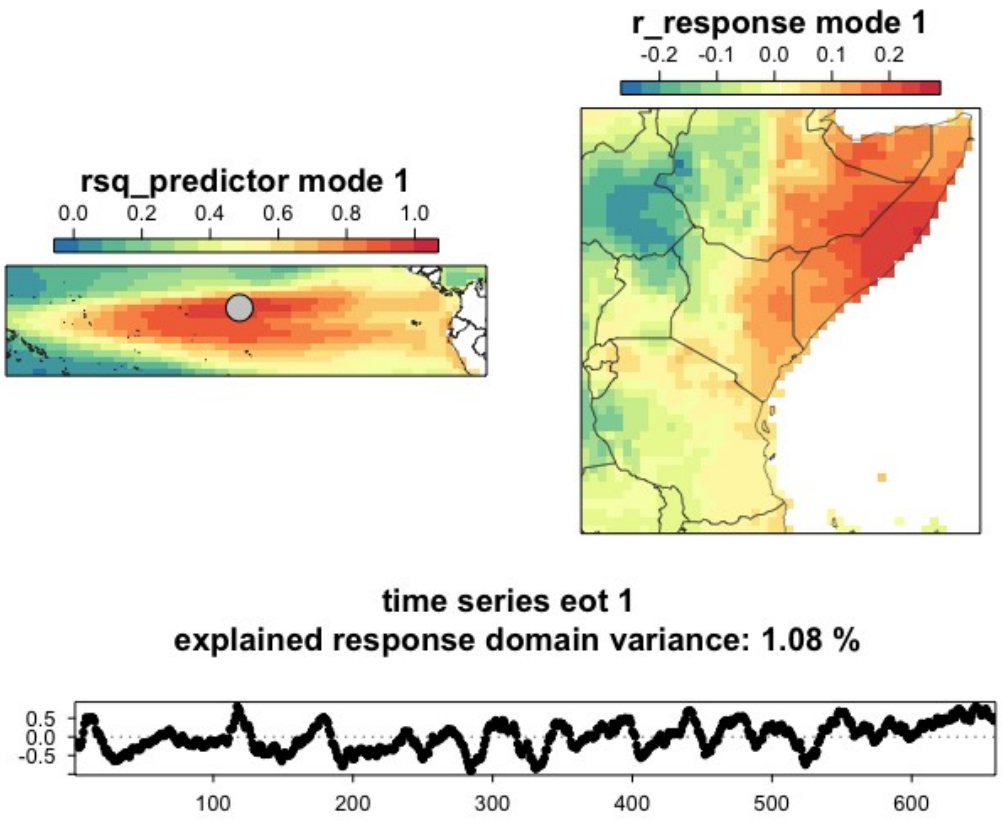

Figure C2. EOT Analysis for the historical period from the GCM simulations. Panels as explained in Figure A1: (Left) The coefficients of determination for the predictor field. (Right) Correlation coefficients of the each pixel of the East Africa (response) domain. (Bottom) Time series at the base point of the mode.

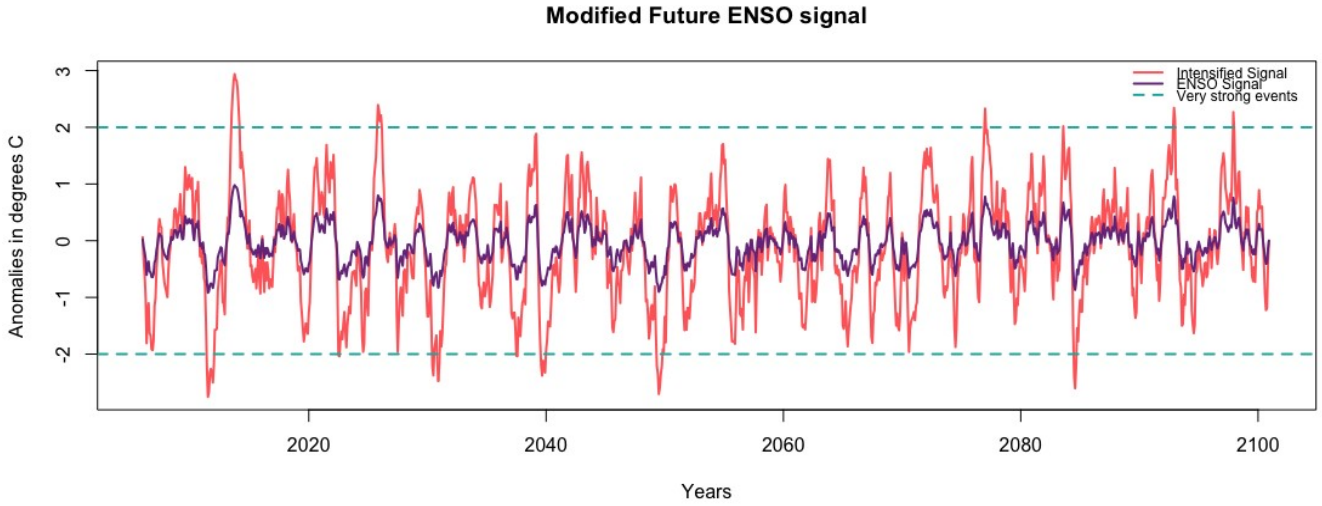

Figure C3. Intensified ENSO signal. Purple line: Future ENSO signal retrieved from GCM outputs for 2006-2100 period. Red Line: Intensified signal such that anomalies peak as strong as recorded amplitudes (± 2.0° C) .Dashed line marks the very strong ENSO event threshold.

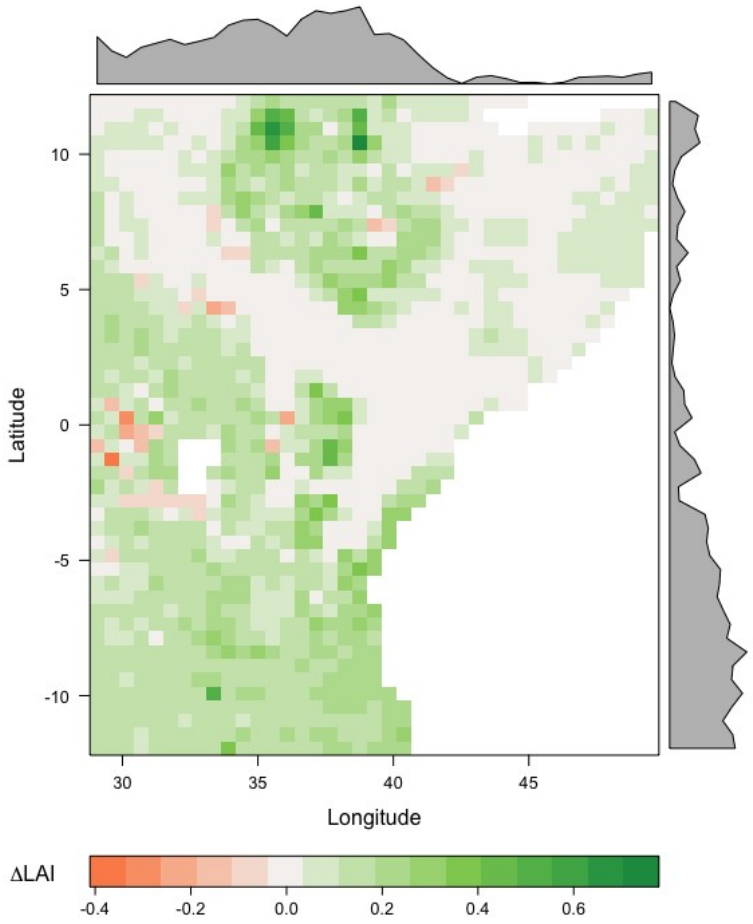

Figure C4. Simulated woody vegetation Leaf Area Index (LAI) differences under future climate scenario RCP8.5 (without any manipulation to the ENSO signal) and present-day (PD). (ΔLAI = RCP8.5 – PD).

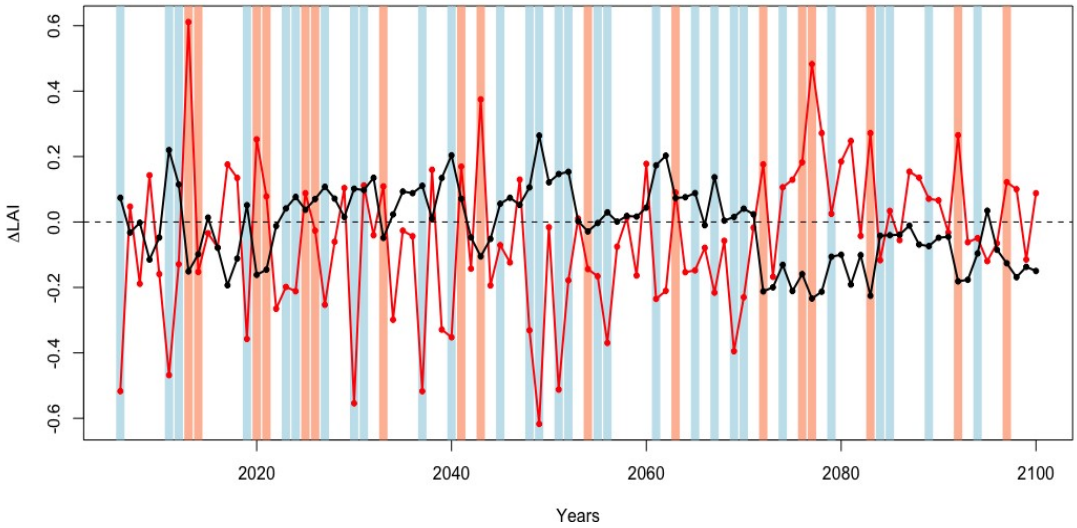

Figure C5. Temporal differences in LAI according to future simulations with and without intensified ENSO contribution (Δ = With_Intensification - Without_Intensification). Black line: Northern transect, Red line: southern transect. Vertical blue lines: All moderate (< -1.0° C) La Nina years identified for the future period (2006-2100), Vertical pink lines: Moderate (> 1.0° C) El Nino years.

C3 Full names of Global Circulation Models and their home Institutions

CCCma-CanESM2: Canadian Centre for Climate Modelling and Analysis - The second generation Canadian Earth System Model (Flato et al., 2000)

CERFACS CNRM-CM5: Centre Européen de Recherche et de Formation Avancée, Centre National de Recherches Météorologiques, Climate Model 5 (Voldoire et al., 2013)

IPSL CM5A-MR: Institut Pierre Simon Laplace Climate Model 5A Medium Resolution (Hourdin et al., 2013)

QCCCE CSIRO Mk3-6-0: Queensland Climate Change Centre of Excellence, Commonwealth Scientific and Industrial Research Organization, Mark 3.6 (Collier et al., 2013)

ICHEC EC-EARTH: Irish Centre for High End Computing, EC-Earth (Sterl et al., 2012)

MIROC5: Atmosphere and Ocean Research Institute (The University of Tokyo), National Institute for Environmental Studies, and Japan Agency for Marine-Earth Science and Technology, Model for Interdisciplinary Research on Climate (Watanabe et al., 2010)

MPI-M ESM-LR: Max Planck Institute for Meteorology, Earth System Model, Low Resolution (Giorgetta et al.,, 2013)

NCC NorESM1-M: Norwegian Climate Centre, Norwegian Earth System Model (Bentsen et al., 2013)

NOAA GFDL-ESM2M: National Oceanic and Atmospheric Administration, Geophysical Fluid Dynamics Laboratory (Dunne et al., 2012)

References

Bentsen, M., et al. (2013): The Norwegian Earth System Model, NorESM1-M - Part 1: Description and basic evaluation of the physical climate, Geosci. Model Dev., 6, 687-720, doi:10.5194/gmd-6-687-2013

Collier, M. et al., 2013, Ocean circulation response to anthropogenic-aerosol and greenhourse gas forcing in the CSIRO-Mk3.6 coupled climate model, Australian Meteorological and Oceanographic Journal, 63, 27-39

Dunne, J.P, et al., 2012, GFDL's ESM2 Global Coupled Climate-Carbon Earth System Models, American Meteorological Society, *http://dx.doi.org/10.1175/JCLI-D-11-00560.1*

Flato, G. M. et al., 2000. "The Canadian Centre for Climate Modeling and Analysis global coupled model and its climate". Climate Dynamics. **16** (6): 451–467. *doi*:*10.1007/s003820050339*.

Giorgetta, M., et al. 2013, Climate change from 1850 to 2100 in MPI-ESM simulations for the coupled model intercomparison project phase 5, J. Adv. Model. Earth Syst., doi:*10.1002/jame.20038*

Hourdin, F., Foujols, MA., Codron, F. et al., 2013, Clim Dyn, 40: 2167. doi:10.1007/s00382-012-1411-3

Sterl, A., Bintanja, R., Brodeau, L. et al., 2012, Clim Dyn, 39: 2631. doi:10.1007/s00382-011-1239-2

Voldoire, A., Sanchez-Gomez, E., Salas y Mélia, D. et al. Clim Dyn (2013) 40: 2091. doi:10.1007/s00382-011-1259-y

Watanabe, M., et al., 2010, Improved Climate Simulation by MIROC5: Mean States, Variability, and Climate Sensitivity, American Meteorological Society, http://dx.doi.org/10.1175/2010JCLI3679.1